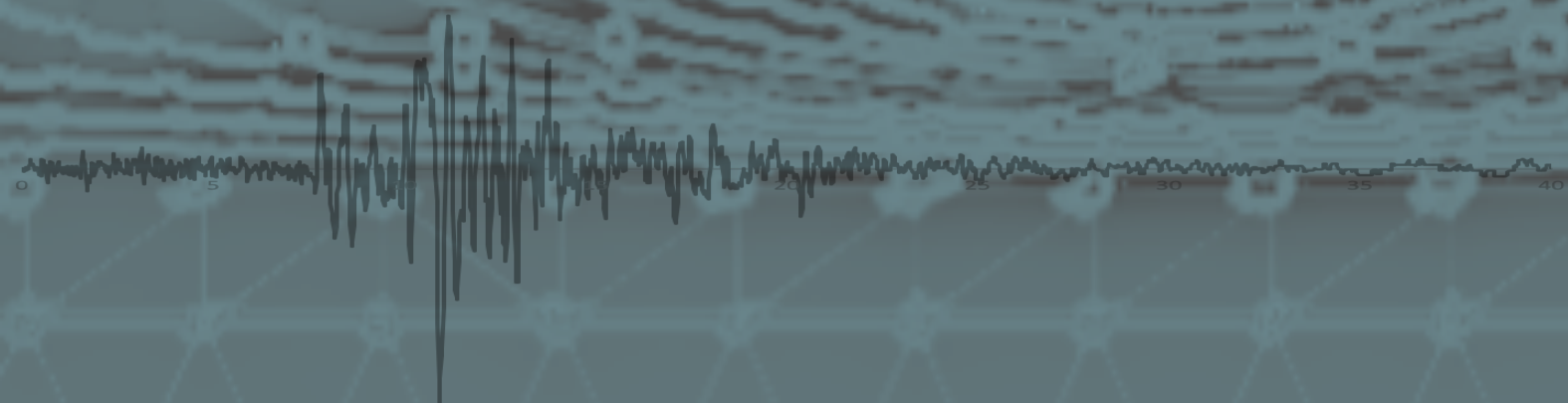


Stability Analysis of Geotextile-reinforced Slope Based on Japan Earthquake in 2011: Yuriage, Natori City Case



Mustaqim

Stability Analysis of Geotextile-reinforced Slope Based on Japan Earthquake in 2011: Yuriage, Natori City Case

By

Mustaqim

in partial fulfilment of the requirements for the degree of

Master of Science
in Geo-Engineering

at the Delft University of Technology,
to be defended publicly on
Tuesday, 30th October 2018

Supervisor:	Dr. Amin Askarinejad	
Thesis committee:	Prof.dr. M.A. Hicks	TU Delft – Geo-engineering
	Dr.ir. Ronald Brinkgreve	TU Delft – Geo-engineering
	Ir. Kristina Reinders	TU Delft – Hydraulic engineering

An electronic version of this thesis is available at <http://repository.tudelft.nl/>.

Acknowledgement

All the praises and thanks be to Allah SWT, The Most Beneficent, so I can finish my study at TU Delft.

First of all, I would like express my gratitude to my supervisor, Dr. Amin Askarinejad, for his continuous and endless supports, helpful discussions, and the opportunity to have my final thesis project located in Japan. I would like to thank Dr.ir. Ronald Brinkgreve who always have time when I need something to discuss and seek for his critical review. Many thanks to Ir. Kristina Reinders and Prof. dr. M.A. Hicks as my committee member who helped and guided me to finish this master thesis.

I want to thank DIMI for the support to fund this thesis site-visit in Japan. I am also grateful for the scholarship from LPDP (Indonesia Endowment Fund for Education), so I can achieve one of my dreams which is to study abroad.

Finally, I want to thank my family for all the support and pray. Special thanks to my mother who is always there for whenever I need and also my grandmother, I know you will be smiling in *Jannah*. I want to say thanks to all my friends and colleagues who helped me through the ups and downs during these past two years in Delft.

Mustaqim

Delft, 30 October 2018

Content

Acknowledgement	v
Content	vii
Abstract	ix
List of Figures	xi
List of Tables	xiii
List of Symbols and Abbreviations	xiv
1 Introduction	1
1.1 Background	1
1.2 Research Questions	2
1.3 Objectives	2
1.4 Limitations of Project	3
2 Literature Review	4
2.1 Seismic Hazard and Damage Categories	4
2.2 Geotextile Application	5
2.3 Input Ground Motion	8
2.4 Limit Equilibrium Method – D-Geo Stability software	9
2.5 Finite Element Method – PLAXIS Software	10
2.5.1 Static Analysis	11
2.5.2 Dynamic Analysis	13
2.6 Rayleigh Damping	17
2.7 Summary and Conclusion	18
3 Project Overview: Yuriage Case	19
3.1 Project Requirements	20
4 Data of Project	22
4.1 Soil Investigation and Layer Schematization	22
4.2 Parameter Correlations	24
4.3 Parameter validation	28
4.4 Rayleigh Damping data	32
4.5 Seismic Design input	32
4.6 Geotextile parameter	36
5 Analysis: Yuriage Case	38
5.1 Limit Equilibrium Method: D-Geo Stability	38
5.1.1 Model	38
5.1.2 Result	40
5.2 Finite Element Method: PLAXIS	40
5.2.1 Geometry and Mesh	40
5.2.2 Model and Boundary Conditions	41

5.2.3	Phases and Analysis.....	42
5.2.4	Results.....	43
5.3	Optimization of Geotextile	54
5.3.1	Tensile Strength and Axial Stiffness.....	55
5.3.2	Length of Geotextile.....	57
5.3.3	Number of Layers	58
6	Conclusions and Recommendations	61
6.1	Conclusions	61
6.2	Recommendations and Fields that require further research	63
	Bibliography	64
A	Standard Penetration Test Data	66
B	Geotextile Properties from Global Synthetics	67
C	Geotextile Properties from TenCate Geosynthetics	68
D	Safety Factor Requirements (Yuriage basic design plan, 2014) (Translated).....	69
E	Disaster category (Yuriage basic design plan, 2014) (Translated)	70
F	Damage Level (Yuriage basic design plan, 2014) (Original Document)	71
G	Unconfined Compression Test for AC1 layer (Yuriage basic design plan, 2014).....	72

Abstract

The use of geotextile for slope strengthening was proven based on the investigation and report by Kuwano, Miyata, and Koseki (2014). Therefore, this research examines the impact of geotextile application on slope stability in newly-elevated area in Yuriage, Natori City, Japan. This project discussed the analysis of geotextile-reinforced slope by comparing the total displacement at the crest of slope between the compaction method as current design and the using of geotextile with further investigation by optimizing the use of geotextile application.

A cross-section of slope with 0.435m height and 29 degrees slope angle were chosen for the geometry of analysis. Two loads acted on the slope such as the uniform load on top of the raised area and dynamic load from the earthquake were defined. Six layers that mostly consist of sandy soils were determined based on the SPT data in 16 locations. The average values of N-SPT were calculated for further parameter correlations based on these values. Furthermore, analyses based on the Limit Equilibrium method and Finite Element Method were selected to analyse the slope stability.

Limit Equilibrium Method using D-Geo stability software based on the Bishop method was taken to define safety factor of slope under uniform load (without earthquake load). The value of safety factor at 1.93 was obtained then compared to the result for the same problem based on the Finite Element Method using PLAXIS 2D with HS Small model that resulted at 2.07 safety factor. Further dynamic analysis was also completed using PLAXIS 2D with UBCSAND model to calculate the total displacement at slope crest without and with geotextile application. The strengthening method using geotextile (500 kN/m tensile strength, 5004 kN/m axial stiffness, 30m length in 5 layers) decreased the total displacement from 0.543m to 0.434m. However, the impact of geotextile is very limited in this case that only decrease 0.109m or about 20% from the total displacement without geotextile. Weak foundation, silty clayey sand layer (AC1) and liquefied layers (AC1 and fine sand AS22) below the slope were observed as the main reasons for this small impact of geotextile. Therefore, geotextile method is not recommended to use in this project given its very limited impact on the total displacement. Furthermore, the soil improvement methods were proposed to tackle these two reasons, such as replacing the soil material (AC1) with stronger soil for the foundation under the slope and/or construct sand pile to minimize the liquefied layer below the slope until AS21 depth, about 6 meters.

Further analysis based on combination of five values of geotextile strengths, four difference lengths, and three number of layers were made to get the optimum used of geotextile by comparing the total displacement at the crest. The first factor that has to be considered is the strength of geotextile because this factor gives more influence in the final total displacement. Secondly, with the high strength of geotextile, the length should be considered first rather than the number of layers based on the impact of both factor on the influence of strength to the total of displacement.

List of Figures

Figure 1. Aerial photo of Yuriage condition after the tsunami (www.city.natori.miyagi.jp)	1
Figure 2. Failure modes for reinforced slopes: (a) internal failure; (b) external failure (Bonaparte et al., 1987).....	7
Figure 3. Internal failure of reinforcement in slopes: (a) reinforcement rupture; and (b) reinforcement pull-out (Bonaparte et al., 1987)	7
Figure 4. Slip surface failure: (a) deep-seated circular surface; and (b) shallow translational surface (Bonaparte et al., 1987).....	8
Figure 5. Type of earthquake motion.....	8
Figure 6. Failure area with vertical slices method.....	9
Figure 7. Force equilibrium for one slice in the method of slice (Deltares, 2016).....	10
Figure 8. Representative of yield contour in principal stress space for cohesionless soil.....	12
Figure 9. Secant and tangent shear modulus reduction curve.....	13
Figure 10. Yield surface in UBCSAND (Beatty and Byrne, 1998).....	15
Figure 11. Hyperbolic hardening rule in UBCSAND (Beatty and Byrne, 1998)	15
Figure 12. Direction of plastic strains associated with location of yield surface (Beatty and Byrne, 1998)	16
Figure 13. Stress ratio history showing loading, unloading, and reloading (Beatty and Byrne, 1998).....	17
Figure 14. Project location in Yuriage (www.google.com/maps).....	19
Figure 15. Project plan area.....	19
Figure 16. Cross-section location.....	20
Figure 17. Cross-section of location	20
Figure 18. Locations of Standard Penetration test.....	22
Figure 19. Geometry of slope and soil layers	24
Figure 20. Relationship between corrected blow count to the relative density (Gibbs & Holtz, 1957).....	25
Figure 21. Consolidated Undrained triaxial test for AC1 from PLAXIS.....	30
Figure 22. Consolidated Drained triaxial test result for all layers	31
Figure 23. Pore pressure ratio for layers use UBCSAND during CDSS test with CSR = 0.25 and $\sigma_v=40$ kPa	32
Figure 24. Location of two seismometer relative to the project location (www.google.com/earth)	33
Figure 25. Original recorded motion at MYG013 (http://www.kyoshin.bosai.go.jp)	33
Figure 26.Original recorded motion at MYG015 (http://www.kyoshin.bosai.go.jp)	34
Figure 27. Motion at surface in both locations based on the Loma Prieta input	35
Figure 28. Seismic input for PLAXIS analysis.....	35
Figure 29. Fast Fourier Transforms of the input	36
Figure 30. Processes of analysis.....	38
Figure 31. Geometry of analysis with D-Geo Stability.....	39

Figure 32. Grid of centre point of circle and horizontal tangent lines	39
Figure 33. Critical circle analysis without geotextile.....	40
Figure 34. Mirrored geometry for the tied degree of freedom boundary.....	41
Figure 35. stages of newly-elevated area for static analysis.....	42
Figure 36. Active pore water pressure for static analysis.....	43
Figure 37. Vertical effective stress (σ_{v0}') for the static analysis.....	44
Figure 38. Shear stress (τ_{xy}) for the static analysis.....	44
Figure 39. failure mechanism on analysis without earthquake load and no geotextile	45
Figure 40. Safety factor for the analysis without earthquake load and no geotextile.....	45
Figure 41. Total displacement at the end of dynamic time for analysis without geotextile.....	46
Figure 42. Total displacement at the cross-section below the crest of slope	46
Figure 43. Total displacement at the crest of slope during dynamic times and the input of motion at bedrock.....	47
Figure 44. Contour line of total displacement at the end of dynamic time for analysis without geotextile	47
Figure 45. Active pore pressure at the end of dynamic time for analysis without geotextile	49
Figure 46. Vertical effective stress at the end of dynamic time for analysis without geotextile ..	49
Figure 47. Liquefied areas corresponding to $r_u > 0.9$ at the end of dynamic times for analysis without geotextile	50
Figure 48. Total displacement at the end of dynamic time for dynamic analysis with geotextile	50
Figure 49. Comparison of total displacement at the crest of slope between the analysis without and with geotextile	51
Figure 50. Vertical effective stress at the end of dynamic time for analysis with geotextile.....	52
Figure 51. Active pore pressure at the end of dynamic time for analysis with geotextile.....	52
Figure 52. Axial forces for all layers of geotextile at the end of dynamic loading	53
Figure 53. Total displacement of geotextile at the end of dynamic time.....	53
Figure 54. Liquefied areas corresponding to $r_u > 0.9$ at the end of dynamic times for analysis with geotextile	54
Figure 55. Influence of strength on total displacement for increasing length of geotextile.....	55
Figure 56. Influence of strength on total displacement for increasing number of layers	56
Figure 57. Comparison of total displacement based on the total length.....	56
Figure 58. Influence of length on total displacement for increasing strength.....	58
Figure 59. Influence of length on total displacement for increasing number of layers	58
Figure 60. Influence of number of layers on total displacement for increasing length of geotextile	59
Figure 61. Influence of number of layers on total displacement for increasing strength of geotextile	60

List of Tables

Table 1. Damage of ground embankment (Yuriage basic design plan, 2014).....	5
Table 2. Combination of damage level and disaster category (Yuriage basic design plan, 2014)	5
Table 3. Hardening Soil Small strain model parameters.....	12
Table 4. Input parameter of UBCSAND.....	17
Table 5. SPT result from field test in Yuriage	23
Table 6. Laboratory data for four layers.....	23
Table 7. Generalized SPT energy ratios (Robertson, 1992).....	25
Table 8. UBCSAND model parameter for dynamic analysis.....	27
Table 9. HS small model parameter input for the static analysis.....	27
Table 10. Linear elastic parameter for bedrock (layer AG3)	28
Table 11. Typical Modulus of Young's modulus of soil (Bowles, 1996).....	28
Table 12. List parameter of HS small model.....	29
Table 13. List parameter of UBCSAND model.....	29
Table 14. Rayleigh damping parameter.....	32
Table 15. Soil parameter in both locations of seismometer (http://www.kyoshin.bosai.go.jp)...	34
Table 16. Geotextile parameters	37
Table 17. Parameter used in D-Geo stability.....	39
Table 18. Distance of total displacement value to the crest of the slope.....	48
Table 19. Combination of parameters	54

List of Symbols and Abbreviations

Symbol in Latin Alphabet

ASTM	American Society for Testing and Material
c	Cohesion
C	Damping matrix
CD	Consolidated Drained triaxial test
CDSS	Cyclic Direct Simple Shear test
CPT	Cone Penetration Test
CSR	Cyclic Stress Ratio
CU	Consolidated Undrained triaxial test
Dr or RD	Relative density
DSS	Direct Simple Shear test
E	Stiffness modulus
e	Void ratio
E'	Effective Young's modulus
EA	Axial stiffness
ER	Energy ratio
f	Yield function / Partial factor for geotextile / Frequency
fa _{C_{hard}}	densification actor
fa _{C_{post}}	Factor that determines the minimum value of the shear modulus during stiffness degradation
FEM	Finite Element Method
FFT	Fast Fourier Transform
g	Plastic potential function
G	Shear modulus
H	Thickness
HS Small	Hardening Soil Small strain
K	Stiffness matrix
KB	Bulk modulus number
KG	Shear modulus number
k _h	Horizontal earthquake factor
LEM	Limit Equilibrium Method
M	Mass matrix
m	Power of stress-level dependency of stiffness
me	Elastic bulk modulus exponent
N	Normal force/reaction
N-SPT	Number of blows SPT
N ₆₀	N-SPT at 60% energy correction
ne	elastic shear modulus exponent
np	Elastic shear modulus exponent
p	Mean stress
Pa	Atmospheric pressure
q	Shear stress / Deviatoric stress
R _f	Failure ratio
r _u	Pore pressure ratio
SF	Safety Factor

SLS	Serviceability Limit State
SPT	Standard Penetration Test
T	Tensile strength
UCT	Unconfined Compression Test
UU	Unconsolidated Undrained triaxial test
V_p	Compression wave velocity
V_s	Shear wave velocity
W	Weight

Symbol in Greek Letter

α and β	Rayleigh coefficients
γ	Unit weight or Shear train
ε	Strain
η	Stress ratio
λ	Wave length
ν	Poisson's ratio
ξ	Damping ratio
ρ	Density
σ	Principal stress
σ_t	Tension cut-off
τ	Shear stress
ϕ	Friction angle
ψ	Angle of dilatancy

1 Introduction

1.1 Background

During Japan's earthquake and tsunami in 2011, many damages happened that related to many sectors, including the geotechnical sector. Based on the field investigation conducted by related parties, there were some slope failures during the earthquake, but some others were still safe under the $M_w=9.0$ -moment magnitude. The result of the investigation concluded that the case where several slopes were safe was actually due to the use of geotextile application. Furthermore, based on the report by Kuwano, Miyata, and Koseki (2014), only less than 1% of the reinforced walls in Tohoku were seriously damaged due to the direct impact of earthquake shaking; more than 90% of them did not show any damage. Therefore, given the extensive and proven impact on geotextile application during the earthquake, this leads to an initiative on exploring the possibility of leveraging the application for an extensive use.



Figure 1. Aerial photo of Yuriage condition after the tsunami (www.city.natori.miyagi.jp)

This thesis project focuses on the post-tsunami reconstruction in Yuriage, Natori City, Japan, which was washed out by tsunami in 2011 as shown in figure 1. This area needs to be reconstructed based on several consideration. Firstly, the resident who lived previously in the area want to come back and live at the same place before the tsunami. Secondly, Yuriage is located near the port where the fishery industry of Natori City and Sendai City rely to this port. Moreover, the needs of housing for people who work at the port is also contribute to the decision of the importance of this area. Finally, one of the famous yet busiest fish markets is also located at the east of this project location toward the sea that escalates the importance of this project.

However, the new area should be strong enough to withstand the earthquake and also expected to be able to minimize the damages of tsunami as the mitigation of this unpredicted natural disaster. Thus, the current reconstruction focuses on raising the elevation of the area using compaction method. Moreover, the slope of the area has to be safe from the earthquake.

Furthermore, this project will provide the analysis geotextile-reinforced slope by comparing the total displacement at the crest of slope between the compaction method as current design and the using of geotextile. Further investigation will also cover the optimization on the use of geotextile application by analysing the length of geotextile, the strength of geotextile (pull-out force/resistance) and also the number of geotextile layer based on the total displacement at the crest.

1.2 Research Questions

Given the background of the research, there are two main research questions:

- How does geotextile reinforcement affect the strength of slope in the newly-elevated area of Yuriage as compared to the compaction method?
- What is the optimum utilization of geotextile to meet the requirement of total displacement and economically constructed for the case with geotextile application?

Further detailed questions are asked to answer these main questions:

- What type of Constitutive Model is suited for the case of dynamic analysis in PLAXIS 2D software?
- How is the stability of current slope design under a specific seismic condition?
 - Does any failure mechanism appear?
 - What is the maximum total deformation at the crest of the slope?

In comparison to the slope with geotextile reinforcement, several questions are asked:

- How different is the total displacement between geotextile method and the compaction method on the dynamic analysis?
- What kind of optimization will be considered to reach the requirement of total displacement at the crest of slope and economically constructed?
 - What is the optimum strength and length of geotextile for this Yuriage case and also number of geotextile layer?

1.3 Objectives

The main objective of this thesis is *checking the stability of slope with geotextile application and its optimization based on the Japan earthquake in 2011*. Two methods are used to investigate the slope, the first is using Limit Equilibrium method using D-Geo Stability software as the preliminary analysis and Finite Element Method using PLAXIS 2D software as the main analysis.

Furthermore, sub-objectives have to be considered as the processes getting into the main objective. They are listed as below:

- Interpretation of field test and lab test data into the required parameters
Correlation from N-SPT to all required parameters while some parameters already determined from the laboratory test.
- Determine the input of seismic motion for the analysis.
The data of seismic input is gathered from two locations of seismometer at the north (Sendai City) and south of this project location (Iwanuma City), where the project location is in the Natori City region (Yuriage).
- Determine the suitable constitutive model for the analysis where most of the soil layer is sandy soil both in the static and dynamic analysis.
- Determine the parameters of optimization for the geotextile application.
Three types of parameter are considered, which are the strength of geotextile, the length of geotextile, and the number of geotextile layer.

1.4 Limitations of Project

There are several limitations in the analyses of this project, which are listed as follow:

1. Data of project is limited with SPT data and some laboratory tests from only one layer (explained more in the chapter 4.1). Therefore, the validation of parameters could not be done properly and only rely on the parameter correlation.
2. The motion input is simplified by adjusting the Loma Prieta motion based on the peak acceleration of 2011 earthquake in two locations of seismometer.
3. The comparison of result (safety factor) between Limit Equilibrium Method and Finite Element Method is limited by the static analysis to review the model used for both methods are correlated to each other.

2 Literature Review

2.1 Seismic Hazard and Damage Categories

The worst effect of the earthquake to the slope is the total failure, which happens in the condition where the slope cannot withstand a large earthquake or long duration of the motion. However, the decrease in strength can also be the cause of damages, called as liquefaction, a condition where the soil was initially able to sustain the loads but due to the decrease in strength; it was not. Some of the evidences from liquefaction were seen during the earthquake in 2011 but washed out by the tsunami (Chian et al., 2012). Thus, the field evidence cannot be adequately documented.

Damage categories are defined based on the basic plan of newly-elevated area of Yuriage. The parts of the original document related to damage categories are compiled in the appendix E and appendix F. Moreover, disaster category based on the basic plan of Yuriage project document is classified as follow:

- Level A: Large damage (Whether the embankment is completely collapsed or the vehicle movement is not possible)
- Level B: Medium Damage (Embankment is partially collapsed, and part of the road may interfere with the collapse)
- Level C: minor damage (small part of embankment is affected, but the traffic might be interrupted)
- Level D: No damage (especially if no abnormality is observed in the embankment)

The damage of embankment is also defined into several levels as shown in table 1. The combination of the damage level and disaster category is presented in table 2.

Table 1. Damage of ground embankment (Yuriage basic design plan, 2014)

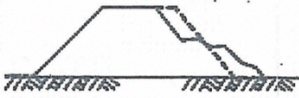



Damage Level	Damage sketch	Explanation
I		Partial failure that does not come to the road above
II		The slip collapse of the embankment/slope or in part of the road line
III		Destruction of the foundation ground and totally collapse all the road above
IV		With the uniform settlement of the embankment that keeping the shape to some extent.

Table 2. Combination of damage level and disaster category (Yuriage basic design plan, 2014)

Damage level	Disaster category	Explanation
I	B	15 cm – 20 cm deformation/displacement
	C	15 cm – 20 cm deformation/displacement
II	A	30 cm – 50 cm deformation/displacement
	B	30 cm – 50 cm deformation/displacement
III	A	-
IV	B	≥50 cm deformation/displacement
	C	≤ 50cm deformation/displacement

Moreover, the requirement of this project is based on the maximum displacement of slope at the crest. The undesirable condition is the damage level III in which all part of the slope including the road/building above the raised area are in total failure. However, the purpose of strengthening of the slope is to provide evacuation road for the people to the safer place. Thus, the minimum condition is the damage level II where only some part of road affected by the instability of slope or no structural damage on the building above. Therefore, the minimum displacement is about 0.5m at the crest of the slope or 10% from the average height of the newly-elevated area of Yuriage.

2.2 Geotextile Application

Given the fact that soil has no or small tensile strength, the method to strengthen the soil could be by reinforcing the it. This method is not a new method, it was started more than 3,000 years

ago in which the early example was found in Iraq. Reed-reinforced were used as construction of levees along the Tiber River by the Romans (Bonaparte, Holtz, & Giroud, 1987). However, the modern of reinforcement started in the 1960s with the development of reinforced earth retaining walls and geotextile stabilization of haul roads and access road. Nowadays, the common method to reinforce the soil is by using either geotextile or geogrid, in which both have experienced rapid developments over the quality of its materials.

Generally, both geotextile and geogrid perform similar functions, while these functions come from different reinforcement mechanisms. Geogrid provides the reinforcement based on the interlocking of geogrid and the soil, which the soil particles have to be in certain criteria to result on optimum function. However, in this case, there is no data of sieving test on the embankment, while the SPT number shows that this soil is categorized as the loose to medium sand. On the other hand, geotextile produces the reinforcement from the friction of geotextile material and soil that in this case the materials could be in wider ranges. Moreover, geotextile also offers other advantages for construction listed as below.

1. Cheaper construction (cost saving): the quantity of fill material can be decreased for steeper slope, which impacts to the reduction on land acquisition cost.
2. Increases on stability; the reinforced slope usually gives larger safety factor or less deformation.
3. Acts as drainage path, which becomes an important role in preventing liquefaction of sandy soil. Geotextile accelerates the dissipation of seismic induced excess pore pressure. However, this behaviour is not simulated in this research.
4. Increase the ductility of the soil mass to resist dynamic load.

D-geo stability requires the tensile strength of geotextile as the input data. However, PLAXIS defines two properties of geotextiles, which are stiffness properties (axial stiffness) and strength properties (tensile strength). Furthermore, several factors contribute to check the long-term design strength that can be obtained by using the formula (1).

$$T_d = \frac{T_c}{f_c \cdot f_d \cdot f_e} \quad (1)$$

Where T_d is the long-term design strength, T_c is the characteristic short-term tensile strength, f_c is the partial factor relating creep, f_d is the partial factor relating damage effect, and f_e is the partial factor relating environmental effect. The value of this factor is presented in the appendix based on the global synthetics company in Australia.

Furthermore, seismic slope stability design is influenced by several factors, such as ground motions at the site, desired slope geometry, the strength of soil, the strength of reinforcement, the strength of soil and reinforcement interaction, and acceptable amount of movement during earthquakes.

Failure might be occurred with varying types of failure and due to different reasons as presented in figure 2. Moreover, two type of failure modes are determined as internal failure in figure 2(a)

that the sliding takes place inside of the reinforced area and external failure in figure 2(b) in which the sliding outside the reinforced soil

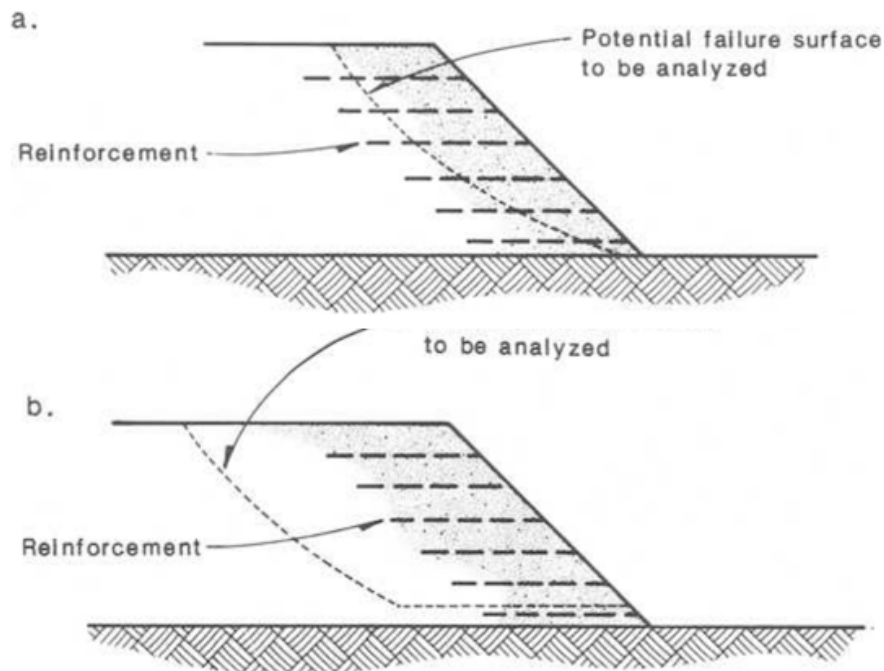


Figure 2. Failure modes for reinforced slopes: (a) internal failure; (b) external failure (Bonaparte et al., 1987)

Furthermore, the internal failure can be caused by two reasons, first due to the reinforcement rupture and second reinforcement pull-out as shown in figure 3(a) and figure 3(b) respectively.

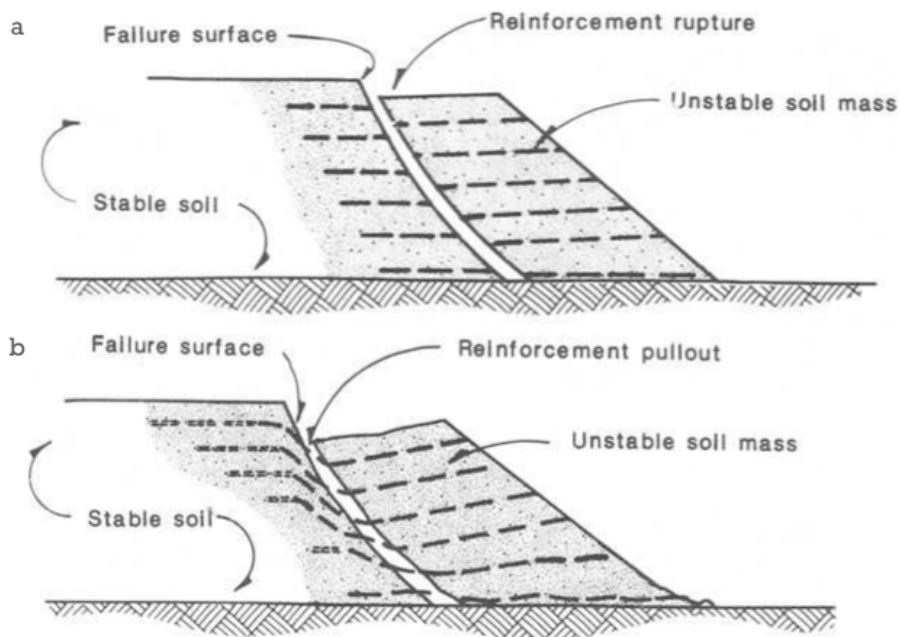


Figure 3. Internal failure of reinforcement in slopes: (a) reinforcement rupture; and (b) reinforcement pull-out (Bonaparte et al., 1987)

In the case of reinforced slope on weak foundation, the type of failure has different pattern as shown in figure 4. The failure line goes through the weak layer until it finds the slip surface. However, the type of slip surface failure is divided based on the thickness of weak layer below the embankment. This could be the deep-seated circular surface as shown in figure 4(a) or shallow translational surface in figure 4(b).

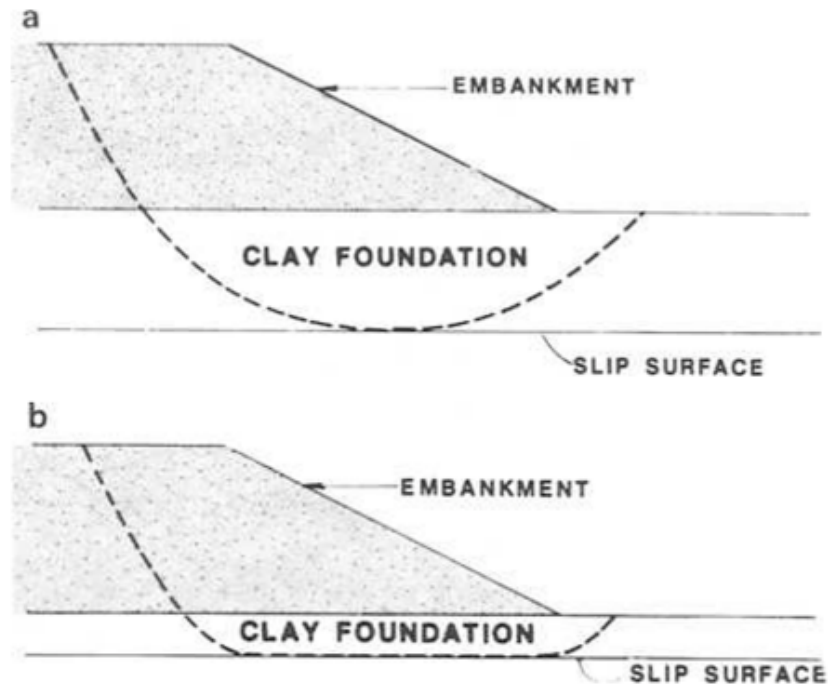


Figure 4. Slip surface failure: (a) deep-seated circular surface; and (b) shallow translational surface (Bonaparte et al., 1987)

2.3 Input Ground Motion

The earthquake motion is based on the time domain data that recorded from the seismometer or other equipment. However, this motion is one of the largest unknowns in any dynamic analysis. There are three types of motion based on the location of where it is recorded as shown in figure 5. The ground motion is the motion at the surface of soil deposit; outcrop motion is the motion that is recorded at the exposed bedrock at the ground surface; bedrock motion is the motion at the base of soil deposit. Furthermore, the seismometer locations for this analysis are found on the ground surface, which means the ground motion is the initial data of the seismic motion.

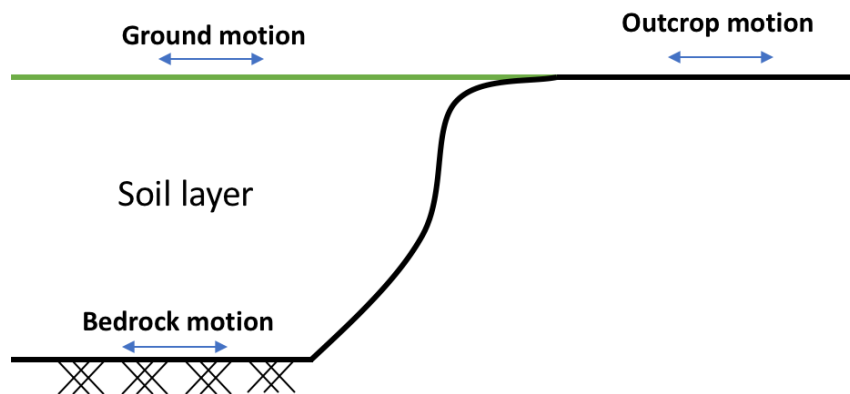


Figure 5. Type of earthquake motion

In this project, the input motion is considered based on the Loma Prieta motion, which was adjusted based on the peak acceleration of original recorded data. Moreover, the project is only limited by a specific motion input of Loma Prieta motion. Therefore, the use of other motions as the input could give a different result on the analysis. However, since the earthquake motion may will never be the same for each earthquake, the use of specific motion of Loma Prieta motions might be one of the limitations of this project.

2.4 Limit Equilibrium Method – D-Geo Stability software

Limit Equilibrium Method is the conventional method to define the slope stability. This method investigates the mass of soil tending to slide under the influence of gravity. Currently, the appearance of some softwares help the analysis of the slope stability, including the use of geotextile as a reinforcement. D-Geo stability is one of the softwares that focuses on this case, which the output of this software is a safety factor. However, the output (safety factor) does not provide the expected deformation of the slope; hence this software will be used as the preliminary analysis of this thesis. The results are intended as the hypothesis and result control for further analysis using PLAXIS software.

The method of slices based on the circular slip plane (Bishop, 1955) is considered to be the method to calculate the safety factor using D-Geo Stability software. This method divides the mass of soil above the slide line into several parts of the vertical slice as shown in figure 6. Moreover, the value of each slice may be different depending on the soil layer for each case, then the soil parameters, effective stress, and pore water pressure are calculated for each slice.

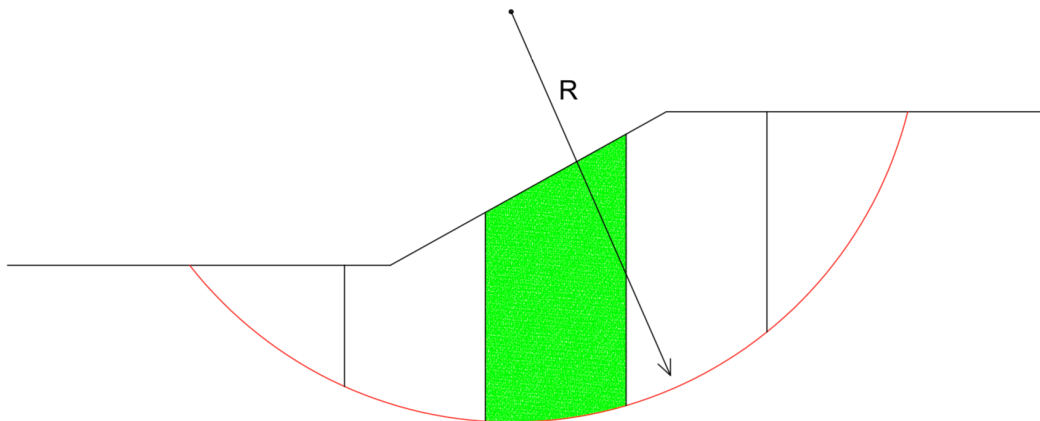


Figure 6. Failure area with vertical slices method

Bishop (1955) considered the driving moment by the soil weight, loads around the centre of the slip circle, and the water pressures. Meanwhile, the resisting moments come from the shear stresses and normal effective stresses that act along the slip circle in which the shear stresses prevent the circular bishop model slipping. Another resisting moment could be from the geotextile as an external part that acts in the slope. Furthermore, the equilibrium state is determined based on the summation of all slices' influence. Therefore, the sum of these driving moments must be equalised by the resisting moments to keep the slope safe, while the ratio of the resisting moments and the driving moments is the output of the analysis (safety factor). The evaluation of equilibrium for a slice includes the forces and also the pressures as presented in figure 7.

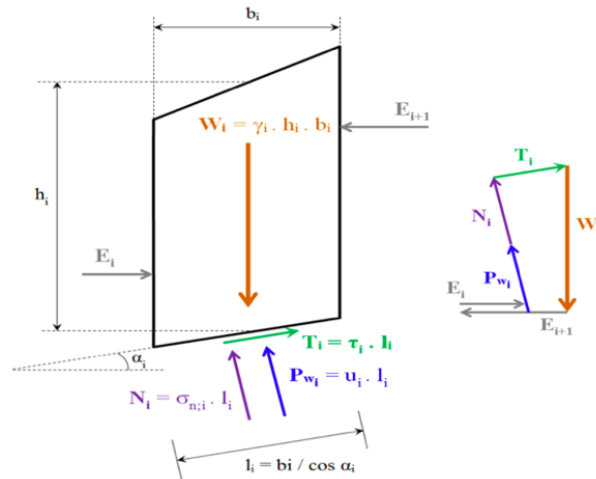


Figure 7. Force equilibrium for one slice in the method of slice (Deltares, 2016)

Where:

W_i : Weight of slice i [kN/m]

T_i : Shear force along of slice i [kN/m]

E_i : Interaction force of slice i with the slice at the left side [kN/m]

E_{i+1} : Interaction force of slice i with the slice at the right side [kN/m]

P_{w_i} : Water force acting on the base of slice i [kN/m]

N_i : The (total) normal reaction of the soil acting on the base of slice i [kN/m]

2.5 Finite Element Method – PLAXIS Software

Finite Element Method has several basic concepts that make this method surpass the Limit Equilibrium Method. First, the Finite Element Method divides the domain of problem into a couple of subdomains, with element equations express each subdomain to the original problem. Furthermore, this is followed by systematically recombining all these element equations into the global system equation for the final calculation. These concepts are adopted by PLAXIS to analyse the geotechnical problem by meshing the geometry of the case from global into local points.

This thesis focuses on seismic analysis on total deformation of slope and the optimisation of geotextile application. The soil profiles in the Yuriage area are mostly dominated by sandy soil that means the possibility of liquefaction occurs during the earthquake is high. Thus, the pore water pressure generation should be considered in the analysis, especially during the dynamic time.

The consequences of liquefaction also depend on the site conditions, seismic loading characteristics, and nature of the structures on the site. Moreover, Idriss and Boulanger (2008) defined three of the most important consequences of liquefaction as follows:

- Loss of shear strength leading to instability of slopes or embankments

- Lateral spreading of mildly sloping ground.
- Settlement caused by reconsolidation of the liquefied soils.

Furthermore, PLAXIS has some constitutive models that can be selected based on the problems and output that want to obtain. The choice of constitutive model is one of the key aspects in advanced numerical modelling because many of the models only work well for specific material types or load paths. Basically, constitutive model works to relate the increment of stress to the increment of strains. However, the more advanced model may include the dilative and contractive behaviour and also can address the elastic and plastic response of the material.

This project considers two types of analysis on the construction of newly-elevated area in Yuriage. Firstly, the stages constructions that only consider the construction of embankment and the uniform load from the traffic above the area. Therefore, these analyses are defined as the static analysis. Secondly, the analysis after all the stages constructions are completed then the earthquake load applied at the base of the bedrock; this analysis is considered as the dynamic analysis. Thus, the constitutive model used for each analysis should be different.

2.5.1 Static Analysis

The first model is the linear elastic model for the bedrock layer (AG3) that consists of gravels. This model was used on both analyses, static and dynamic analysis. Linear elastic model is the simple model that relates the stress increments to the strain increments according to Hooke's law. Moreover, the bedrock behaviour was simulated based on this linear elastic model because the material is much stronger and stiffer than the rest of layer and also this bedrock layers is not expected to experience plastic straining. The required parameters to describe this material behaviour is only the stiffness in term of Young's modulus (E) and Poisson's ratio (ν). meanwhile, the other stiffness parameters are computed based on the elasticity theory.

AC2 layer is another layer that use the same model for both static and dynamic analysis. This layer has much similarities with the first later AC1 but has been deposited for long time. AC2 layer has small possibility to be liquified because this layer is the cohesive layer and also it has been deposited for long time that make the stiffness is even greater. The Hardening Soil Small strain (HS Small) model was selected to analyse the behaviour of this soil, which is an elastoplastic type of hyperbolic model. This model describes the soil stiffness much accurate compared to the linear elastic model and even better than the Hardening Soil model since the increasing of stiffness at small strain is also considered.

During the static analysis, all layers (except AG3) were modelled with the same HS Small model with the parameters are presented in table 3. The Hardening Soil Small model has several main characteristics as listed below:

- Stress-dependent stiffness behaviour according to a power law
- Hyperbolic stress-strain relationship in axial compression

- Plastic strain by mobilising friction (shear hardening)
- Plastic strain by primary compression (compaction hardening)
- Elastic unloading/reloading
- Failure behaviour according to Mohr-Coulomb criterion
- Small strain stiffness

Table 3. Hardening Soil Small strain model parameters

c	(Effective) cohesion
φ	(Effective) angle of internal friction
ψ	Angle of dilatancy
$E50-ref$	Secant stiffness in standard drained triaxial test
$Eoed-ref$	Tangent stiffness for primary oedometer loading
$Eur-ref$	Unloading / reloading stiffness (default $Eur-ref = 3 E50-ref$)
m	Power for stress-level dependency of stiffness
$\gamma_{0.7}$	Shear strain at which $G_s = 0.722 G_0$
$G_0 ref$	Reference shear modulus at very small strains
ν_{ur}	Poisson's ratio for unloading-reloading (default $\nu_{ur} = 0.2$)
$p-ref$	Reference stress for stiffnesses (default $p-ref = 100 \text{ kN/m}^2$)
K_0-nc	K_0 -value for normal consolidation (default $K_{nc} = 1 - \sin\varphi$)
R_f	Failure ratio

Hardening Soil small model is the more advanced model compared to the elastic perfectly-plastic model because the yield surface of hardening plasticity model is not fixed, but it can expand due to plastic straining. Moreover, the yield contour in principal stress and also the cap is presented in figure 8.

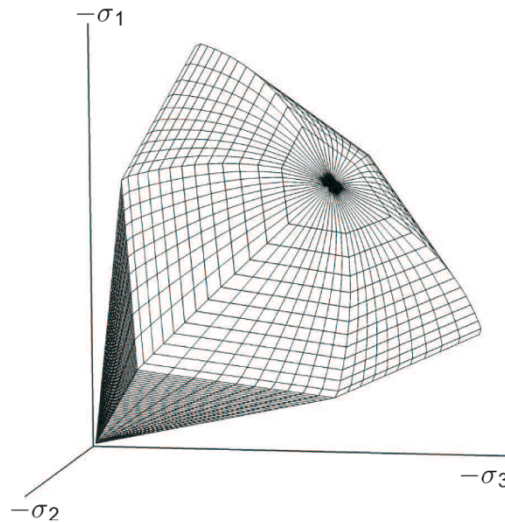


Figure 8. Representative of yield contour in principal stress space for cohesionless soil (Brinkgreve et al., 2018)

Furthermore, the quasi-elastic tangent shear modulus is determined by integrating the secant stiffness modulus reduction curve over the actual shear strain increment. The reduction of stiffness that used in the model is presented in the figure 9.

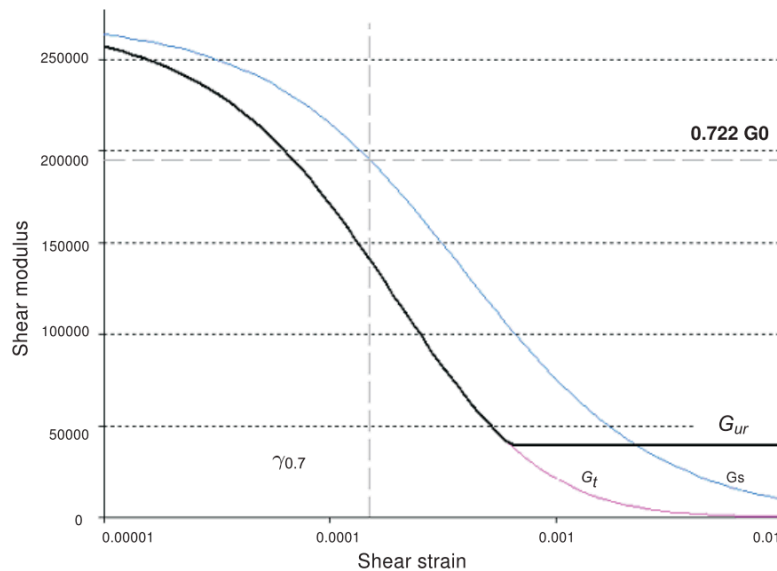


Figure 9. Secant and tangent shear modulus reduction curve (Brinkgreve et al., 2018)

Given all the advantages of this model, HS small is not suitable for the dynamic analysis with some limitations, especially for earthquake load in the liquefiable soil. HS small model does not incorporate a gradual softening during cyclic loading that means this model is not suitable for problems with softening roles. Moreover, softening due to dilatancy and debonding effects are not considered. More importantly, this model does not cover the irreversible volumetric straining nor liquefaction behaviour. Meanwhile, the liquefaction is one of the crucial parts that need to be identified in this project.

2.5.2 Dynamic Analysis

Beside the fact that constitutive has strength and weakness, especially for the complex analysis that need advanced model, Beaty & Perlea (2011) proposed some features that might be considered when selecting and using the constitutive model for an advanced analysis.

- The formulation of the constitutive model should adequately address the key feature of the anticipated soil behaviour. These may include the relationship between shear stiffness and strain, stress level dependence, generation of pore pressure, and strain softening.
- It should have sound theoretical basis.
- It should reasonably model the stress-strain and pore pressure generation in both monotonic and cyclic laboratory test. Moreover, direct comparison between the numerical simulations and laboratory test data should be available.
- It should reasonably capture the behaviour describe by the empirical relationships for liquefaction triggering and post-liquefaction behaviour.
- The selection of input parameters should be reasonably transparent, particularly in cases where direct calibration to laboratory data is not possible.
- Successful use of model should be documented through back-analysis of case history.

Given the requirements of the constitutive model as explain above and the specific problems for this project such as earthquake loads and the presence of liquefiable layer, a proper selection among the available models have to be more selective. Finally, the UBCSAND model seems the most suitable constitutive model for this case with several main characteristics listed below.

- Plastic strain by mobilising friction, similarities with shear hardening in Hardening Soil model
- Different flow rule, allowing for static liquefaction
- Accumulation of plastic strains upon cyclic loading
- Accumulation of pore pressure in undrained cyclic loading
- Liquefaction behaviour

This model was developed by Puebla, Byrne, & Phillips (1997) to create liquefaction response, while Beaty and Byrne (1998) adapted this model for seismic evaluation and applied to the response analysis. This model is the advanced model for the seismic analysis with liquefiable soil layer yet relatively easy to use with some required parameters are needed from the laboratory and in situ test. UBCSAND is an effective stress model based on the classic plasticity theory.

The elastic behaviour is assumed to be isotropic that specified by a bulk modulus, K_B^e , and a shear modulus, K_G^e , that can be calculated using these following formulas.

$$K_B^e = k_B^e \times P_A \times \left(\frac{P'}{P_A} \right)^{me} \quad (2)$$

$$K_G^e = k_G^e \times P_A \times \left(\frac{P'}{P_A} \right)^{ne} \quad (3)$$

Where P' is mean effective stress, P_A is the reference stress defined as the atmospheric pressure (100 kPa), k_B^e and k_G^e are the bulk and shear modulus numbers respectively, and me and ne are the elastic bulk and shear modulus index that has the same default value at 0.5.

The critical yield surface is based on the Mohr-Coulomb yield function (f_m) as given in equation (4) and represented by the radial line from the origin in stress space as shown in figure 10.

$$f_m = \frac{\sigma'_{max} - \sigma'_{min}}{2} - \left(\frac{\sigma'_{max} - \sigma'_{min}}{2} + c' \cot \varphi'_p \right) \sin \varphi_{mob} \quad (4)$$

Where σ'_{max} and σ'_{min} are the maximum and minimum principal stresses, c' is the effective cohesion, and φ'_p and φ_{mob} are the peak and mobilised friction angle respectively.

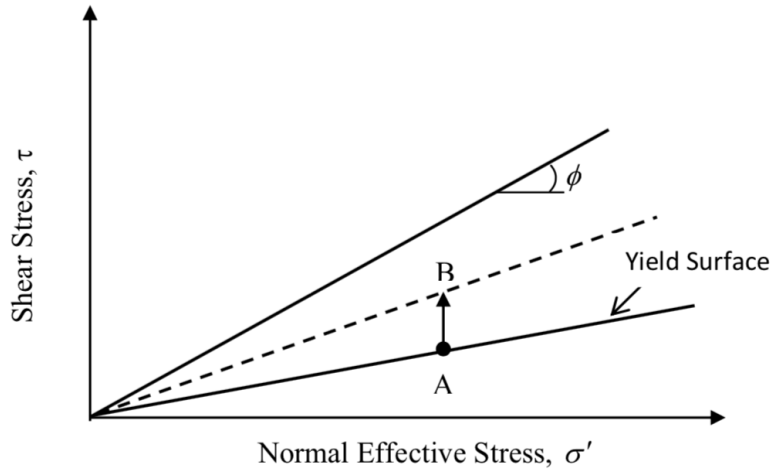


Figure 10. Yield surface in UBCSAND (Beatty and Byrne, 1998)

The yield surface and flow rule control the plastic strain, which once the yield surface is reached and the loading continues, this results in plastic strains, both shear and volumetric. The plastic hardening is described by the hyperbolic hardening rule (Beatty and Byrne, 1998) as shown in figure 11. The hardening rule relates the plastic shear strain increment ($\delta\gamma^p$) and the stress ratio increment ($d\eta$) as shown in formula (5).

$$\delta\gamma^p = \frac{1}{G^p/\sigma'} \cdot d\eta \quad (5)$$

Where G^p is the plastic shear modulus, σ' is the effective stress, and assuming a hyperbolic relationship between η and γ^p :

$$G^p = G_i^p \cdot \left(1 - \frac{\eta}{\eta_f} \cdot R_f\right)^2 \quad (6)$$

Where, G_i^p is the plastic shear modulus at a low level of stress ratio, η_f is the stress ratio at failure (equal to $\sin \varphi_p$), φ_p is the peak friction angle, and R_f is the failure ratio that varies between 0.7-0.98 and decreases with increasing relative density.

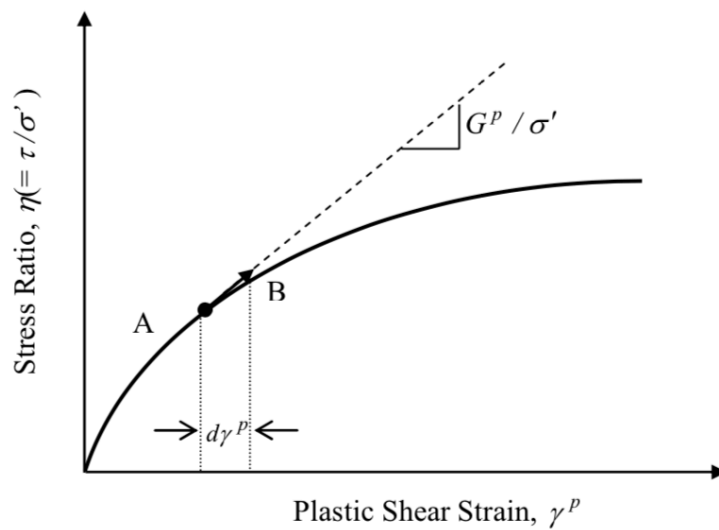


Figure 11. Hyperbolic hardening rule in UBCSAND (Beatty and Byrne, 1998)

The plastic potential function (g) is based on the Drucker Prager that formulated as:

$$g = q - \frac{6 \sin \psi_m}{3 - \sin \psi_m} (p + \cot \varphi_p) \quad (7)$$

Where q is the equivalent shear stress, p is the mean effective stress, ψ_m is the mobilised dilatancy angle, and φ_p is the peak friction angle. Furthermore, the plastic volumetric strain ($d\varepsilon_v^p$) is defined by the flow rule with this following formula.

$$d\varepsilon_v^p = \sin \psi_m \times \delta\gamma^p \quad (8)$$

$$\sin \psi_m = \sin \varphi_m - \sin \varphi_p \quad (9)$$

Where ψ_m is the mobilised dilatancy angle, $\delta\gamma^p$ is the plastic shear strain, φ_m is the mobilised friction angle, and φ_p is the peak friction angle. Moreover, yield loci and the corresponding direction of the plastic strains that resulted the flow rule is shown in figure 12. Shear induces plastic expansion or dilation when the stress ratios greater than the constant volume friction angle φ_{cv} .

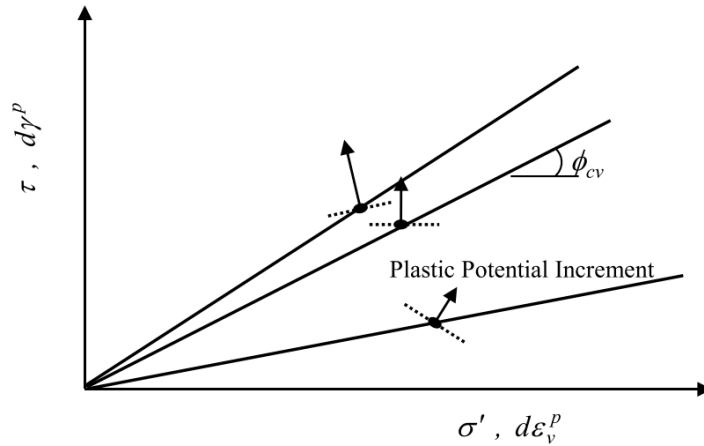


Figure 12. Direction of plastic strains associated with location of yield surface (Beaty and Byrne, 1998)

The first-time loading is defined when the current load increment pushes the yield surface outside the previous maximum stress ratio limit. Furthermore, when the increment of loading occurs less than previous stress ratio, the sand is assumed to behave plastically with stiffer plastic modulus than the first-time loading. However, not all loading generates plastic strains; elastic strain is assumed when the reloading occurs with the stress ratio is less than or equal to the previous value. During this reloading, no plastic shear and volumetric strains accumulated. Furthermore, once the previous stress ratio is reached, the plastic strain will be recurred. This loading, unloading, and reloading is presented in the figure 13. The input of parameters for the UBCSAND are summarized in table 4.

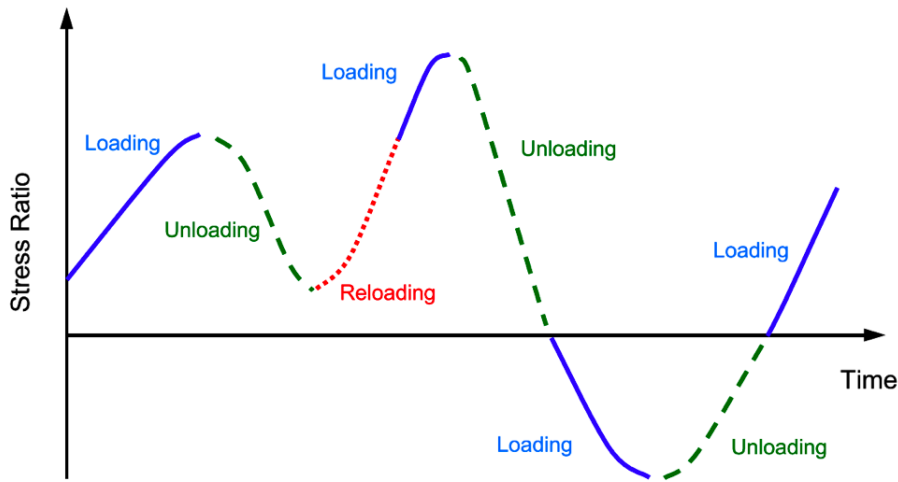


Figure 13. Stress ratio history showing loading, unloading, and reloading (Beaty and Byrne, 1998)

Table 4. Input parameter of UBCSAND

ϕ_{cv}	Friction angle at constant volume
ϕ_p	Peak friction angle
c	Effective cohesion
K_G^e	Elastic shear modulus number
K_G^p	Plastic shear modulus number
K_B^e	Elastic bulk modulus number
m_e	Elastic bulk modulus exponent
n_e	Elastic shear modulus exponent
n_p	Plastic shear modulus exponent
R_f	Failure ratio
P_a	Reference stress which is equal to the atmospheric pressure
fac_{hard}	Densification factor
$(N1)_{60}$	Corrected N-SPT value
fac_{post}	Factor that determines the minimum value of the shear modulus during stiffness degradation

2.6 Rayleigh Damping

Material damping is caused by viscous properties of soil, friction, and the development of irreversible strains during the dynamic calculations. One of the simple methods to determine material damping is using Rayleigh damping, which is a numerical feature in a damping matrix C as shown in formula below.

$$C = \alpha M + \beta K \quad (10)$$

Where the M is mass matrix, K is stiffness matrix, and α and β are the Rayleigh coefficients that calculated based on the input of target damping ratio and two target frequencies. From the equation above, the higher α , the more the lower frequencies are damped; and the higher β , the more the higher frequencies are damped.

Damping ratio (ξ) is the common parameter used to determine the damping parameter identification, which for the critical damping is chosen equal to 1 percent. Furthermore, Hudson,

Idriss & Bairkhae (1994) and Hashash & Park (2002) suggested to select the first target frequency as the first natural frequency of the soil deposit (f_1) that can be calculated using equation (11), while the second target frequency is the closest odd integer larger than the ratio f_p/f_1 . The f_p is the predominant frequency of the input motion, which can be determined from the input Fourier spectrum.

$$f_1 = \frac{v_s}{4H} \quad (11)$$

Where v_s is the shear wave velocity in m/s that is the function of shear modulus G [kN/m^2], and H is the thickness of soil deposit in m.

2.7 Summary and Conclusion

Many studies have been conducted across the world related to the slope stability, various methods were also used to analyse the behaviour and the safety of slope under static or dynamic load and combination of them. However, not all slopes can withstand the loads without any improvement on the slope and its surrounding area. One of the slopes strengthening methods is by reinforcing slope using geotextile. This method provides tensile strength by the friction of soil and the geotextile that increases the strength of slope under loading, which in this case resistance of slope to dynamic loading. Moreover, other advantages of geotextile are also given as explained in [chapter 2.2](#).

The use of Limit Equilibrium Method (LEM) is a conventional method for engineers and researcher, even though this method may be considered as conservative, yet it is very established. This method can provide an estimate safety factor without requiring initial condition, which becomes the reason for this method being really favored by engineers. On the other hand, the safety factor cannot define expected deformation during the earthquake loading, in which deformation provides a better indicator of slope performance. The appearance of many softwares to analyse the problem with this method, like D-GEO Stability, facilitates the engineers to do faster calculation and analysis. The output from such software could be used as the hypothesis and as result control for another method. Nowadays, the use of Finite Element Method (FEM) provides the expected deformations output, which gives the better understanding of the slope performance, especially during the earthquake loading. However, the selection of constitutive model has to be more selective since the choice of constitutive model is one of the key aspects in advanced numerical modelling because many of the models only work well for specific material types or load paths.

Finally, after reviewing the literature above, considering the fact from the field, and an interview with related party in Japan, the final thesis focuses on the slope stability analysis and optimization of application in regards to the strength, length, and the number of layers based on the case of a newly-elevated area in Yuriage, Japan. The analysis will be based on the Finite Element Method with the help of PLAXIS software.

3 Project Overview: Yuriage Case

The project is located in Natori City (about 10 Km from Sendai City) as shown in the map of figure 14. The area of this project is around 0.56 Km² (1.2 Km length and 0.46 Km wide) in which the plan of the raised area is presented in figure 15. Furthermore, some criteria were determined to select the critical cross-section within the area of this newly elevated area. The first criteria is the distance of uniform loads (structure and traffic above the embankment) to the slope crest. The second one is the location of cross section that face the sea, which will be hit first when the tsunami occurs, hence it should be strong enough to withstand the prior earthquake.



Figure 14. Project location in Yuriage (www.google.com/maps)

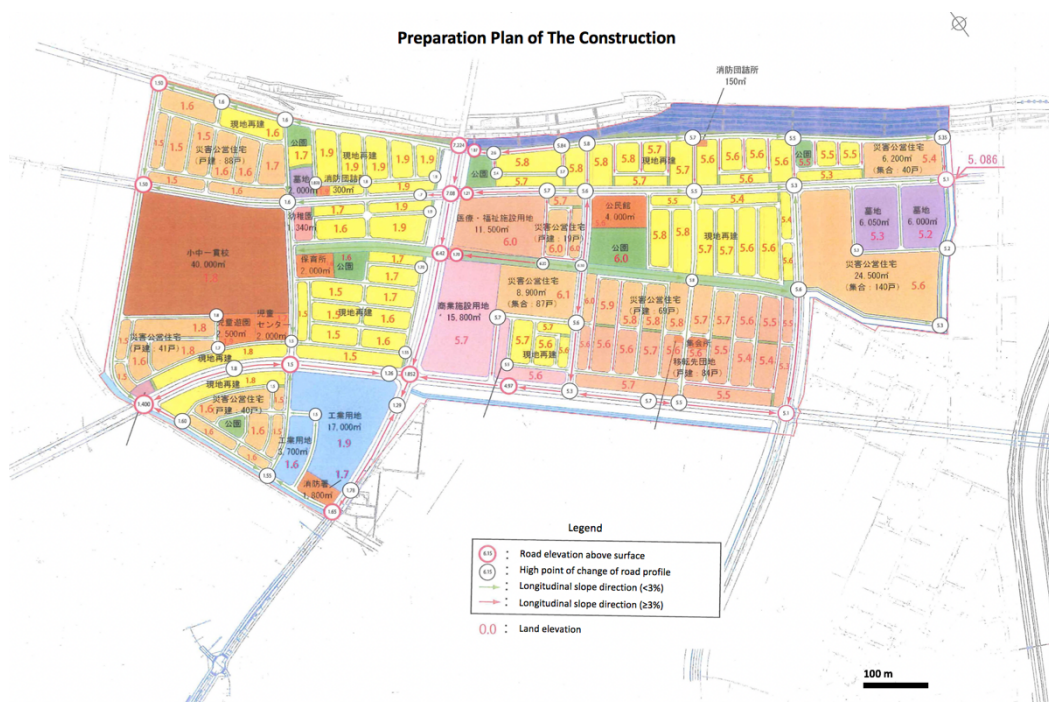


Figure 15. Project plan area

Based on the criteria above, a critical cross-section was chosen at the nearest part of the shoreline as given in figure 16. Moreover, the critical cross-section of this location is presented in figure 17 with slope angle 29 degrees and 4.35 m height. More importantly, the uniform load is lining until the slope crest that might affect the stability of slope. therefore, the structure above could be affected by the instability of slope.

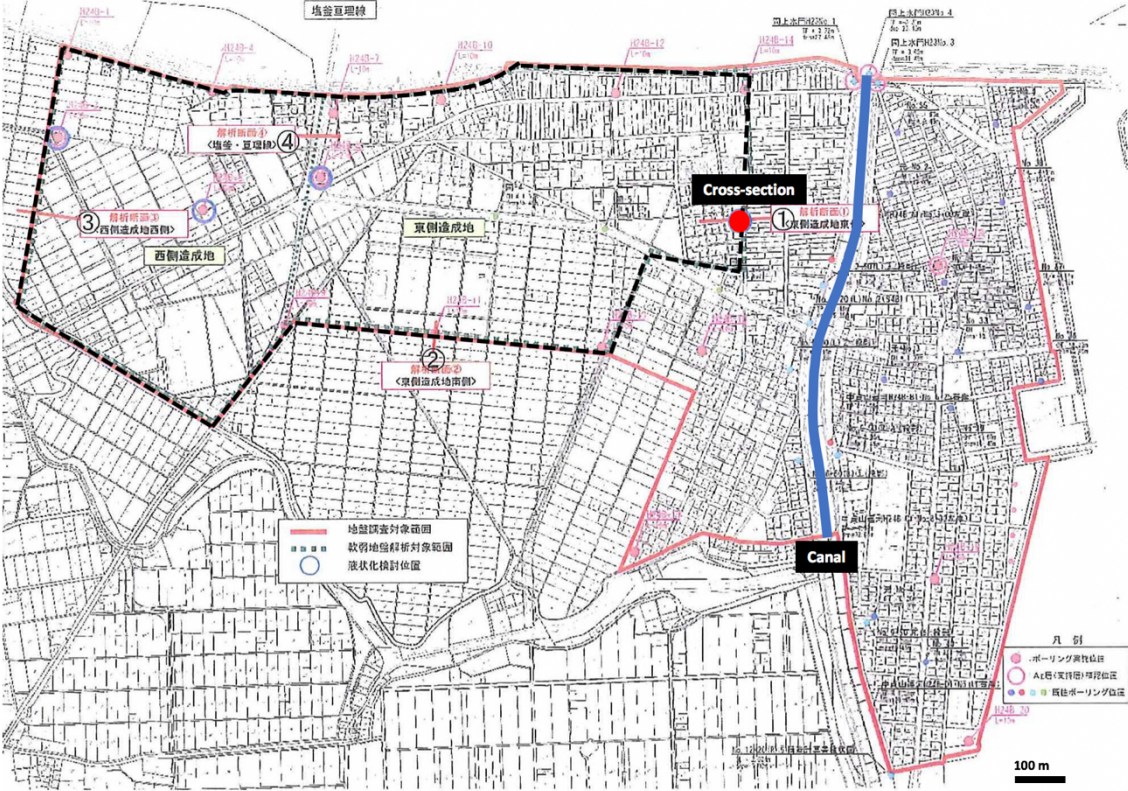


Figure 16. Cross-section location

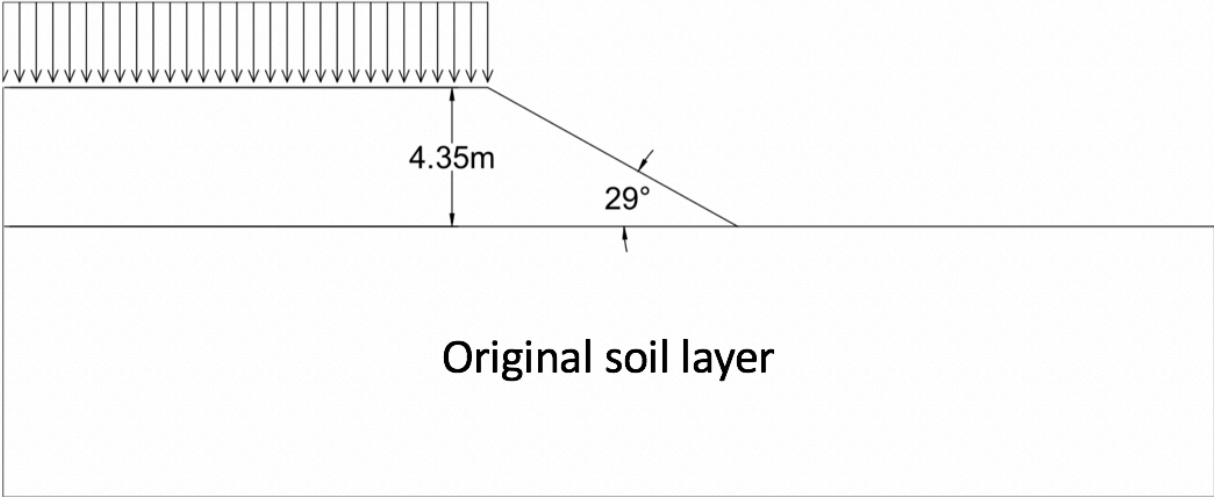


Figure 17. Cross-section of location

3.1 Project Requirements

The requirement was defined differently for static and dynamic analysis. The static analysis is based on the safety factor output, while the dynamic analysis is based on the total displacement at the crest of slope. Both requirements are determined from the Yuriage basic plan documents which are included in the appendix D, appendix E, and appendix F.

Furthermore, all analyses were based on the Serviceability Limit State (SLS) because no design factor was considered. First, the initial data such as the loads has no explanation whether it has considered the design factor. hence, it is assumed that the loads do not consider the design factor. Second, the value of N-SPT was based on the average value without any further consideration of design factor. Third, the parameters correlations were also neglected the design factor.

Furthermore, the requirement was defined for the static analysis, which was based on the safety factor. The minimum safety factor was selected at 1.5, this is based on the requirement of the project (Yuriage basic design, 2014), included under appendix D.

Moreover, the requirement for dynamic analysis is included in table 1 ([chapter 2.1](#) on about the damage of ground embankment). Given the fact that the analysis was based on the SLS, the partial failure should be considered as the worst-case scenario for this analysis. Therefore, the damage level II is selected as the category of partial failure that has the maximum total displacement up to 0.5m or about 10% from the average height of the raised area. However, the height of slope in the cross section is about 4.35m, less than the average height of raised area (around 5m). Thus, the requirement for the total displacement was adjusted to 10% of the slope height (around 0.435m / 43.5cm).

4 Data of Project

Waltham (2009) defined three stages of ground investigation to obtain the data for the project as per below:

1. Initial stage, covering the desk study of available data, walkover survey & visual assessment, and preliminary report and fieldwork plan.
2. Main stage, initiated by the fieldwork (geological mapping or geophysical survey if necessary, trial pit, borehole including SPT, and CPT). After one or more parts have been done, the laboratory testing might be necessary to get more detailed data (usually soils), and end by the final report.
3. Review stage, covering the monitoring during excavation or construction.

The requirement of complete data of the project will help to accelerate the engineering preparation. Moreover, this complete data increases the chance of a project to meet the construction requirements. The complete data can predict the cost of the project more accurately. Furthermore, this project has some data of Standard Penetration Test (SPT) at several locations within the project area and also laboratory test for some layers.

4.1 Soil Investigation and Layer Schematization

Natori City prefecture provided some data of the project, such as the Standard Penetration Test (SPT) data, the data of the embankment (unit weight and internal friction angle), and also some lab test results for some layers. First, SPT was done at 18 locations in the Yuriage area. However, only 14 locations of SPT are within the area of newly-elevated area as shown in figure 18. Second, some laboratory tests were also completed but only the first layer (AC1) has detailed data while layer AS21, layer AS22, and layer AS3 have limited data from sieving test.

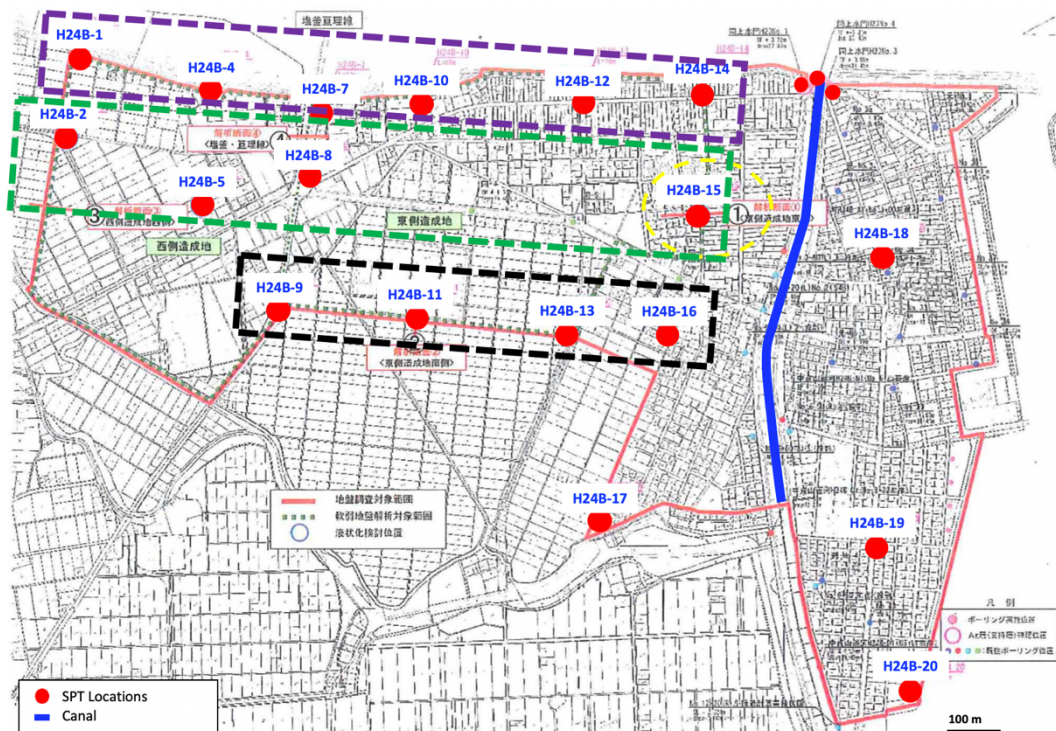


Figure 18. Locations of Standard Penetration test

Based on the SPT data, it was concluded that there are six different layers of soil below the newly elevated area that summarized in table 5. The results of N-SPT are the average value from the 14 locations. Meanwhile, the original data of this SPT is presented in the Appendix A. Moreover, the result of laboratory test from four layers of soil is presented in table 6. The data of SPT and laboratory test show that the AC1 layer is the soft soil layer, which can be concluded that the newly elevated area of Yuriage is built on top of soft soil layer. Therefore, there are two possibilities of failure type either the deep-seated circular surface or shallow translational surface.

Table 5. SPT result from field test in Yuriage

Layer	Thickness [m]	Name	Type	N-SPT range	N-SPT average
0	4.35	B1/embankment	Fine-medium Sand	8-9	8.50
1	2.10	AC1	Silty Clayey Sand	0-6	1.89
2	3.90	AS21	Fine Sand	1-24	11.85
3	1.70	AS22	Medium-coarse Sand	15-50	36.29
4	13.4	AS3	Medium-coarse Sand	12-49	26.99
5	1.60	AC2	Silty Clayey Sand	5-22	13.00
6	5.30	AG3	Gravel	31-50	50.95

Table 6. Laboratory data for four layers

Sample location number		H25-B15				
Sample Number		T15-1	P15-2	P15-6	P15-10	
Soil symbol		Ac1	AS21	AS22	AS3	
Sampling top (below GL)		1			m	
Sampling bottom (below GL)		1.78			m	
sampling center (below GL)		1.39			m	
Parameter	Symbol	Value				Unit
Wet density	pt	1.741	-	-	-	g/cm ³
Dry density	pd	1.2	-	-	-	g/cm ³
Solid density	ps	2.597	-	-	-	g/cm ³
Moisture content	Wn	45.02	-	-	-	%
Void ratio	e	1.164	-	-	-	
Degree of saturation	Sr	100	-	-	-	%
Stone (<75mm)	-	0	0	0	0	%
Gravel (2mm - 75mm)	-	0.3	0	1.3	2.3	%
Sand (0.075mm - 2mm)	-	49.3	90.6	90.1	87.9	%
Silt (0.005mm-0.075mm)	-	26.6	9.4	8.6	9.8	%
Clay (<0.005mm)	-	23.8				%
Maximum diameter	Dmax	4.75	4.75	9.5	9.5	mm
Uniformity coefficient	Cu	-	2.92	6.01	6.07	
60% particle size D60		0.1369	0.240	0.600	0.472	mm
50% particle size D50	-	0.073	0.21	0.507	0.392	mm
30% particle size D30		0.011	0.162	0.3472	0.2527	mm
20% particle size D20	-	0.0031	0.1381	0.2634	0.184	mm
10% particle size D10	-	-	0.0821	0.0998	0.0778	mm
Liquid Limit	LL	40.6	-	-	-	%
Plastic Limit	PL	23.2	-	-	-	%
Plasticity Index	PI	17.4	-	-	-	%
Liquid index	LI	1.25	-	-	-	%
Consistency Index	CI	-0.25	-	-	-	%
Classified symbol of soil	-	CLS	S-F	S-F	S-F	-
Unconfined compressive clay	qu	29.3				kN/m ²
Secant Stiffness in standard drained Triaxial test	E50	1202				kN/m ²
Compression Index	Cc	0.392				-
Precompression stress	Pc	55.44				kN/m ²

Furthermore, based on the location of cross section and the data of SPT at the location, the geometry of slope and soil underneath are portrayed in figure 19 where the phreatic line is the blue line in the depth of -1.3m.

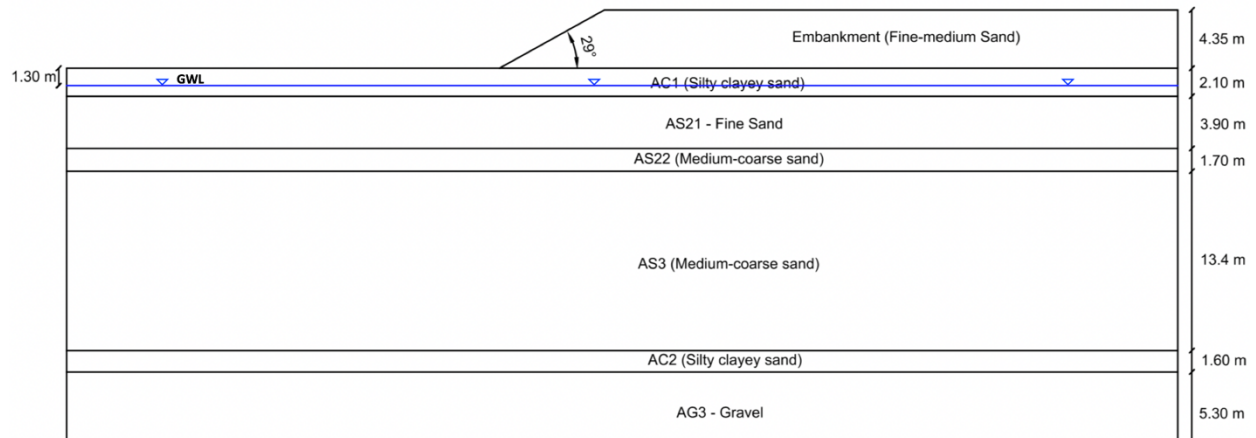


Figure 19. Geometry of slope and soil layers

Two types of load were considered, for which these might affect the stability of the slope. However, there is no explanation from the project documents on whether the loads have already considered the design factor. Thus, the assumption made that the load has no design factor consideration which leads to conclusion that the analysis is based on the Serviceability limit State. Moreover, the two loads are explained below:

1. Uniform load: come from the building and traffic above the embankment, which counts for about 10.8 kN/m².
2. Earthquake load: this is based on the Japan 2011 earthquake from the nearest seismometer location (MYG013 and MYG015).

4.2 Parameter Correlations

Given the existing data of this project is limited to the SPT data. In order to calculate other parameters, parameter correlations should be taken. Moreover, the input parameters of UBCSAND have to be defined prior to the Finite Element Method analysis using PLAXIS software. All the required parameters for this constitutive model are listed in [chapter 2.5](#), while all the input parameters are presented at the end of this chapter.

Firstly, based on the average N-SPT data, the N-value has to be corrected to 60% energy level (N_{60}) for the design value using this formula.

$$N_{60} = N \frac{ER_i}{60} \quad (12)$$

ER_i is the energy ratio in percentage and N is the blow amount value from SPT test at field. Seed et al. (1985) and Skempton (1986) defined the 60% energy represents a historical average for different SPT system to get the empirical value. The SPT energy ratios is showed in table 7. However, the average value of 1.2 is selected for the $ER_i/60$ due to the semi-automatic SPT equipment was used for the test.

Table 7. Generalized SPT energy ratios (Robertson, 1992)

Location	Hammer	Release	ER _i (%)	ER _i /60
North and South America	Donut	2 turns of rope	45	0.75
	Safety	2 turns of rope	55	0.92
	Automatic	Trip	55-83	0.92-1.38
Japan	Donut	2 turns of rope	65	1.08
	Donut	Auto-trigger	78	1.30
China	Donut	2 turns of rope	50	0.83
	Automatic	Trip	60	1.00
United Kingdom	Safety	2 turns of rope	50	0.83
	Automatic	Trip	60	1.00
Italy	Donut	Trip	65	1.08

The first parameter to determine is the Relative Density. This parameter will be used as the input to calculate the unit weight. The correlation of corrected blow count to the Relative density value has been defined by as shown in figure 20.

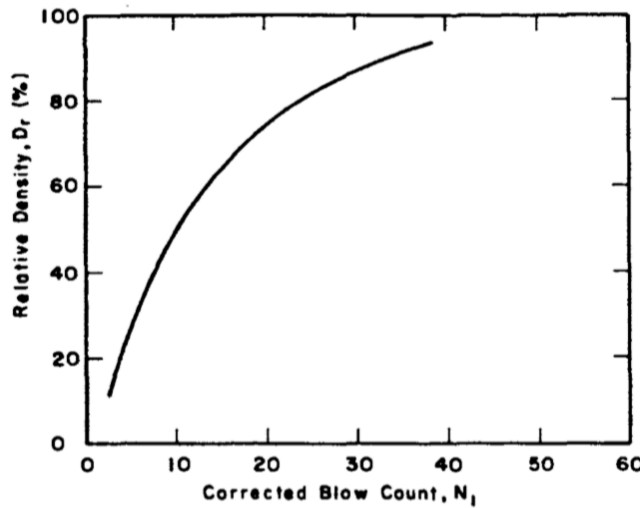


Figure 20. Relationship between corrected blow count to the relative density (Gibbs & Holtz, 1957)

Furthermore, the unit weight, dry (γ_{dry}) and saturated (γ_{sat}), can be calculated directly with these formulas by Brinkgreve & Engin (2010).

$$\gamma_{dry} = 15 + 4.0 RD/100 \quad [\text{kN/m}^3] \quad (13)$$

$$\gamma_{sat} = 19 + 1.6 RD/100 \quad [\text{kN/m}^3] \quad (14)$$

Where RD is the relative density of soil in percentage. Moreover, the initial void ratio (e_{init}) can be driven from the formula by Anbazhagan et al. (2017) based on the value of N_{60} -SPT with 60% energy correction as written below.

$$e_{init} = 1.202N_{60}^{-0.217} \quad (15)$$

Internal friction angles, constant volume and peak, can be calculated from two different formulas. The internal friction angle at constant volume (ϕ_{cv}) was defined by Peck et al. (1974) in equation 16 while the peak internal friction angle (ϕ_p) is determined by Beaty and Byrne (2011) in equation 17. Both parameters were determined based on then-SPT value at 60% energy correction (N_{60}) from SPT.

$$\varphi_{cv} = 54^\circ - 27.6034 \exp(-0.014 \times N_{60}) \quad [\text{degrees}] \quad (16)$$

$$\varphi_p = \varphi_{cv} + \frac{N_{60}}{10} + \max\left(0; \frac{N_{60} - 15}{5}\right) \quad [\text{degrees}] \quad (17)$$

The cohesive soil is only found at layer AC1 and layer AC2. Layer AC1 has the data from laboratory test in which the value of cohesion was calculated directly by the half of the unconfined compressive clay (q_u) value. Moreover, the value for AC2 layer was defined at the same value with AC1.

Beatty and Byrne (2011) also proposed some equations based on the value of N_{60} in order to define parameters for the analysis using UBCSAND model. All equations are presented below, such as elastic shear modulus K_G^e (equation 18), elastic bulk modulus K_B^e (equation 19), plastic shear modulus K_G^p (equation 20), and failure ratio R_f (equation 21).

$$K_G^e = 21.7 \times 20 \times N_{60}^{0.3333} \quad (18)$$

$$K_B^e = 0.7 K_G^e \quad (19)$$

$$K_G^p = K_G^e \times N_{60}^2 \times 0.003 + 100 \quad (20)$$

$$R_f = 1.1 \times N_{60}^{-0.15} \quad (21)$$

Furthermore, modulus exponent for elastic, plastic, and bulk modulus were set as default 0.5, 0.4, and 0.5 respectively. The values of densification factor fac_{hard} and fac_{post} were set at 1.0 for both.

The input parameters for the interface and material are the same. Moreover, the dilatancy angle (ψ) is defined based on the formula from Bolton (1986) for plane strain case as shown in equation 22 based on the value of peak friction angle (φ_p) and constant volume friction angle (φ_{cv}). The rate of stress dependency of the interface stiffness is set as default value at 0.5.

$$\varphi_p - \varphi_{cv} = 0.8 \psi \quad [\text{degrees}] \quad (22)$$

Finally, all the input parameters for analysis using UBCSAND, for the dynamic analysis, is summarized in table 8.

Table 8. UBCSAND model parameter for dynamic analysis

Symbol	Parameter	Value					Units
		B1	AC1	AS21	AS22	AS3	
Dr	relative density	50.85	10.44	62.73	96.21	89.59	%
γ_{dry}	Dry unit weight	19.00	12.24	17.51	18.85	18.58	kN/m3
γ_{sat}	Saturated unit weight	19.00	17.75	20.00	20.54	20.43	kN/m3
einit	initial void ratio	0.726	1.164	0.676	0.53	0.565	-
ϕ_{cv}	Friction angle at constant volume	30	27.26	31.38	39	36.46	Degrees
ϕ_p	Peak friction angle	30.00	27.26	32.80	45.00	43.18	Degrees
c	Effective cohesion	10	15	0	0	0	kPa
K_G^e	Elastic shear modulus number	940	570	1050	1525	1382	-
K_G^p	Plastic shear modulus number	394	109	737	8778	4447	-
K_B^e	Elastic bulk modulus number	658	399	735	1068	967	-
me	Elastic bulk modulus exponent	0.5	0.5	0.5	0.5	0.5	-
ne	Elastic shear modulus exponent	0.5	0.5	0.5	0.5	0.5	-
np	Plastic shear modulus exponent	0.4	0.4	0.4	0.4	0.4	-
Rf	Failure ratio	0.78	0.97	0.74	0.62	0.65	-
Pa	Reference stress which is equal to the atmospheric pressure	100	100	100	100	100	kPa
σ_t	Tension cut-off	0	0	0	0	0	
fac hard	Densification factor	1	1	1	1	1	-
(N1)60	Corrected N-SPT value	10.20	2.27	14.22	43.55	32.38	Times
fac post	Factor that determines the minimum value of the shear modulus during stiffness degradation	1	1	1	1	1	-

On the other hand, Hardening Soil Small strain model was used during the staged construction for static analysis. Therefore, all layer but the Gravel required the parameter of HS small model that summarized in table 9 with the value of Poisson's ratio (ν) was taken the same at 0.2.

Table 9. HS small model parameter input for the static analysis

Symbol	Parameter	Value						UNITS
		B1	AC1	AS21	AS22	AS3	AC2	
c	(Effective) cohesion	0	15	0	0	0	15	kN/m2
ϕ	(Effective) angle of internal friction	30	27.26	31.38	39	36.46	31.81	degrees
ψ	Angle of dilatancy	0	0	1.78	10	8.39	2.1	degrees
σ_t	Tension cut-off and tensile strength	0	0	0	0	0	0	kN/m2
E_{50-ref}	Secant stiffness in standard drained triaxial test	30,510	1,202	37,638	57,726	53,754	43,248	kN/m2
$E_{oed-ref}$	Tangent stiffness for primary oedometer loading	30,510	1,202	37,638	57,726	53,754	43,248	kN/m2
E_{ur-ref}	Unloading / reloading stiffness (default $E_{ur-ref} = 3 E_{50-ref}$)	91,530	3,606	112,914	173,178	161,262	129,744	kN/m2
m	Power for stress-level dependency of stiffness	0.54	0.67	0.50	0.40	0.42	0.47	-
$\gamma_{0.7}$	Shear strain at which $G_s = 0.722 G_0$	1.5E-04	1.9E-04	1.4E-04	1.0E-04	1.1E-04	1.3E-04	
G0 ref	reference shear modulus at very small strains	94578	67099	102656	125423	120921	109014	kN/m2

However, some parameters in table 9 have to be calculated based on the value of relative density (RD) as shown in these equations (R. Brinkgreve & Engin, 2010)

$$E_{50}^{ref} = 60000 \cdot RD/100 \quad [\text{kN/m}^2] \quad (23)$$

$$E_{oed}^{ref} = 60000 \cdot RD/100 \quad [\text{kN/m}^2] \quad (24)$$

$$E_{ur}^{ref} = 180000 \cdot RD/100 \quad [\text{kN/m}^2] \quad (25)$$

$$G_0^{ref} = 60000 + 68000 \cdot RD/100 \quad [\text{kN/m}^2] \quad (26)$$

$$\gamma_{0.7} = (2 - RD/100) \cdot 10^{-4} \quad [-] \quad (27)$$

$$m = 0.7 - RD/320 \quad [-] \quad (28)$$

In addition, the input parameters of linear elastic model for the engineering bedrock, layer AG3, are presented in table 10.

Table 10. Linear elastic parameter for bedrock (layer AG3)

Symbol	Parameter	Value	Units
γ_{dry}	Dry unit weight	19.00	kN/m ³
γ_{sat}	Saturated unit weight	20.60	kN/m ³
e _{init}	initial void ratio	0.49	-
E'	Effective Young's modulus	200,000	kN/m ²
G	Shear modulus	83333	kN/m ²
E _{oed}	Oedometer Modulus	222222	kN/m ²
V _s	Shear wave velocity	199.2	m/s
V _p	Compression wave velocity	325.3	m/s

Some data of linear elastic model have to be determined further by using parameter correlation. Firstly, the Young's modulus (E') was determined around 200,000 kN/m² based on Bowles (1996) for dense gravel as shown in table 11. Moreover, the value of Shear Modulus (G) was calculated based on the value of Young's modulus by using equation (29), while Oedometer modulus (E_{oed}) was calculated using equation (30) with the same Poisson's ratio at 0.2. The shear wave velocity (V_s) and compression wave velocity (V_p) were defined by equation (31) and equation (32) respectively. Meanwhile, the value of density was calculated using formula $\rho = \gamma/g$, where γ is the unit weight [kN/m³] and g is gravity [m/s²].

$$G = \frac{E'}{2(1 + \nu')} \quad [\text{kN/m}^2] \quad (29)$$

$$E_{oed} = \frac{E'(1 - \nu')}{(1 + \nu')(1 - 2\nu')} \quad [\text{kN/m}^2] \quad (30)$$

$$V_s = \sqrt{G/\rho} \quad [\text{m/s}] \quad (31)$$

$$V_p = \sqrt{E_{oed}/\rho} \quad [\text{m/s}] \quad (32)$$

Table 11. Typical Modulus of Young's modulus of soil (Bowles, 1996)

Soil	E_s , MPa
Clay	
Very soft	2-15
Soft	5-25
Medium	15-50
Hard	50-100
Sandy	25-250
Glacial till	
Loose	10-150
Dense	150-720
Very dense	500-1440
Loess	15-60
Sand	
Silty	5-20
Loose	10-25
Dense	50-81
Sand and gravel	
Loose	50-150
Dense	100-200
Shale	150-5000
Silt	2-20

4.3 Parameter validation

The more advanced constitutive model for the analysis usually requires greater number of parameters for calculation. These parameters often cannot be defined directly from laboratory

test. Therefore, validation of the parameters is crucial to ensure that the parameters used in the model has similar behaviour with the test in the laboratory. However, nowadays, some correlations are available to determine the parameters that were already validated by the author. Moreover, Marcuson et al. (2007) and Idriss and Boulanger (2008) defined the validation of models showed a strong stress path dependency.

PLAXIS soil element test was used to validate the input parameters in this project. Ideally, the calibration by curve fitting could provide good results if the stress paths in the problem are similar with test data (laboratory test). However, the limitation of this validation is that it has only one layer of the laboratory data, other layers only have the sieving test data and N-SPT. Moreover, the laboratory test for the first layer (AC1) is also limited to only the Unconfined Compression Test (UCT). Therefore, the comparison of result between PLAXIS and laboratory test data is only for the first layer (AC1). However, the other layers were also tested in PLAXIS; but cannot be validated. The list of parameters and also the methods to obtain the parameters is summarized in table 12 and table 13 for HS small model and UBCSAND model respectively.

Table 12. List parameter of HS small model

Name	Symbol	Unit	Method	Default
(Effective) cohesion	c	kPa	CD or DSS	0
(Effective) angle of internal friction	ϕ	Degrees	CD or DSS	-
Angle of dilatancy	ψ	Degrees	CD or DSS	-
Secant stiffness in standard drained triaxial test	E_{50-ref}	kPa	CD or DSS	-
Tangent stiffness for primary oedometer loading	$E_{oed-ref}$	kPa	Oedometer	= E_{50-ref}
Unloading / reloading stiffness	E_{ur-ref}	kPa	CD or DSS	= 3 E_{50-ref}
Power for stress-level dependency of stiffness	m	-	Curve fit	0.5
Shear strain at which $G_s = 0.722 G_0$	$\gamma_{0.7}$	-	DSS	-
Reference shear modulus at very small strains	G_0 ref	kN/m ²	DSS	-
Poisson's ratio for unloading-reloading	ν_{ur}	-	CD or CU	0.2
Failure ratio	R_f	-	Curve fitting	0.9

Table 13. List parameter of UBCSAND model

Name	Symbol	Unit	Method	Default
Cohesion	c	kPa	CD or DSS	0
Constant volume friction angle	ϕ_{cv}	Degrees	CD or DSS	-
Peak friction angle	ϕ_p	Degrees	CD or DSS	-
Elastic shear modulus number	K_{e_G}	-	Curve fitting	-
Plastic shear modulus number	K_{p_G}	-	Curve fitting	-
Elastic bulk modulus number	K_{e_B}	-	Curve fitting	-
Elastic bulk modulus exponent	n_e	-	Curve fitting	0.5
Elastic shear modulus exponent	n_m	-	Curve fitting	0.5
Plastic shear modulus exponent	n_p	-	Curve fitting	5
Failure ratio	R_f	-	Curve fitting	0.9
Atmospheric pressure	P_a	kPa	Standard value	100
Tension cut-off	σ_t	kPa	-	0
Densification factor	f_{ac_hard}	-	Curve fitting	1
SPT value	N_{60}	-	In-situ test	-
Post liquefaction factor	f_{c_post}	-	Curve fitting	0.2-1

Laboratory data for the first layer is based on the Unconfined Compression Test. Meanwhile, this test was not available in PLAXIS soil element test, but the Unconsolidated Undrained (UU) triaxial test is supposed to give the similar result. However, in the PLAXIS soil element test, the Consolidated Undrained (CU) triaxial test was selected with the K_0 approach to represent the field condition. Therefore, the value of horizontal stress was defined with the available data of depth of sample and the density of the soil. The original data of laboratory test for this sample is presented in appendix G. Furthermore, the soil element test was done with the horizontal stress (cell pressure) about 12.81 kN/m² and K_0 about 0.54. Moreover, the output from PLAXIS soil element test is presented in figure 21 with the comparison from the laboratory test of UCT. The result of this analysis is different from the laboratory test in which the secant stiffness is much greater than what obtained from the laboratory test.

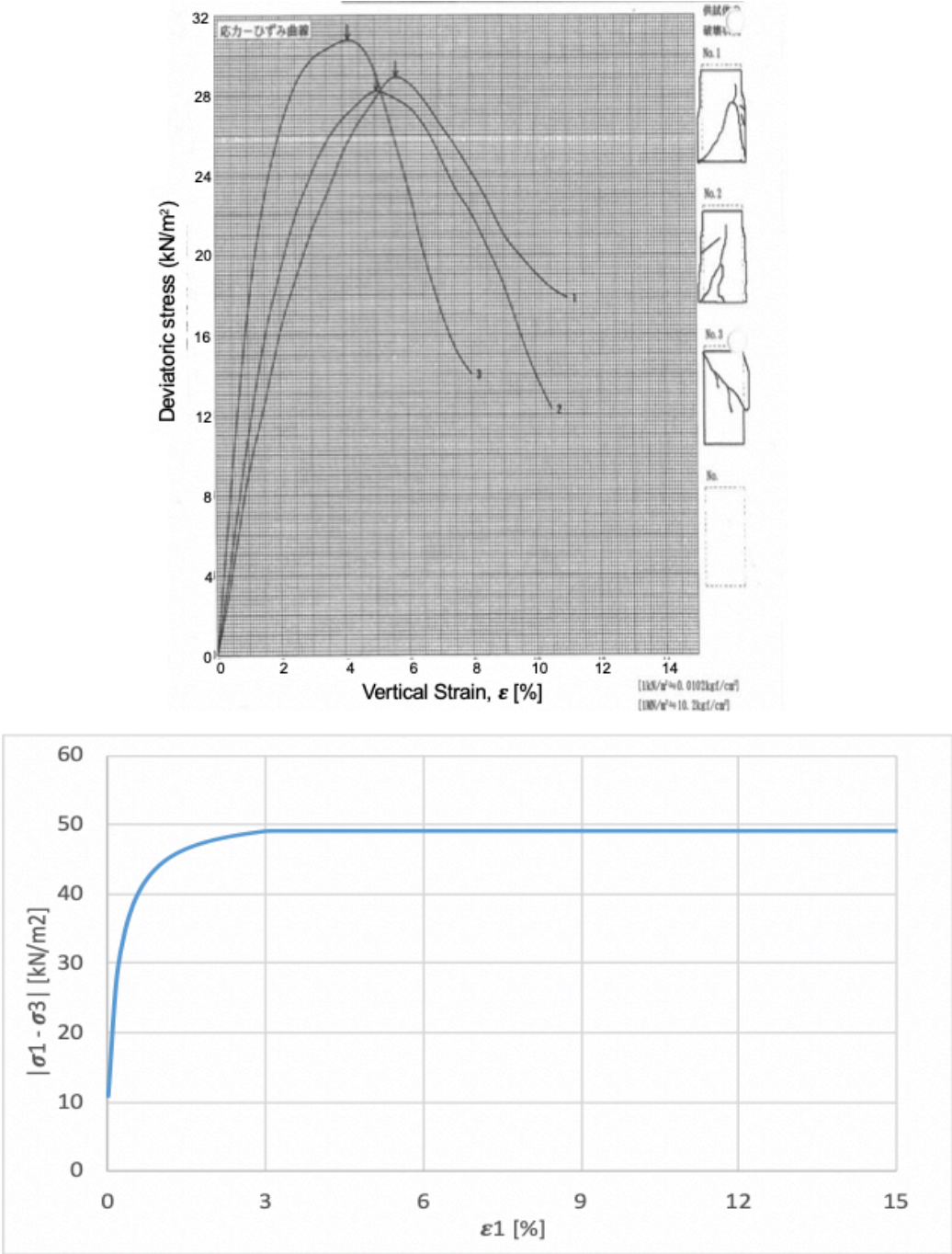


Figure 21. Consolidated Undrained triaxial test for AC1 from PLAXIS and UCT from Laboratory test

Furthermore, the Consolidated Drained (CD) triaxial tests were done for all layers except the bedrock (AG3). Unfortunately, the validation is also not possible due to no laboratory tests for these layers. CD triaxial test with cell pressure to 40 kN/m^2 were done for all layers. The purpose of this CD test is to check the rationality of result based on the stress strain curve that related with the stiffness of soil. The result from all layers are summarised in figure 22.

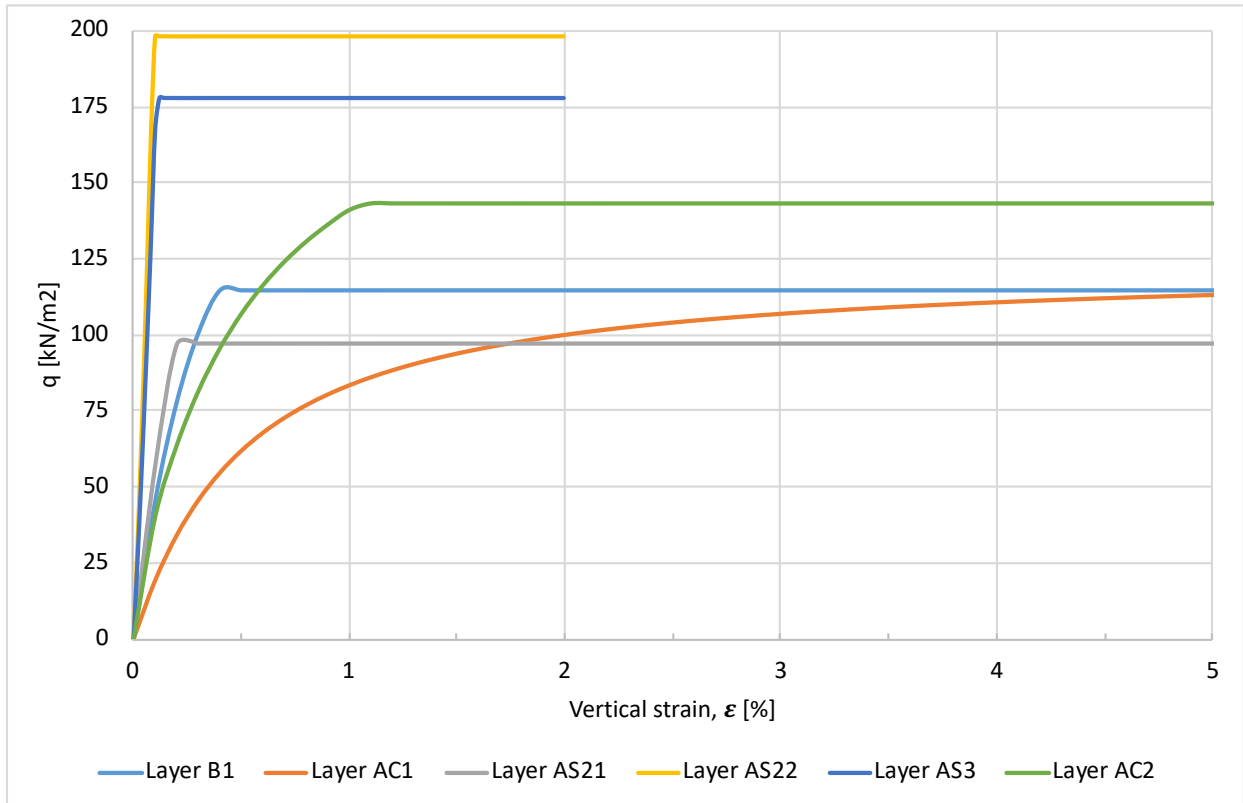


Figure 22. Consolidated Drained triaxial test result for all layers

From figure 22, it can be seen that the stiffest layer is the layer AS22 and followed by AS3 with almost vertically stress strain relationship. Moreover, the weakest layer is the first layer AC1 with gentle slope of stress-strain relationship. However, this stress-strain relationship should be validated with the laboratory result such that the relationship is similar for each layer. From this stress-strain relationship, the stiffness parameters could be determined and also the internal friction angle and the cohesion.

Cyclic DSS test was also completed to check the pore pressure ratio over the number of cycles, which related to the potential of liquefaction. The tests were based on cyclic stress ratio (CSR) 0.25 and the initial vertical stress 40 kN/m^2 with stress control. Moreover, the result for all layers is shown in figure 23. This figure shows no liquefaction occurs in layer AS22 and AS3 that has the N_{60} about 43.55 and 32.38 respectively. Both layers are defined as the dense layer with sandy soil with small possibility of liquefaction. Moreover, the most liquefiable layer is found at the first layer (AC1), weak layer with N_{60} equal to 2.27, that tend to be liquefied at the first cycle. Layer AS21 and B1 have similar pore pressure ratio within the number of cycles less than 6. However, for number of cycles more than 6, the pore pressure ratio of B1 increases over the number of cycles while the AS21 shows almost the same pattern of ratio.

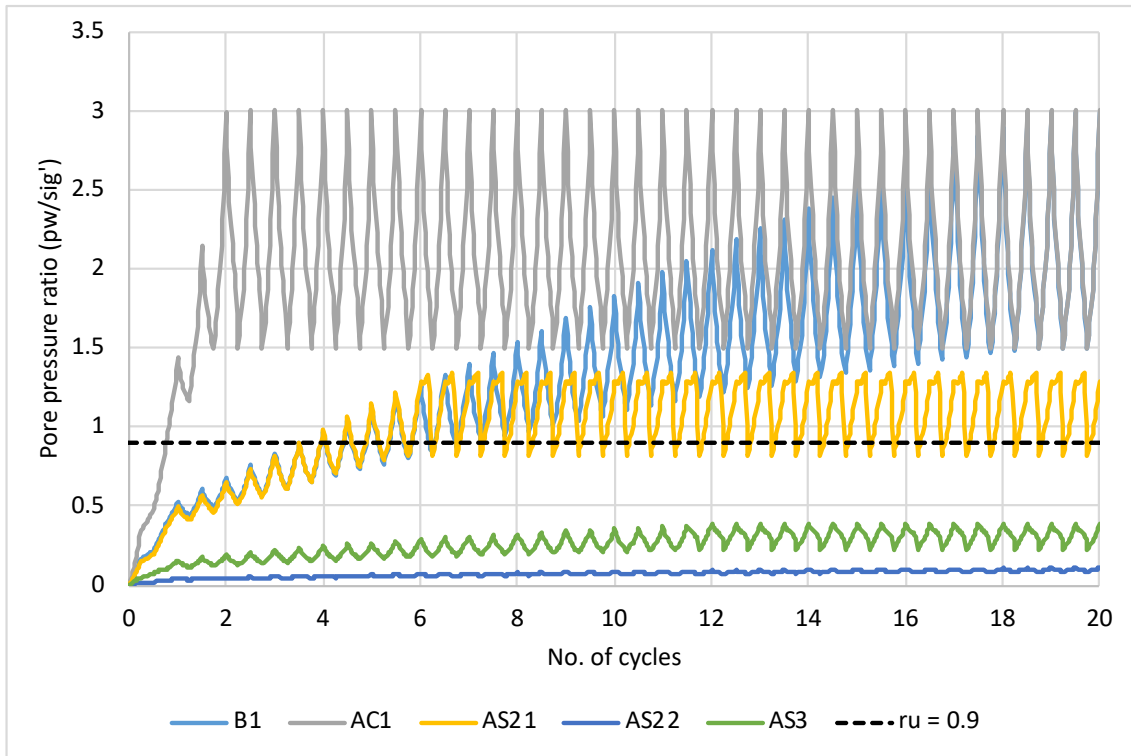


Figure 23. Pore pressure ratio for layers use UBCSAND during CDSS test with CSR = 0.25 and $\sigma_v=40$ kPa

The validation of all parameters cannot be completed due to limitation of data from the laboratory. However, the validation should be done by comparing the result between PLAXIS soil element and laboratory data. The comparison could be from the triaxial (CD) test, Direct Simple Shear test (DSS) as shown in table 12 and 13. However, some parameters have to be adjusted with curve fitting method such the curve from PLAXIS and Laboratory show similarities.

4.4 Rayleigh Damping data

There are three required parameters to determine α and β of Rayleigh coefficients. First is the damping ratio (ξ) that set as 1 percent for critical camping. The second is the first target of frequency and the third is the second target of frequency that already discussed in [chapter 2.6](#). Therefore, the calculation based on the soil parameters for each layer were done and the results are summarized in table 14.

Table 14. Rayleigh damping parameter

Symbol	Parameter	Value							Units
		B1	AC1	AS21	AS22	AS3	AC2	AG3	
f1	Frequency of soil / first target	0.73	0.15	0.79	0.97	0.93	0.84	1.80	Hz
fp/f1	Second target	5	17	5	3	3	3	3	Hz
α	Rayleigh alpha	0.0801	0.0187	0.0857	0.0921	0.0892	0.0825	0.1414	-
β	Rayleigh beta	5.56E-04	1.86E-04	5.50E-04	8.02E-04	8.10E-04	8.29E-04	6.63E-04	-

4.5 Seismic Design input

There are two locations of seismometer near the project area, the first is in the north and the second in the south toward the project location. The locations of seismometer are shown in figure

24 in which each location has the same distance about 10 km to the area of the project. Moreover, the distance from the epicentre of earthquake to these three locations are about 170 km. The soil profiles in each location are totally different that resulting two different peak accelerations. The first location, MYG013, recorded the peak acceleration at 1.52g while the second location, MYG015, recorded much lower peak acceleration value at 0.42g. The recorded motion for each location is given in figure 25 and figure 26 respectively that collected from National Research Institute for Earth Science and Disaster Resilience (<http://www.kyoshin.bosai.go.jp>). Moreover, the soil data of these two locations are summarised in table 15.



Figure 24. Location of two seismometer relative to the project location (www.google.com/earth)

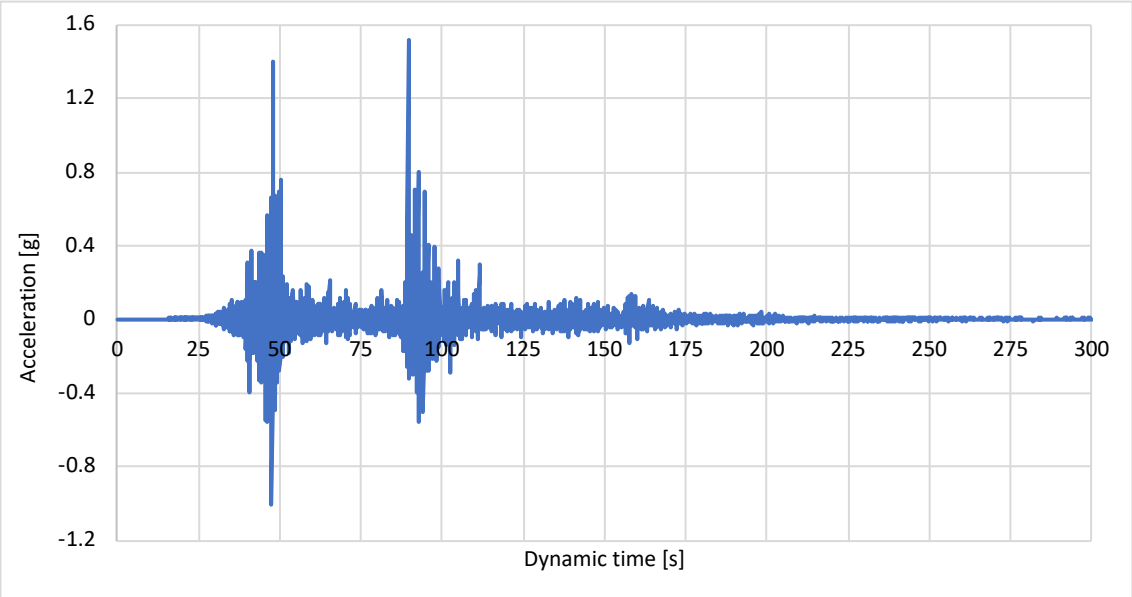


Figure 25. Original recorded motion at MYG013 (<http://www.kyoshin.bosai.go.jp>)

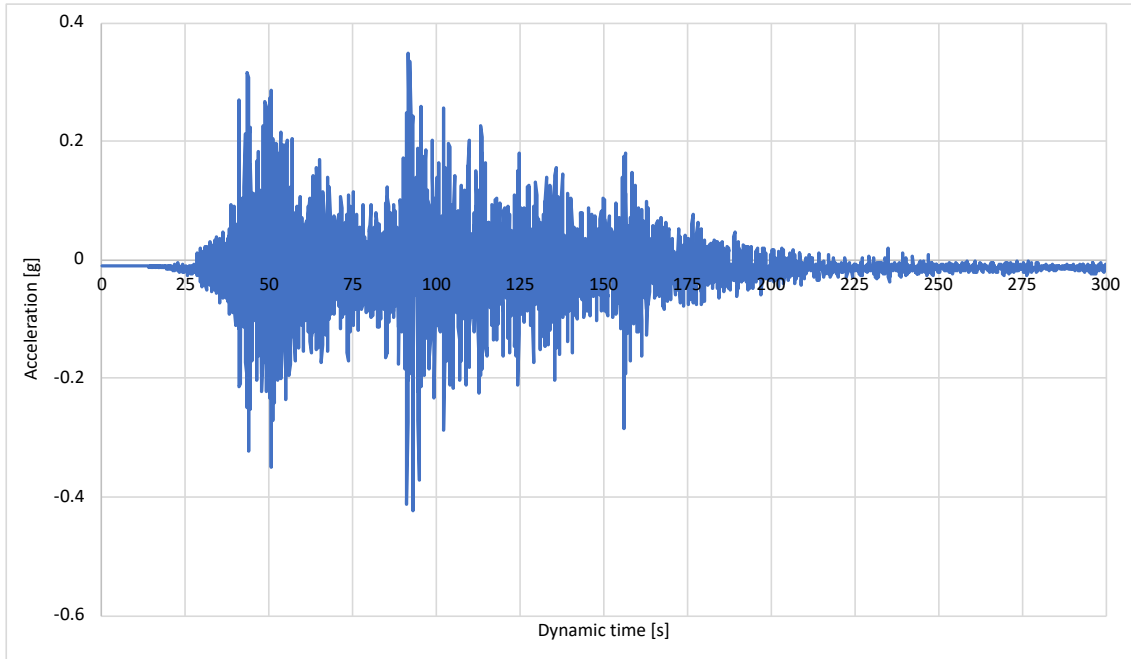


Figure 26. Original recorded motion at MYG015 (<http://www.kyoshin.bosai.go.jp>)

Table 15. Soil parameter in both locations of seismometer (<http://www.kyoshin.bosai.go.jp>)

Seismometer	Layer Number	Thickness	Unit Weight	Shear Velocity	Gmax
		[m]	[kN/m ³]	[m/s]	[kPa]
MYG013	1	0.85	16.30	70	8100
	2	0.80	16.00	100	16300
	3	3.50	15.87	147	35000
	4	1.35	19.70	170	58100
	5	7.50	20.50	406	344600
MYG015	1	1.00	15.70	100	16000
	2	2.00	15.80	100	16100
	3	1.00	16.20	100	16500
	4	1.00	17.40	180	57500
	5	7.00	18.10	220	88900
	6	6.00	18.60	250	118500
	7	3.00	19.70	410	337700

The processes of motion to get the seismic input at the base of layer (engineering bedrock) were done based on the simplification of the signal input from adjusted Loma Prieta motion. Firstly, the amplification factors were calculated for both seismometers based on the Loma Prieta motion as the input at the bottom. The amplification factor is defined as the ratio of peak acceleration at the top of soil (surface) and the peak acceleration at the base as the input. The calculation was done by using Proshake software and the output motion (at the surface) for both locations is presented in figure 27.

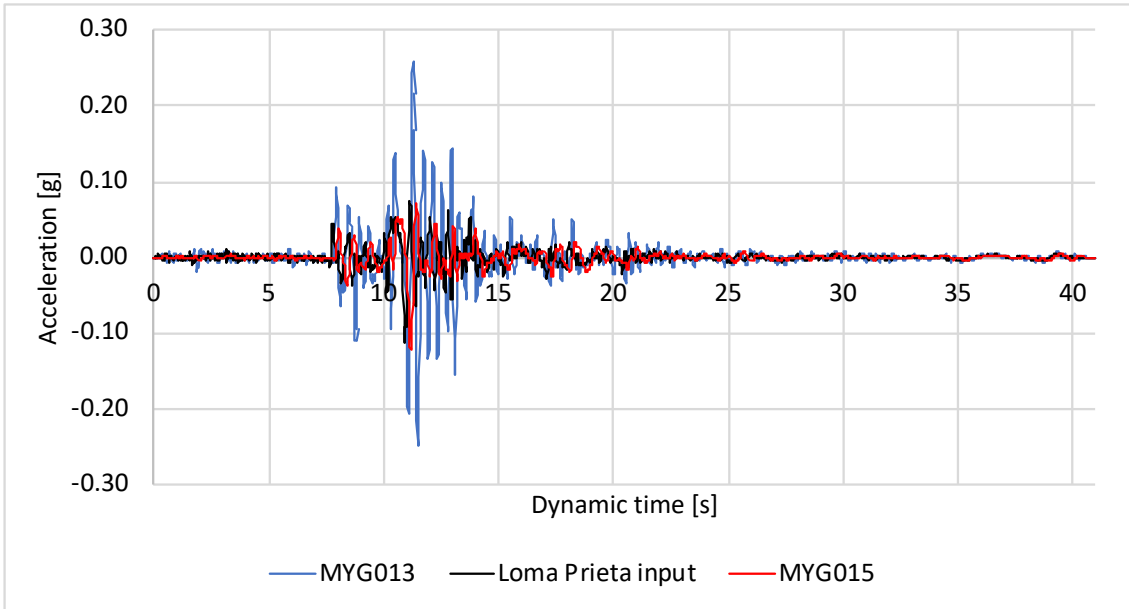


Figure 27. Motion at surface in both locations based on the Loma Prieta input

Moreover, based on the result of analysis in figure 27, the amplification was determined at 2.29 for MYG013 and at 1.08 for MYG015. Loma Prieta motion at the bottom (as the input) has to be adjusted by dividing the peak acceleration of original recorded motion at surface to the amplification factor. Therefore, the peak acceleration of Loma Prieta as the input at the bottom was determined to 0.66g for MYG013 and 0.39g for MYG015. Furthermore, to get the input at the engineering bedrock of project's location, the calculated average value based on these two peak accelerations resulted in the peak acceleration input for this research at 0.53g as shown in figure 28 for the adjusted Loma Prieta motion.

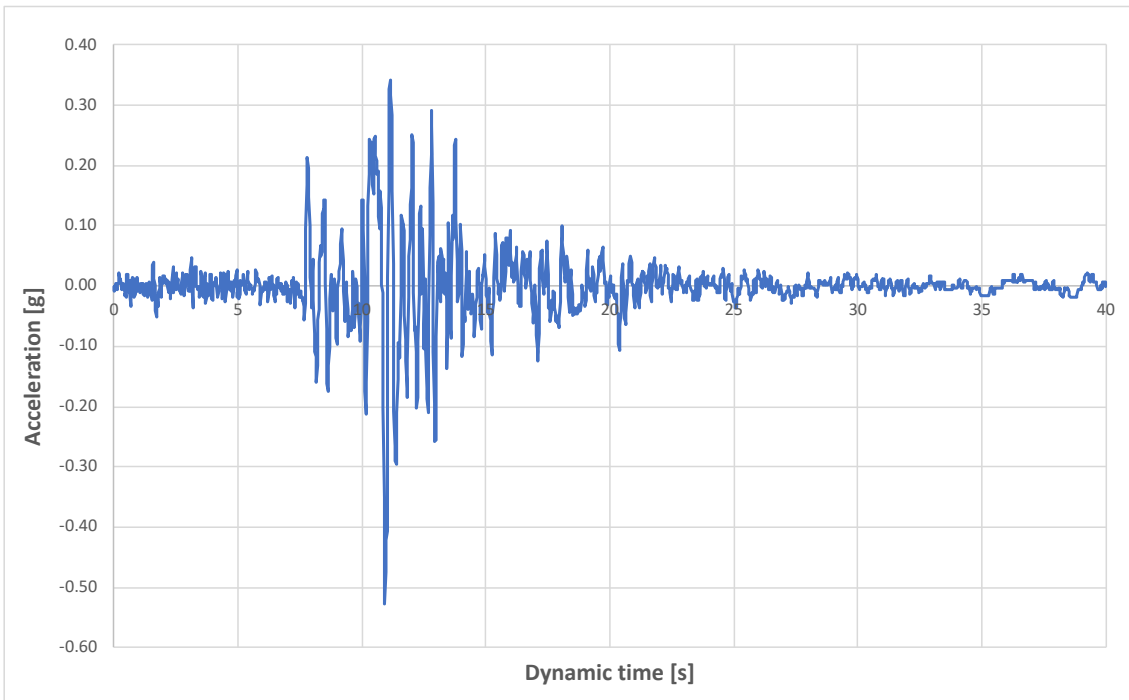


Figure 28. Seismic input for PLAXIS analysis

However, these processes of motion analysis have some drawbacks because many assumptions were present. First, the motion used was simplified by using Loma Prieta motion in a condition

where the characteristic of each earthquake is different. However, the fact that each earthquake will not produce the same motion is also the reason to take this adjusted Loma Prieta motion as the input motion. Second, the process of taking the amplification factor was not valid for all earthquake motion; it was specific for the motion that is used in this research (Loma Prieta). Therefore, the proper analysis of motion should be defined for other case of analysis based on the original recorded motion. Additionally, deconvolution analysis has to be done based on the input at the surface to get the motion at the bedrock. Meanwhile, the process of motion analysis in this research was made without deconvolution analysis instead of the motion at the surface, it was on the bedrock.

The Fast Fourier Transform based on the input motion in figure 28 was done to determine the frequency of the seismic input at the bedrock. The result of this FFT were used as the input for the Rayleigh damping calculation. The analysis was done using *Seismosignal* software in which the result is presented in figure 29. The maximum Fourier amplitude is at 0.29 g*second at the frequency around 2.5 Hz.

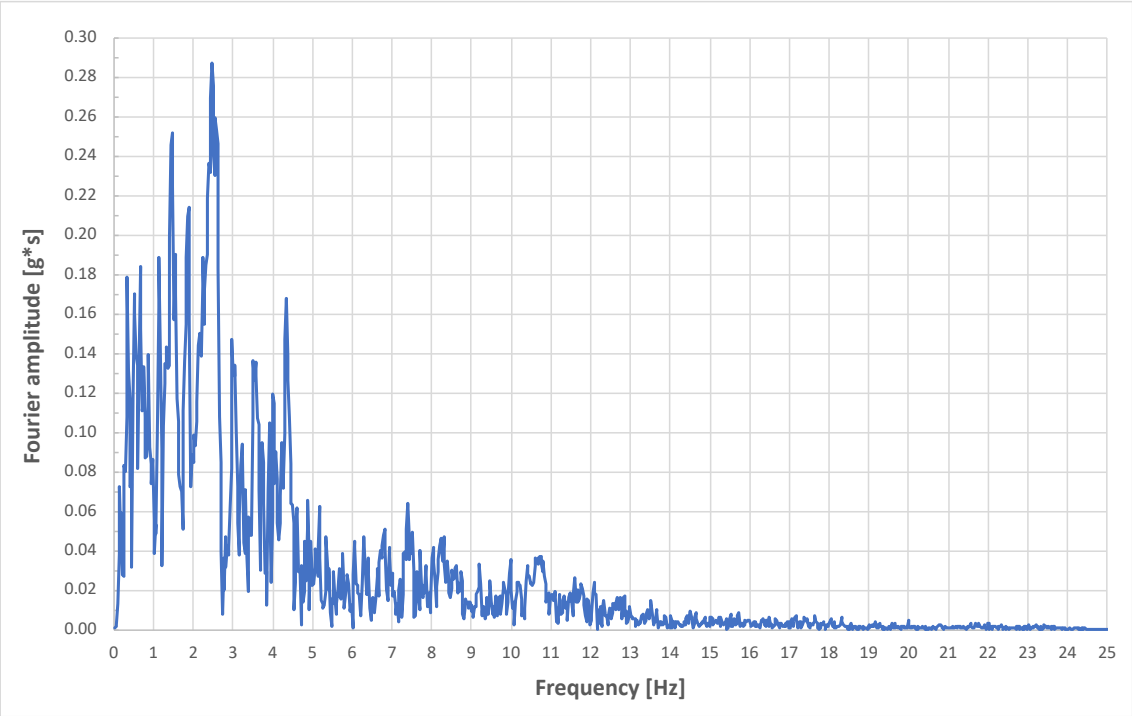


Figure 29. Fast Fourier Transforms of the input

4.6 Geotextile parameter

There are two input parameters for the analysis using PLAXIS. First, the tensile strength [kN/m] of geotextile that usually provided by the manufacturer. Moreover, the strain in percentage at short term strength is also provided. Based on the value of tensile strength and strain, the second main parameters can be calculated by dividing the value of tensile strength to the strain, which resulting the axial stiffness (EA) in kN/m unit. The axial stiffness is not provided by the manufacturer; therefore, this parameter was determined by the user based on the linear elastic perfectly plastic approximation.

The material type can be considered either in elastic or elastoplastic that has different input. Firstly, the elastic material needs axial stiffness as the input. Secondly, the elastoplastic type requires both parameters, axial stiffness and tensile strength. Moreover, the elastoplastic material type was used this analysis.

The method to determine tensile strength is based on ASTM D 4594. This method considers clamping the entire width of sample and pull to get the value of tensile strength. Furthermore, the total strain is also recorded in which to calculate the axial stiffness (EA) of the geotextile. The parameters of geotextile (tensile strength and strain) were collected from the Global Synthetics (<http://globalsynthetics.com.au>) and TenCate Geosynthetics (<https://www.tencategeo.eu/>), while the axial stiffness (EA) values were calculated based on the ratio of tensile strength over the strain. The parameters of geotextile are summarized in table 16, while the original data from both companies are included in the appendix B and appendix C.

Table 16. Geotextile parameters

Name	Tensile strength	Design life	fc Creep rupture	fd Construction damage	fe Environmental effect	Long-term design strength	Strain	Axial Stiffness
	[kN/m]	[years]	[-]	[-]	[-]	[kN/m]	[%]	[kN/m]
PEC 50*	50	120	1.55	1.02	1.1	28.8	10	288
GT 200/50	200	60	1.45	1.1	1.05	119	10	1194
GT 400/50	400	60	1.45	1.05	1.05	250	10	2502
GT 800/50	800	60	1.45	1.05	1.05	500	10	5004
GT 1200/100	1200	60	1.45	1.05	1.05	751	12	6255

* TenCate Geosynthetics

5 Analysis: Yuriage Case

This chapter discusses the analysis using D-Geo Stability and PLAXIS 2D. However, the main analysis is using the PLAXIS 2D in which the focus and detail of explanation is more to the PLAXIS. Moreover, the optimization of geotextile application is based on the Finite Element Method using PLAXIS software. The analyses are illustrated in figure 30 as the processes of calculation.

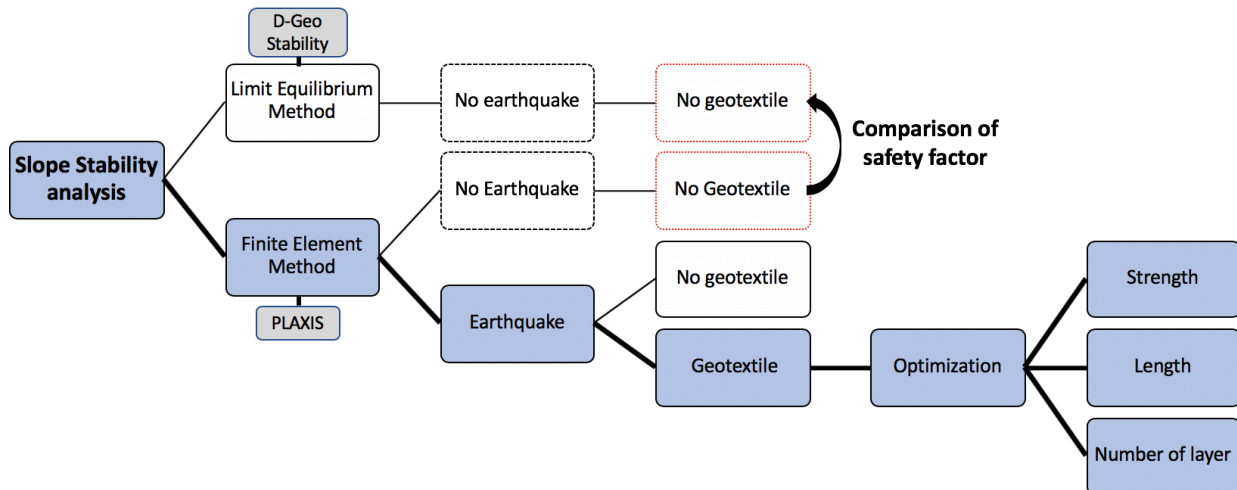


Figure 30. Processes of analysis

5.1 Limit Equilibrium Method: D-Geo Stability

Limit Equilibrium Method using D-Geo stability software was used as the initial analysis with Safety Factor as the output. The output will be compared with the PLAXIS output for which the safety factor from these two methods needs to be similar. Therefore, the model used for the analysis based on these two approaches would be correct if the output is similar. Limit Equilibrium Method is conventional method, especially for dynamic analysis. This software only considers the single value of seismic input that is defined as horizontal earthquake factor (k_h). Moreover, the changes in soil behaviour during the earthquake cannot be seen. Lastly, the input for dynamic calculation is too large to be calculated by such simple approach used by this software.

5.1.1 Model

Bishop model was used to analyse the slope of newly elevated area in Yuriage. The case for the LEM analysis did not consider the earthquake loading and geotextile application. The geometry of the analysis is based on the D-Geo stability software shown in figure 31 below, while the parameters used are summarized in table 17.

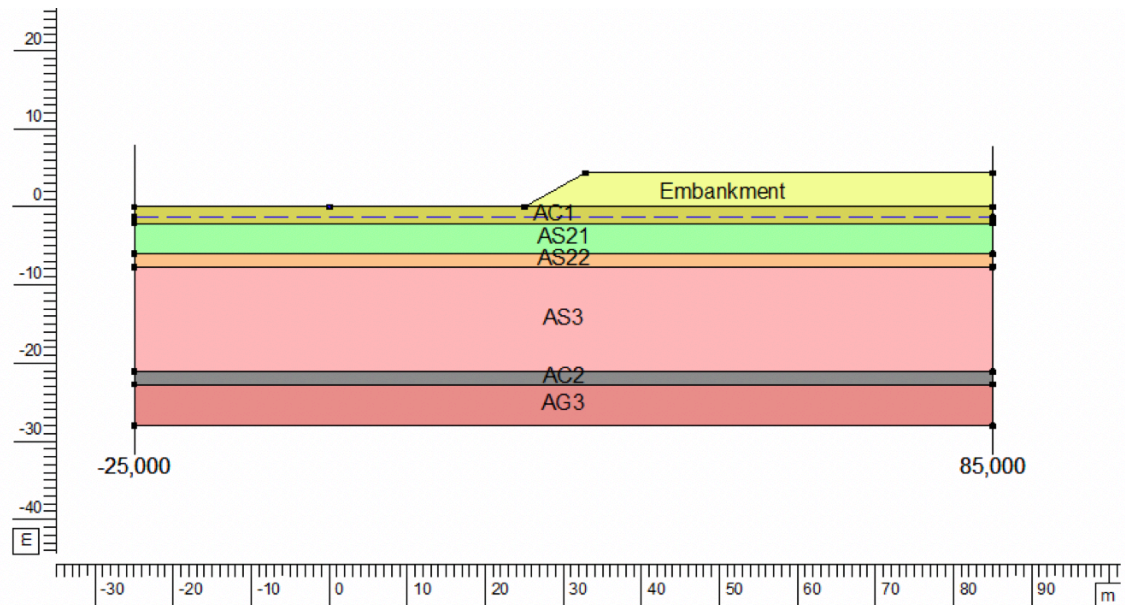


Figure 31. Geometry of analysis with D-Geo Stability

Table 17. Parameter used in D-Geo stability

Symbol	Parameter	Value							UNITS
		B1	AC1	AS21	AS22	AS3	AC2	AG3	
γ_{dry}	Dry unit weight	19.00	12.24	17.51	18.85	18.58	17.88	19.00	kN/m ³
γ_{sat}	Saturated unit weight	19.00	17.75	20.00	20.54	20.43	20.15	20.60	kN/m ³
c	Effective cohesion	10	15	0	0	0	15	0	kN/m ²
ϕ_{cv}	Friction angle at constant volume	30	27.26	31.38	39	36.46	31.81	42.27	Degrees
ψ (psi)	Angle of dilatancy	0	0	1.78	10	8.39	2.1	10	Degrees

D-Geo stability determines the critical slip circle in an iterative way. The trials are based on a grid of centre points and a set of horizontal tangent lines. These two factors (centre point and tangent line) can move towards the direction with the lowest safety factor during the calculation process. The grid of centre points and set of horizontal tangent lines is shown in figure 32.

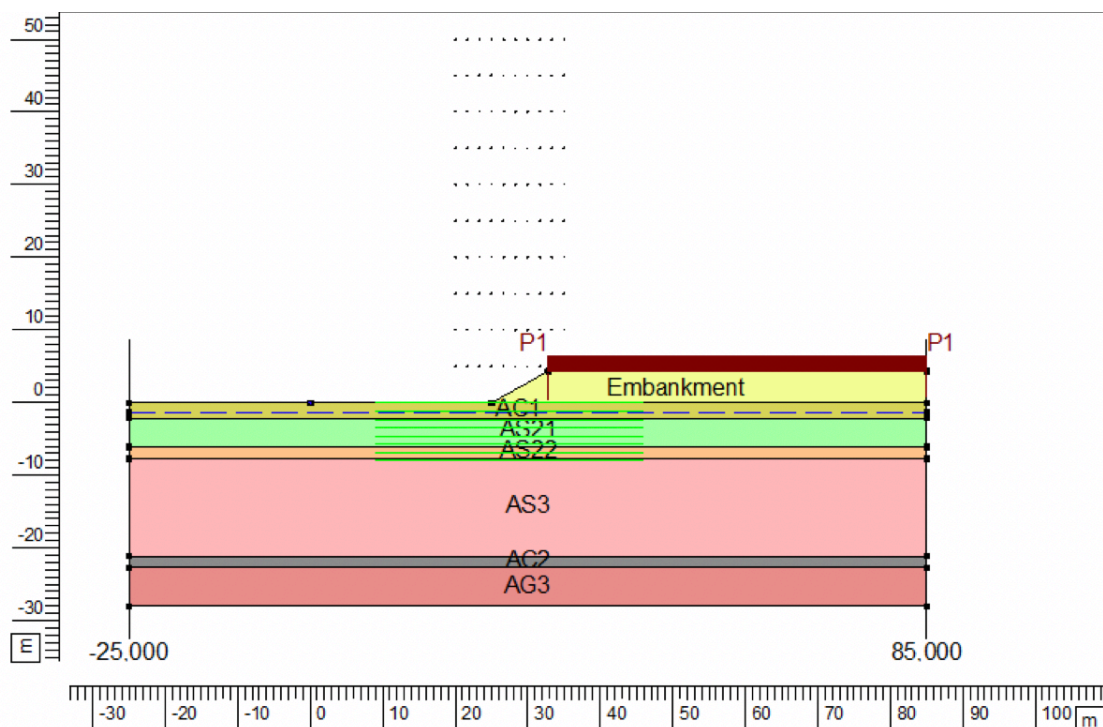


Figure 32. Grid of centre point of circle and horizontal tangent lines

5.1.2 Result

The analysis considers the uniform load without reinforcement and seismic input. The output of safety factor from this analysis is 1.93 with the radius of the circle around 10m as shown in figure 33. Moreover, it can be seen that the critical circle goes to the toe of the slope even though the layer AC1 is soft soil layer. Furthermore, the safety factor from this analysis met the requirement of minimum safety factor 1.5 as explained in [chapter 3.1](#).

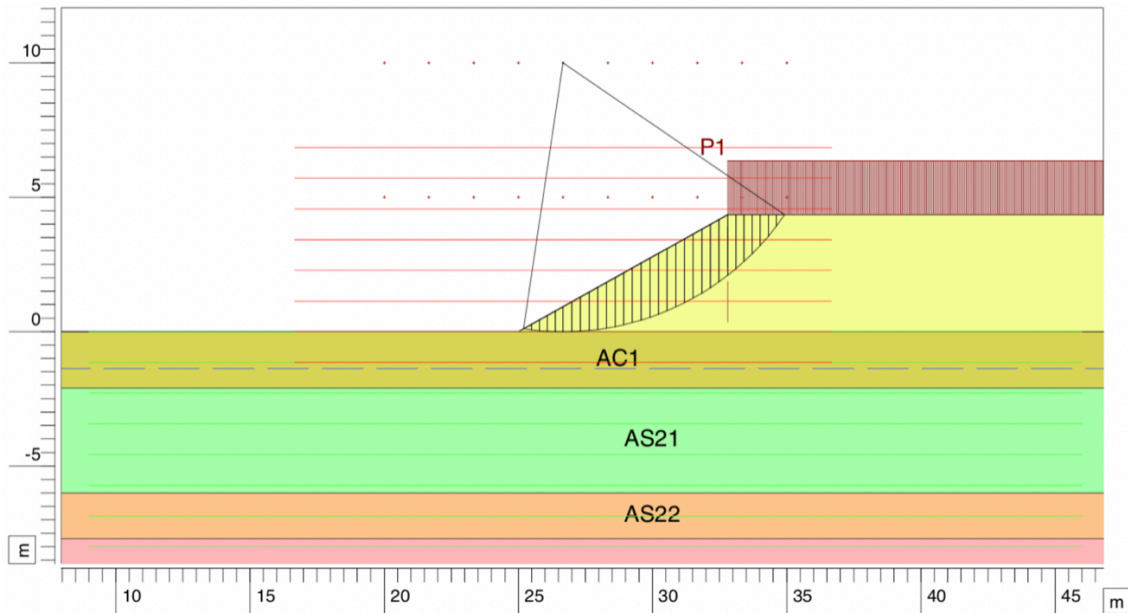


Figure 33. Critical circle analysis without geotextile

5.2 Finite Element Method: PLAXIS

5.2.1 Geometry and Mesh

The geometry used in PLAXIS is based on figure 15 but adjustment has to be made in the horizontal boundary where the left and right boundaries do not influence the slope in the analysis. Therefore, distance from the crest of slope to the left boundary is at 57.15 m and distance from toe of slope to the right horizontal boundary is at 75 m. With such distance, it is expected that the slope will not be affected.

Furthermore, geometry has to be divided into finite element to perform finite element calculations. A composition of finite elements is called a mesh. The mesh is based on a robust triangulation procedure. The size of the mesh needs to be sufficiently fine to get the accurate results. However, the very fine mesh is also bad for calculation time. Kuhlmeier and Lysmer (1973) suggested to use the size of mesh based on the wavelength (λ) that is associated with the frequency of input motion. Moreover, the minimum size of mesh is about one-eighth of the wavelength value. The formula to determine this wave length is shown in formula (33).

$$\lambda = \frac{V_s}{f} \quad (33)$$

Where V_s is the lowest shear wave velocity that is defined from the first layer (AC1) and about 16.8 m/s. f is the frequency from the input motion at the base as shown previously in figure 27 with value of 2.5 Hz. Moreover, the minimum wavelength at 6.72m was calculated using equation 33. Thus, the size of mesh is less than or equal to one-eighth of the minimum wavelength at 0.84m. moreover, the *fine* element distribution was selected in mesh option in PLAXIS.

5.2.2 Model and Boundary Conditions

Slope of newly-elevated area in Yuriage was analysed in two-dimensional finite element analysis. Plane strain model with 15-noded triangular elements was selected for the geometry in which the displacements and strains in z-direction were assumed to be zero. However, the normal stresses in this direction were considered in the analysis.

The boundary conditions of this project were considered differently between the static and the dynamic analysis. The standard fixities were assigned for static analysis, where the horizontal fixities in the X_{max} and X_{min} and vertical fixities in the Y_{min} as the bottom boundary.

However, for the dynamic analysis, the boundary is more complicated in regards to the reflection and absorption of the motion. Thus, proper boundary has to be chosen for each part. Two types of boundary can be considered in the lateral; free field and tied degree of freedom. However, based on analysis by Makra (2013), there is not much difference in terms of the outputs (total displacement, effective stress, and pore pressure ratio) from these two types. However, the tied degree of freedom is simpler than the free field boundary because tied degree only requires to switch off the default fixities.

Finally, the tied degree of freedom was chosen as the boundary in this analysis as proposed by Zienkiewicz, Bicanic & Shen (1998). This boundary connects the nodes on the same elevation at the left and right model boundaries. Therefore, all the nodes are characterised by the same vertical and horizontal displacement. However, this boundary only works when the boundaries are free to move. Thus, there are no fixities in the vertical boundaries, or switch off the default fixities during the dynamic analysis. Moreover, the distribution of nodes along the vertical boundaries must be identical (same y-coordinate). Therefore, the geometry of the case analysis has to be mirrored to meet these requirements. The mirrored geometry along with uniform load is shown in figure 34.

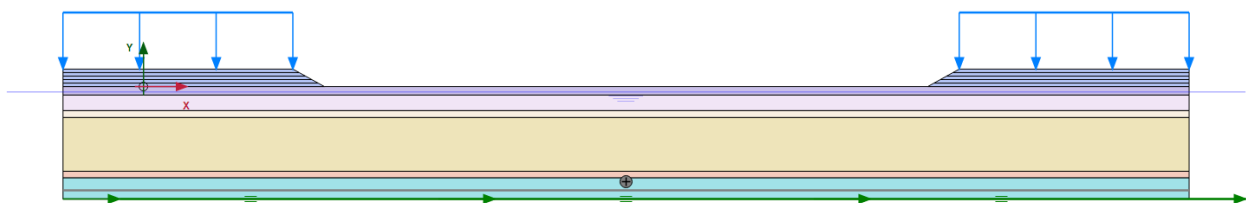


Figure 34. Mirrored geometry for the tied degree of freedom boundary

The third boundary is at the bottom where the input of motion is applied. Since the bedrock engineering is also modelled in the analysis, the most appropriate boundary is to assume the compliant base. Moreover, the dynamic impedance remains the same because the input wave

propagates from the part of bedrock outside the model to inside the model. Furthermore, the half of input is considered for this type of base boundary because the wave has the upward and downward propagating waves, but only the upward is considered in the analysis.

5.2.3 Phases and Analysis

There are two analyses considered in this research, static and dynamic analysis. Firstly, for the static analysis using HS Small strain model, there are several phases that are considered for staged constructions. These phases denote the construction of embankment that consist of 5 layers of soil compaction with same height at 0.87m (5 stages) and the geotextiles installation (for analysis with geotextile) on each part of embankment (5 stages). Afterward, the uniform loads are applied on the top of the raised area, where all these stages are sketched in figure 35.

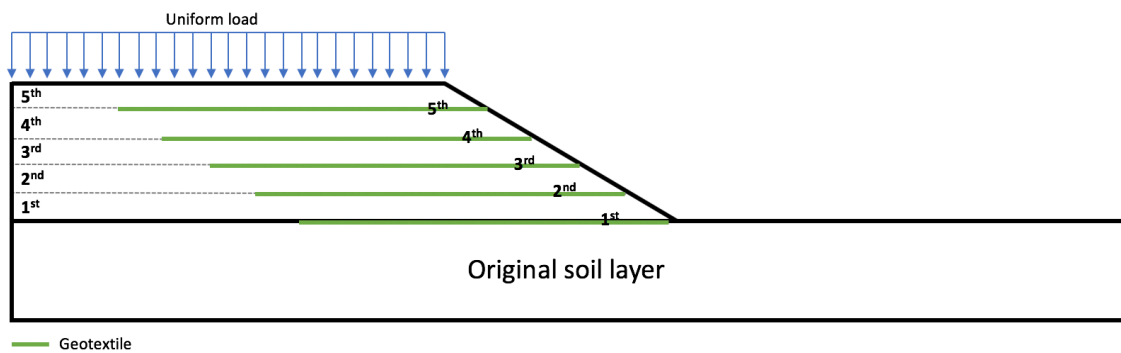


Figure 35. stages of newly-elevated area for static analysis

The next stage is to calculate the dynamic analysis but with different constitutive model; using UBCSAND instead of HS Small strain. In order to change the model, one more step has to be defined as “nil step”. This step is a plastic calculation phase in which no additional loading is applied. Besides the aim of changing the material model, this plastic nil step is sometimes required to restore the equilibrium.

The static analysis of this project is intended to give comparison result based on the safety factor value for the same case as the D-Geo Stability analysis. Moreover, the safety calculation in PLAXIS is called phi/c reduction. In safety approach, the shear strength parameter, $\tan \phi$ and cohesion of soil as well as the tensile strength are successively reduced until failure of the structure occurs (Brinkgreve et al., 2018). However, the approach of safety factor calculation is similar in which the safety factor is the ratio of available strength to the strength at failure.

Moreover, the dynamic analysis provides other outputs compared to the static analysis that resulting safety factor. Several outputs are expected from the dynamic analysis to be considered in this research, such as the total displacement, pore water pressure, pore pressure ratio, effective vertical stress, and the axial forces on the geotextile.

5.2.4 Results

5.2.4.1 Static Analysis – Comparison to D-Geo Stability Result

The static analysis is based on the calculation before the earthquake load is being considered, which in this case some stages of construction for the newly elevated area and the area where the geotextiles are installed. Thus, all these stages are in the static analysis with Hardening Soil small strain model in which the uniform load applied on top of the raised area was also considered.

The first output is active pore pressure as shown in figure 36 where the part above the phreatic line has zero pore pressure value.

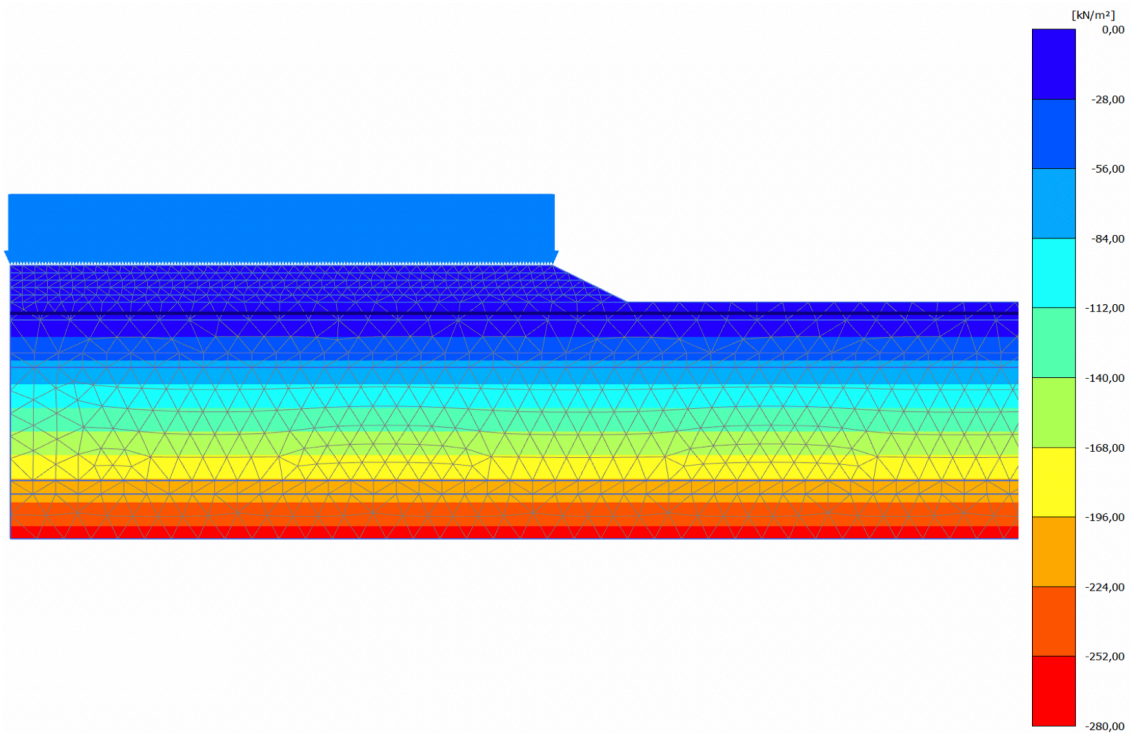


Figure 36. Active pore water pressure for static analysis

The effective vertical effective stress (σ'_v) and shear stress (τ_{xy}) are presented in figure 37 and 38 respectively. Vertical effective stress increases within the construction of newly elevated area. This can be seen with the higher value of effective stress, within the same layer, on the part below the embankment compared to the right part where there is no elevated area.

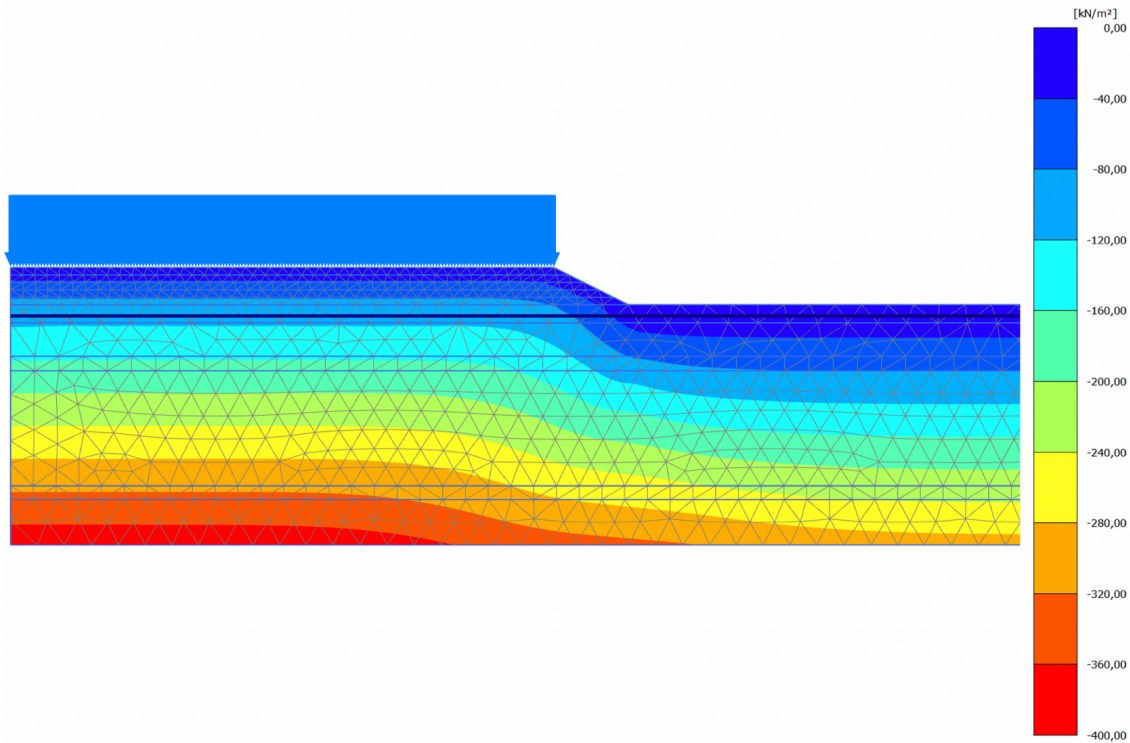


Figure 37. Vertical effective stress ($\sigma_{v0'}$) for the static analysis

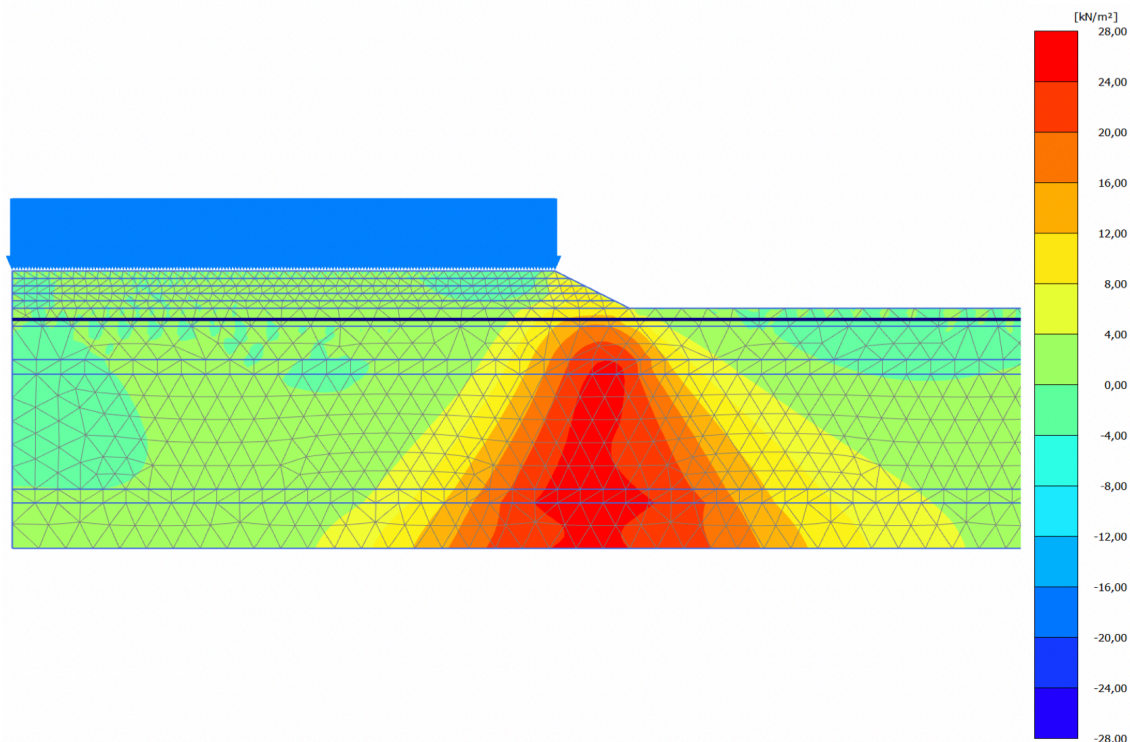


Figure 38. Shear stress (τ_{xy}) for the static analysis

Furthermore, this analysis aims to compare the output from PLAXIS to D-Geo stability based on the safety factor value. The failure mechanisms from both analyses shows similarity in result as shown in figure 39. The failure line goes through the toe of slope with safety factor about 2.07 as shown by the flat line in figure 40. The value is similar to the result of D-Geo stability that has the safety factor 1.93 for the same case. From this result, since the minimum safety factor of 15 is reached, no improvement is necessary in the slope for condition without earthquake load.

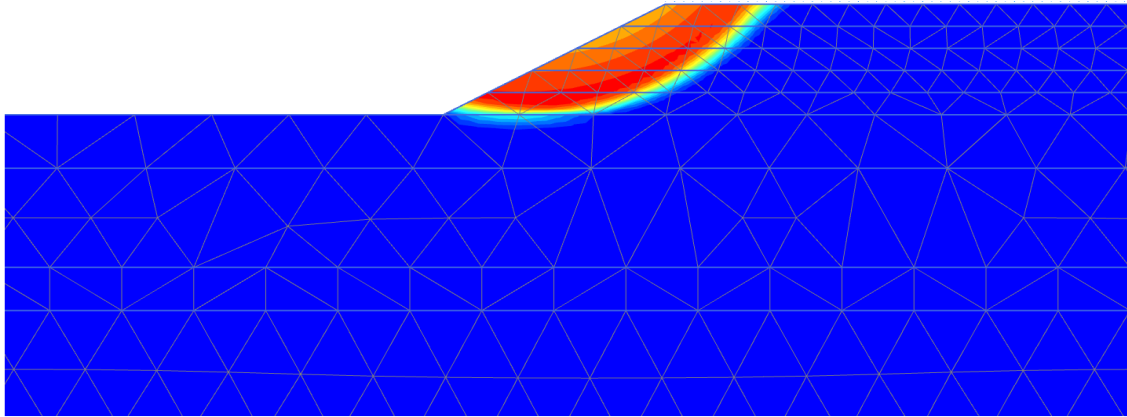


Figure 39. failure mechanism on analysis without earthquake load and no geotextile

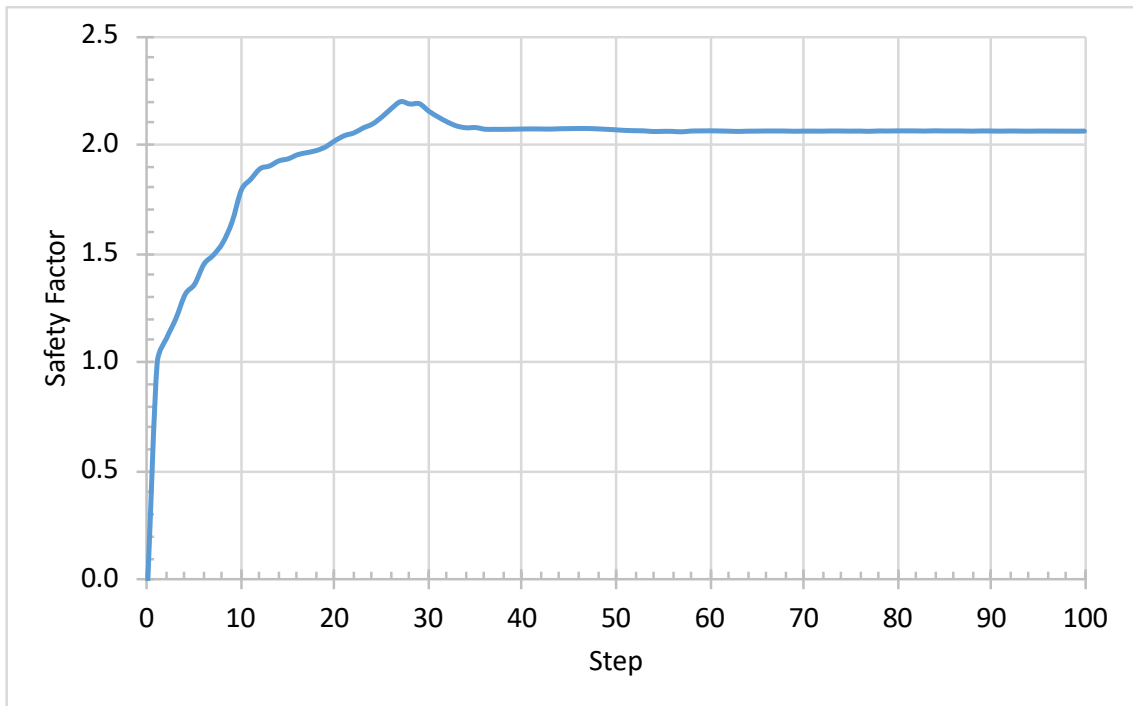


Figure 40. Safety factor for the analysis without earthquake load and no geotextile

5.2.4.2 Dynamic Analysis

Dynamic analysis using UBCSAND model is the main part of the analysis. It was done in the stage where the acceleration input at the bedrock is applied. However, before this stage is calculated, one more stage is added; namely “nil step”, where no action was taken except for changing the model for analysis that was previously using HS small model to UBCSAND for the dynamic analysis. However, the bedrock layer (AG3) remains in linear elastic model. The AC2 was also assigned with the same model using HS small due to the cohesive soil and small possibility of liquefaction.

5.2.4.2.1 Without Geotextile

The analysis in this part considered all the loads (uniform and earthquake loads), but there is no geotextile installed. This case aims to check the stability of the slope based on total displacement. Furthermore, the output from this analysis determined the minimum length of geotextile for further analysis. The total displacement of the slope is shown in figure 41.

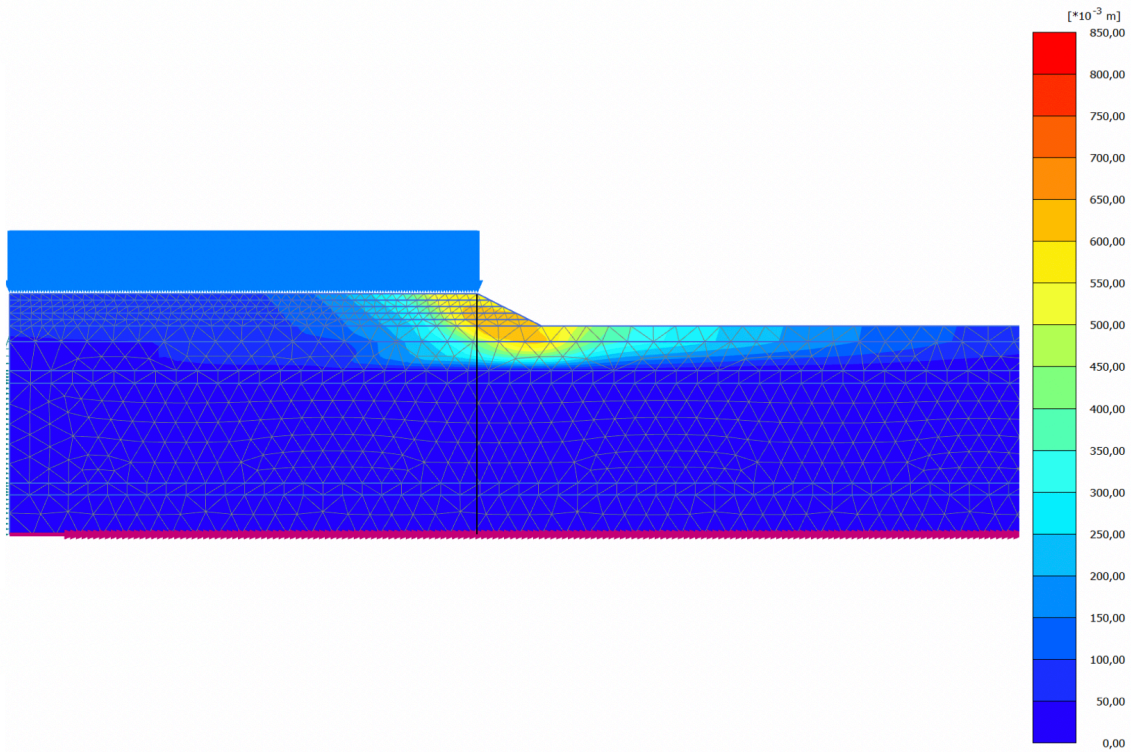


Figure 41. Total displacement at the end of dynamic time for analysis without geotextile

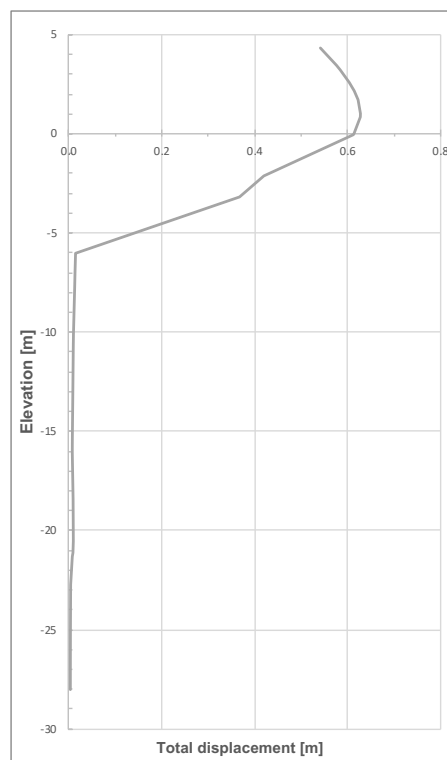


Figure 42. Total displacement at the cross-section below the crest of slope

Moreover, from figure 41, a cross-section was taken vertically from the slope crest (black line) to check the value of total displacement along this section. The result is presented in figure 42 as the maximum total displacement is located around the elevation $\pm 1\text{m}$ with a value of 0.629m . However, the total displacement at the crest of the slope is 0.543m , which is less than the maximum total displacement at the elevation $+1\text{m}$ at the same cross-section. Unfortunately, the

total displacement exceeded the maximum allowable value about 0.435m. Furthermore, the total displacement during the dynamic times and the acceleration input are presented in figure 43.

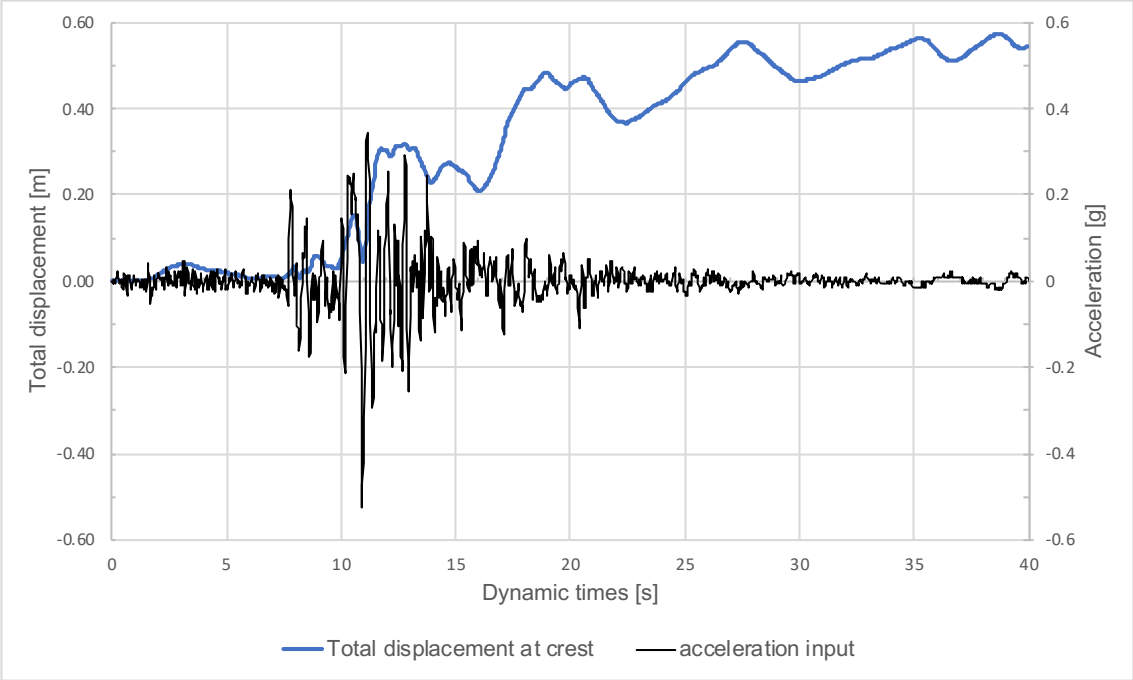


Figure 43. Total displacement at the crest of slope during dynamic times and the input of motion at bedrock

The plastic strain mostly occurred after the peak acceleration motion input at the time around 11 seconds as shown in figure 43. At this stage, the soil particles are restructured due to the shake that do not come back to the initial position (irreversible strain).

Furthermore, given the fact that the minimum requirement was not reached, the improvement of slope stability has to be considered, which in this case using the geotextile application. The first step is to determine the minimum length of geotextile in which the reinforcements have to be placed outside the failure area. Therefore, the contour line of total displacement is the basis of the minimum length requirement for further analysis as shown in figure 44. The distance of total displacement point to the crest is summarized in table 18.

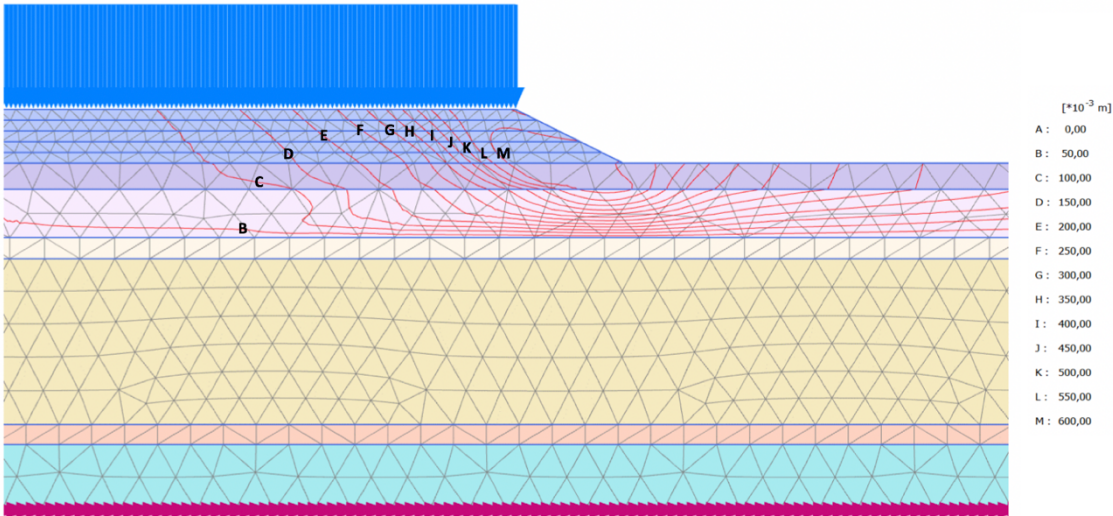


Figure 44. Contour line of total displacement at the end of dynamic time for analysis without geotextile

Table 18. Distance of total displacement value to the crest of the slope

Displacement [m]	Distance [m]
0.1	26
0.15	20
0.2	16.1
0.25	12.8
0.3	10.7
0.35	9.4
0.4	8.1

From figure 44 and table 18, and also based on SLS requirement of 0,435m, the minimum length of 10m was chosen as the initial length for the analysis. Moreover, lengthier geotextile will be considered based on the further output.

Active pore pressure at the end of dynamic time is shown in figure 45. Pore pressure developed significantly compared to the result before the earthquake occurred in figure 36. Therefore, the effective vertical stress also changed with the effect of increases active pore pressure. The new effective stress is presented in figure 46 as the part below the slope mostly decreases and also some parts in the second layer below the raised area as shown in blue colour (lower value).

The last part to check is the liquefaction, which can be defined by the ratio of pore pressure (r_u). This ratio is determined as the change in effective vertical stress over the initial effective vertical stress ($r_u = 1 - \frac{\sigma'_v}{\sigma'_{v0}}$). However, this term has a drawback as even at the place where there should no change in pore pressure (above phreatic level), the effective stress can change when the soil deforms. Moreover, the parts of soil above phreatic level are assumed in undrained condition in PLAXIS, which is one of the limitations for this software. Thus, there will be the parts where liquefaction should not occur (above phreatic level), but sometimes the ratio shows the soil is liquefied. Therefore, the value of pore pressure ratio above the phreatic line could be ignored. The evidence of this case could be seen in the analysis with geotextile application in which the pore pressure ratio more than 0.9, defined as the liquefied layer, occur at the part above the phreatic level (newly elevated area part).

Finally, the ratio of pore pressure for the analysis is given in figure 47 that clearly shows liquefaction occurring in the first, second, and fourth layer of soil. Also, the second layer AS21 is the most vulnerable layer to shearing. Moreover, this layer is the loose fine sand that is very sensitive to be liquefied during the earthquake.

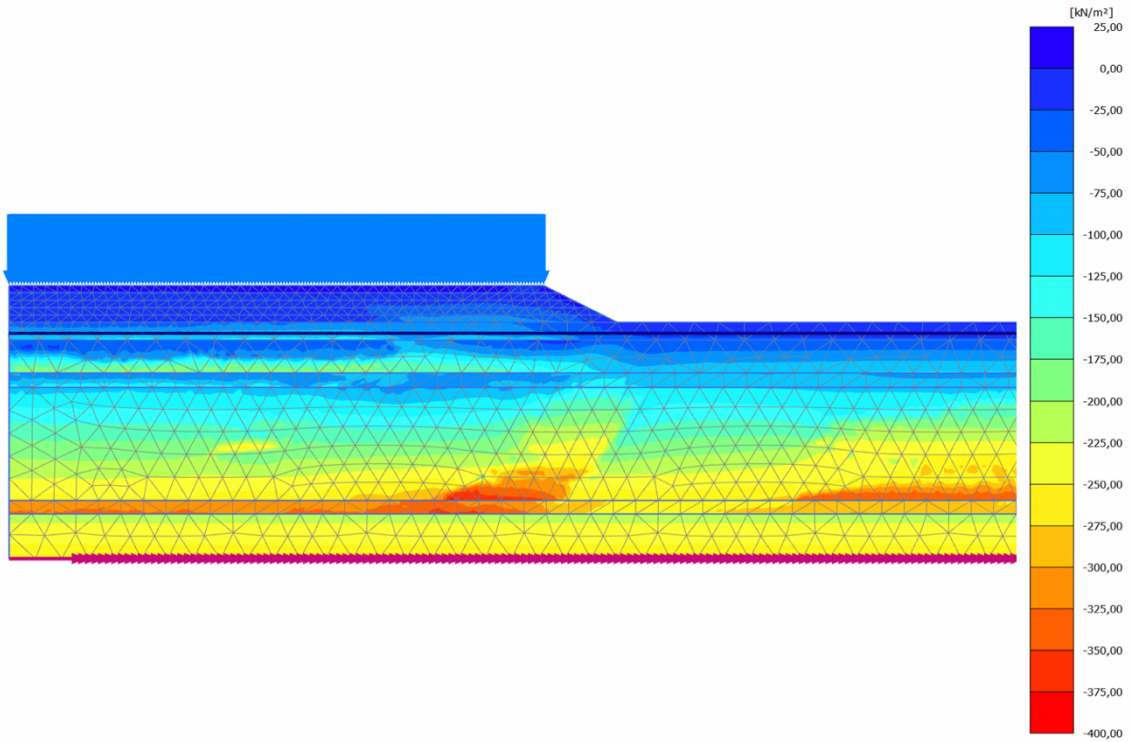


Figure 45. Active pore pressure at the end of dynamic time for analysis without geotextile

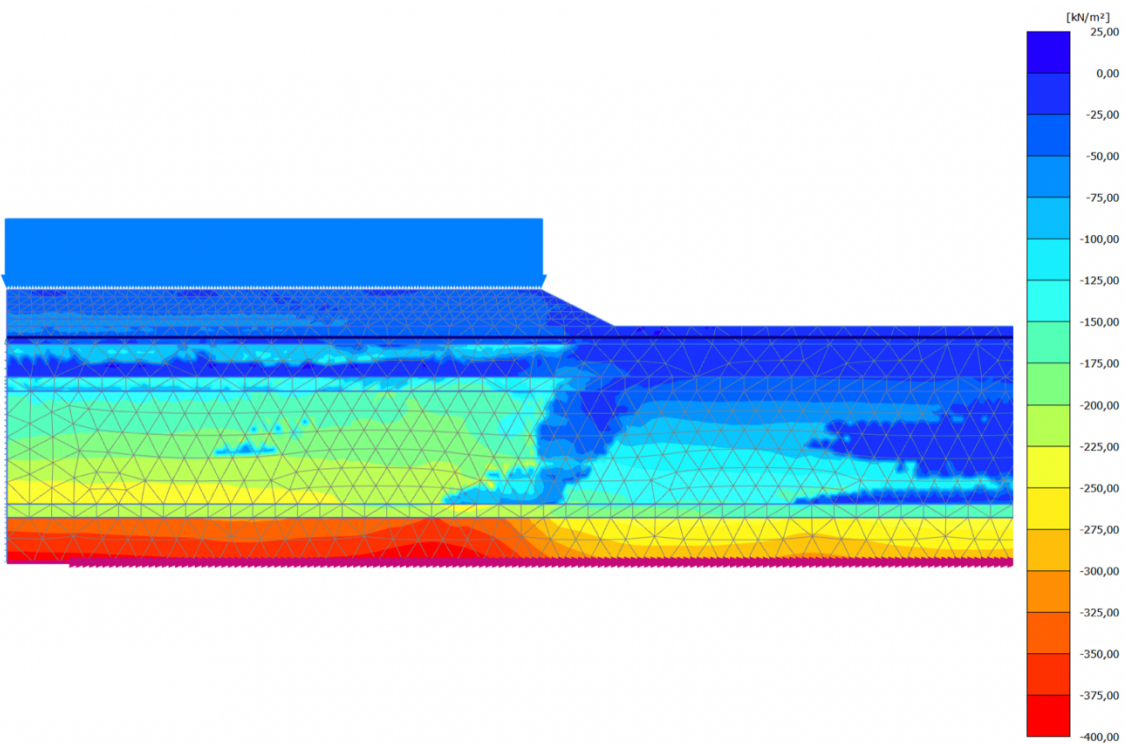


Figure 46. Vertical effective stress at the end of dynamic time for analysis without geotextile

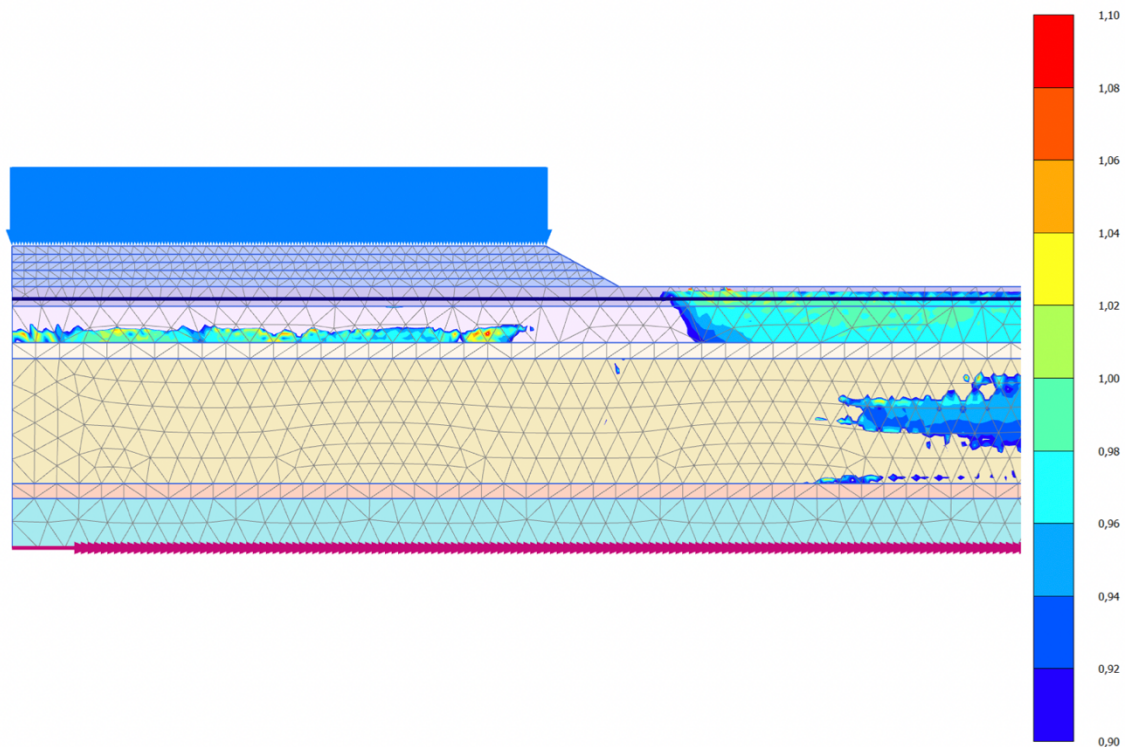


Figure 47. Liquefied areas corresponding to $r_{uv} > 0.9$ at the end of dynamic times for analysis without geotextile

5.2.4.2.2 With Geotextile

Further analysis was done by considering the geotextiles for slope stability improvement. The length is taken as the 30m in 5 layers of geotextile with the tensile strength 500 kN/m and axial stiffness (EA) 5004 kN/m (10% strain). The total displacement at the end of the dynamic time is presented in figure 48 with the maximum value at 0.434 m.

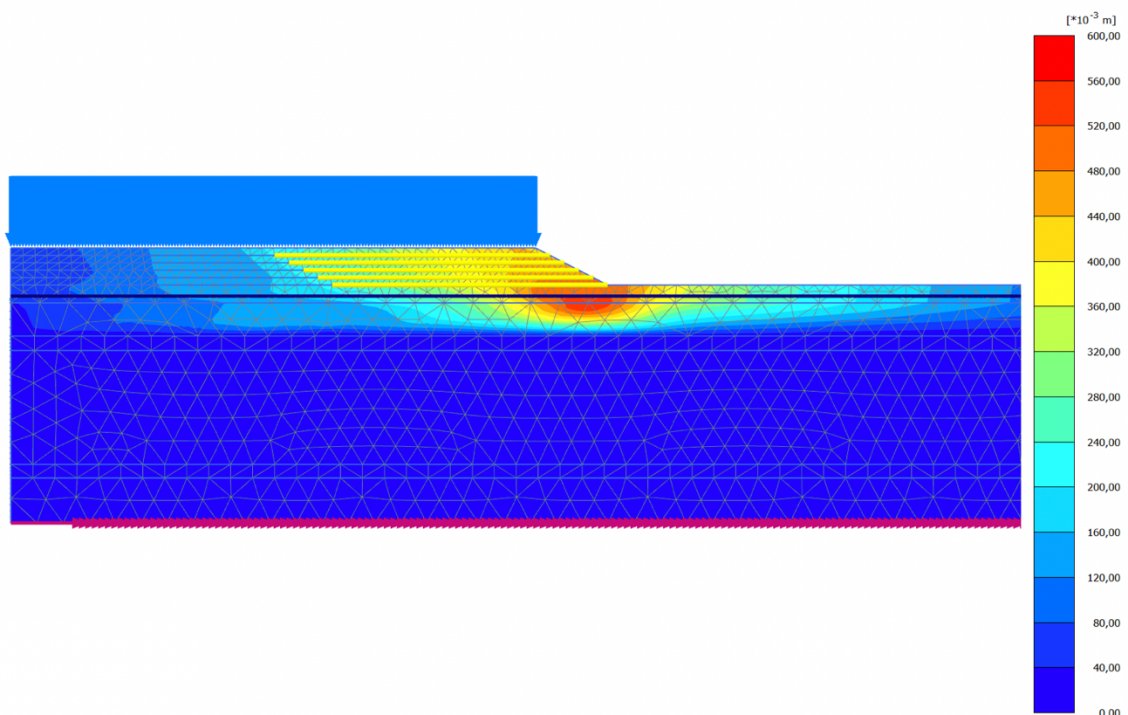


Figure 48. Total displacement at the end of dynamic time for dynamic analysis with geotextile

Moreover, the same pattern of failure is observed, where the part near the toe of slope deformed the most. Some conclusions can be out of this, which are the weak layer (AC1) induced the slope

instability and also layers below the embankment (AC1 and AS22) were liquefied during the dynamic time. Therefore, the failure of slope will always occur as long as the weak layer remains the same and no improvement on the liquefiable layers. The better parameters of geotextile will decrease the total settlement at crest but might be in small scale because no improvement is made on the source that make the slope failed.

Furthermore, the total displacements at the crest of slope during the dynamic time is presented in figure 49, while the total displacement for analysis without geotextile is also included for comparison. The total displacement at the end of dynamic time for the analysis using geotextile reached 0.434m that is within the maximum requirement of total displacement of 0.435m.

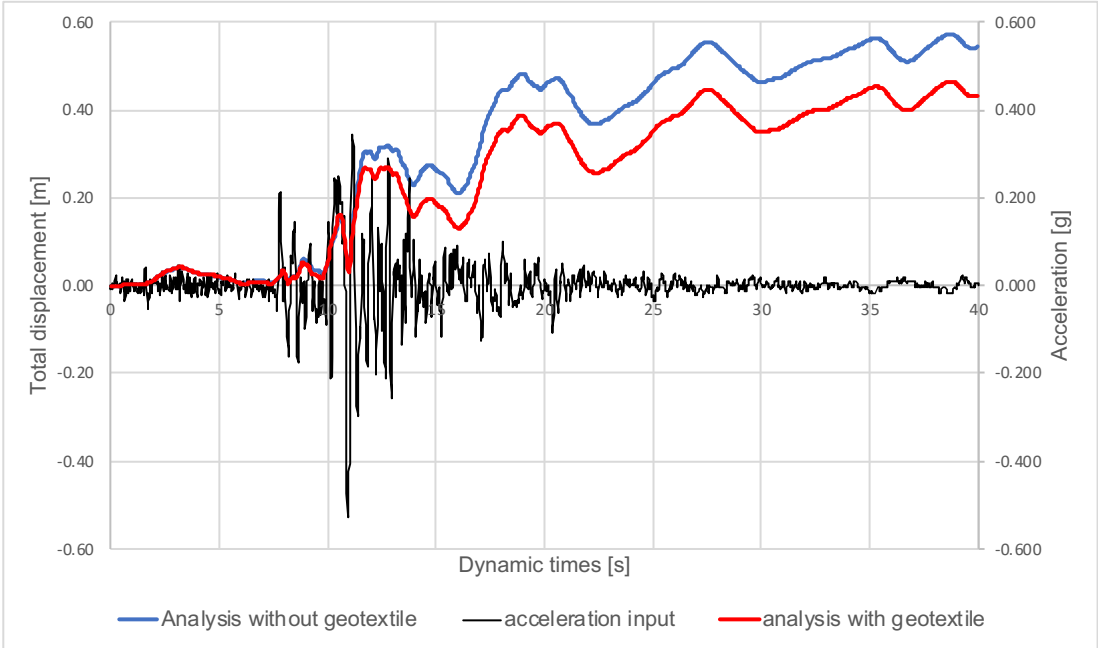


Figure 49. Comparison of total displacement at the crest of slope between the analysis without and with geotextile

The difference in total displacement from these two analyses could be seen after peak acceleration occurred as shown in figure 49 at time around 11 seconds. The red-line has less total displacement (plastic strain) right after the peak acceleration compared to the blue line for the no geotextile analysis. In conclusion, the installation of geotextile is proven to decrease the total displacement of the slope at the crest from about 0.543m to around 0.434m, with the difference around 0.109m (about 20%). Moreover, the effective vertical stress and active pore pressure are also presented in figure 50 and figure 51 respectively, which are most likely the same with the analysis without geotextile.

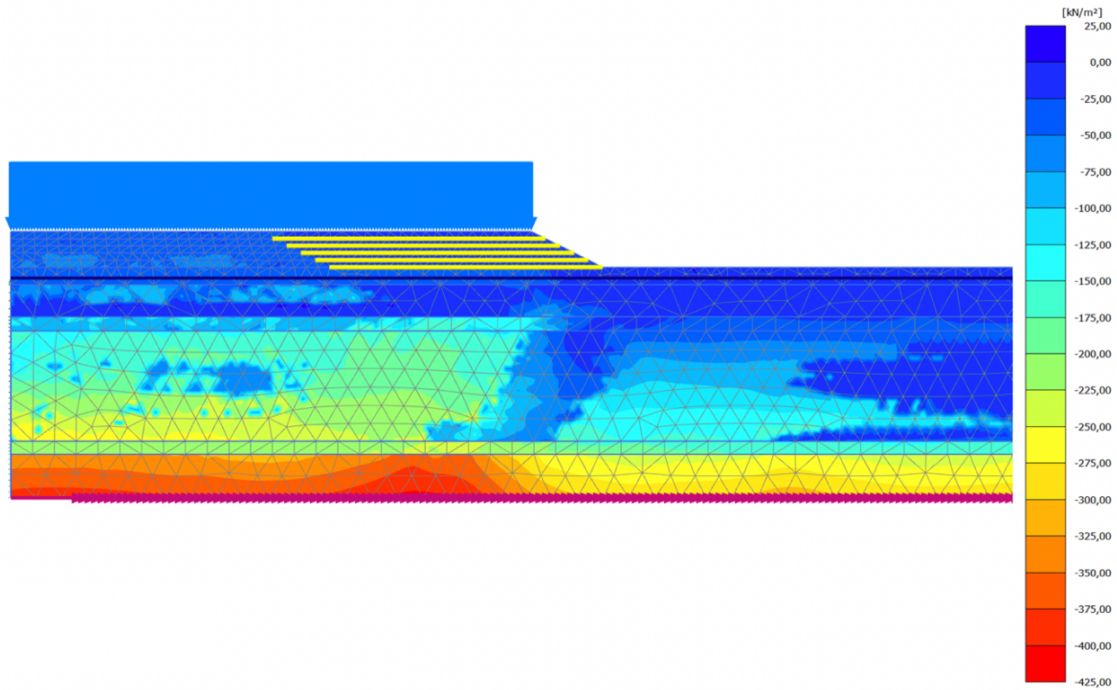


Figure 50. Vertical effective stress at the end of dynamic time for analysis with geotextile

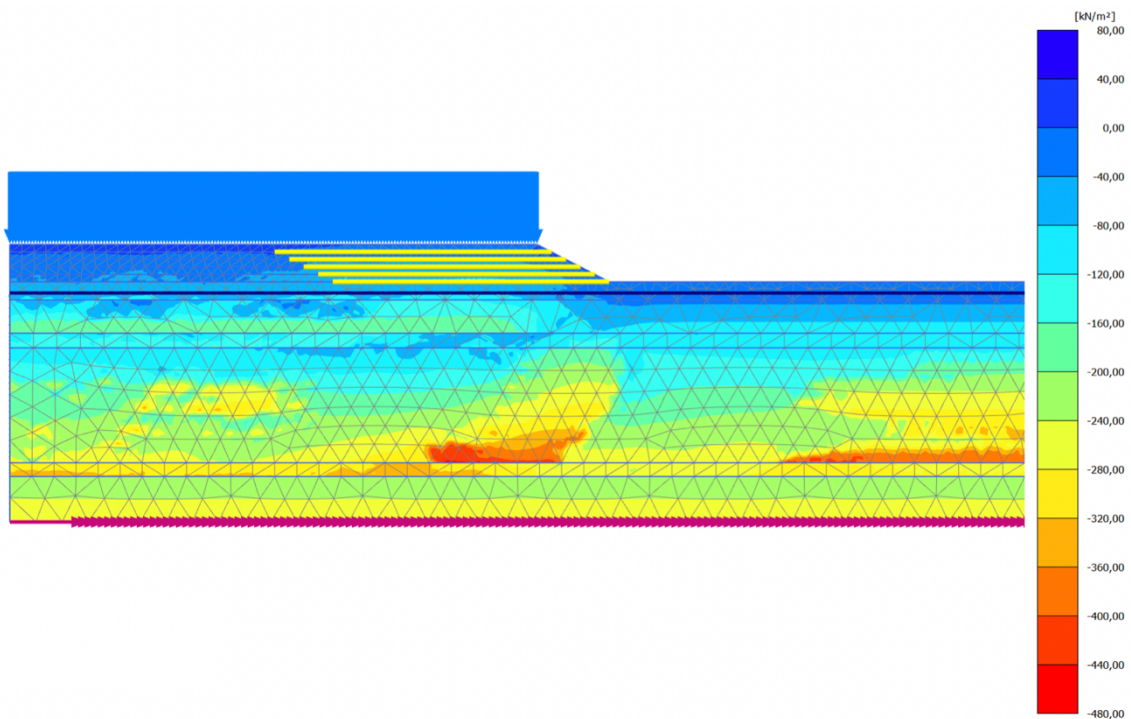


Figure 51. Active pore pressure at the end of dynamic time for analysis with geotextile

The axial force of the geotextile is shown in figure 52 with maximum force around 87.54 kN/m. The output shows parts of geotextile near the toe of the slope have zero or almost zero axial forces. The reason for this case is because parts of geotextile suffer compression instead of tension while geotextile can only have tension. Furthermore, the total displacement for the geotextile is presented in figure 53 with maximum value at 0.494m.

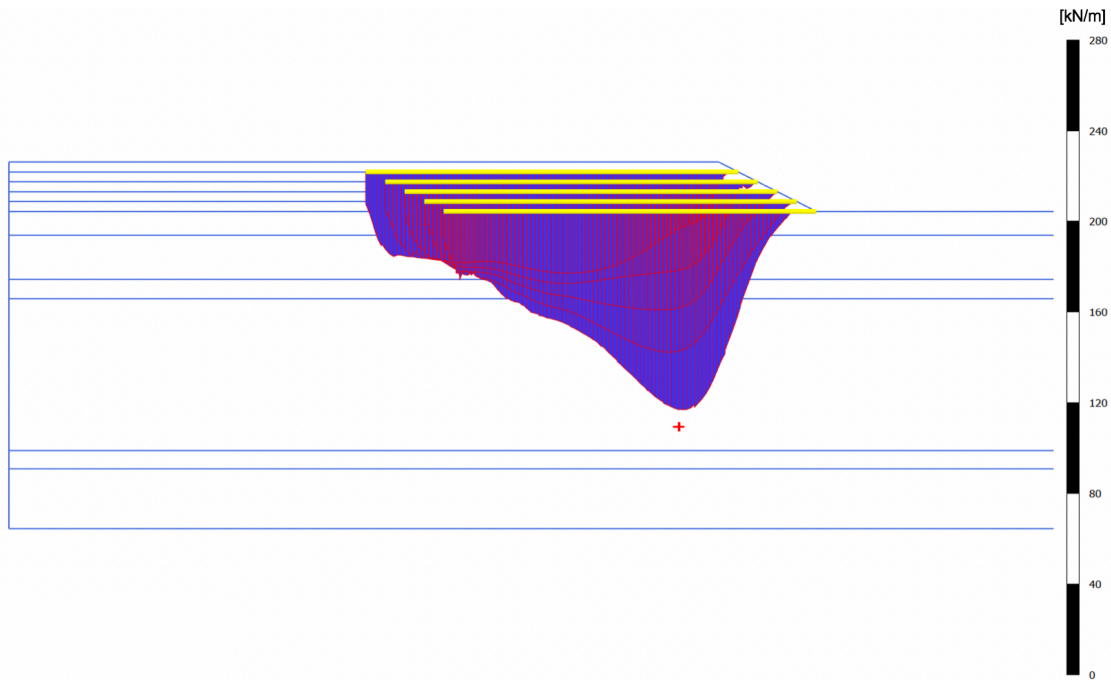


Figure 52. Axial forces for all layers of geotextile at the end of dynamic loading

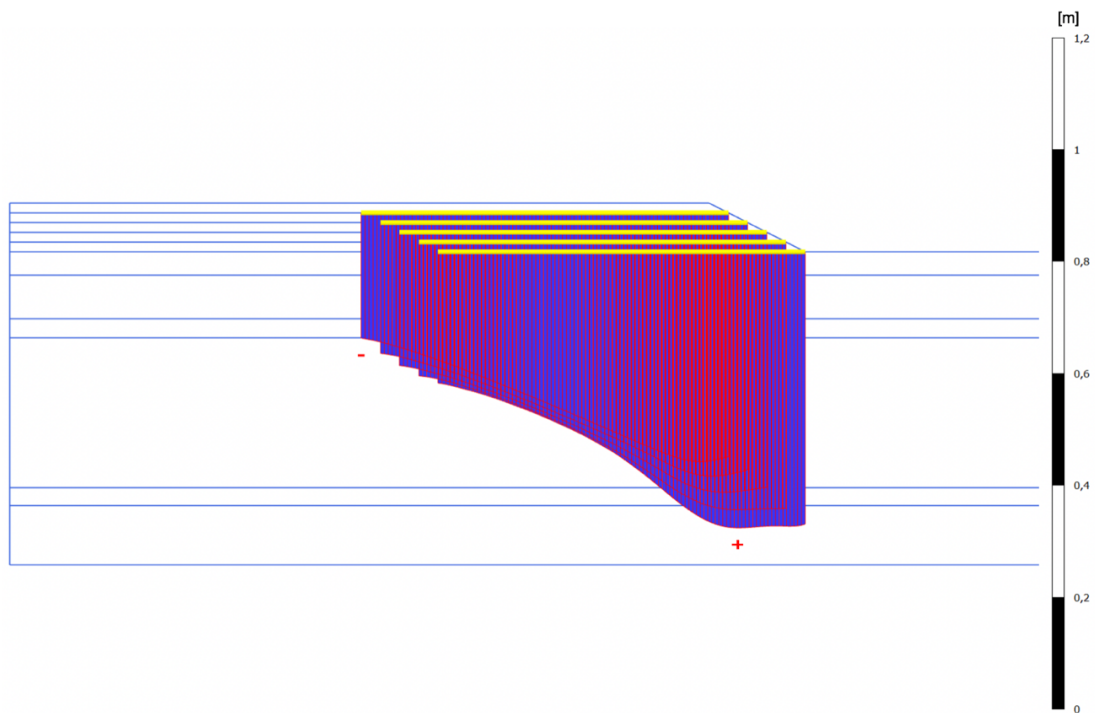


Figure 53. Total displacement of geotextile at the end of dynamic time

Liquefaction area is presented in figure 54 that is indicated by pore pressure ratio more than 0.9. Moreover, the most part of the second layer (AS21) are liquefied at the end of dynamic time. This result shows an agreement with the output of effective vertical stress in figure 50. The part where the effective stress decreases is the same part where liquefaction occur. Liquefaction area in the geotextile parts can be ignored because of the limitation of this approach as explained in previous chapter. PLAXIS assume soil above the phreatic level is in undrained condition, one of the limitations of this software, and also the part that has pore pressure ratio more than 0.9 appear due to decreasing of effective stress value at the deformed soil.

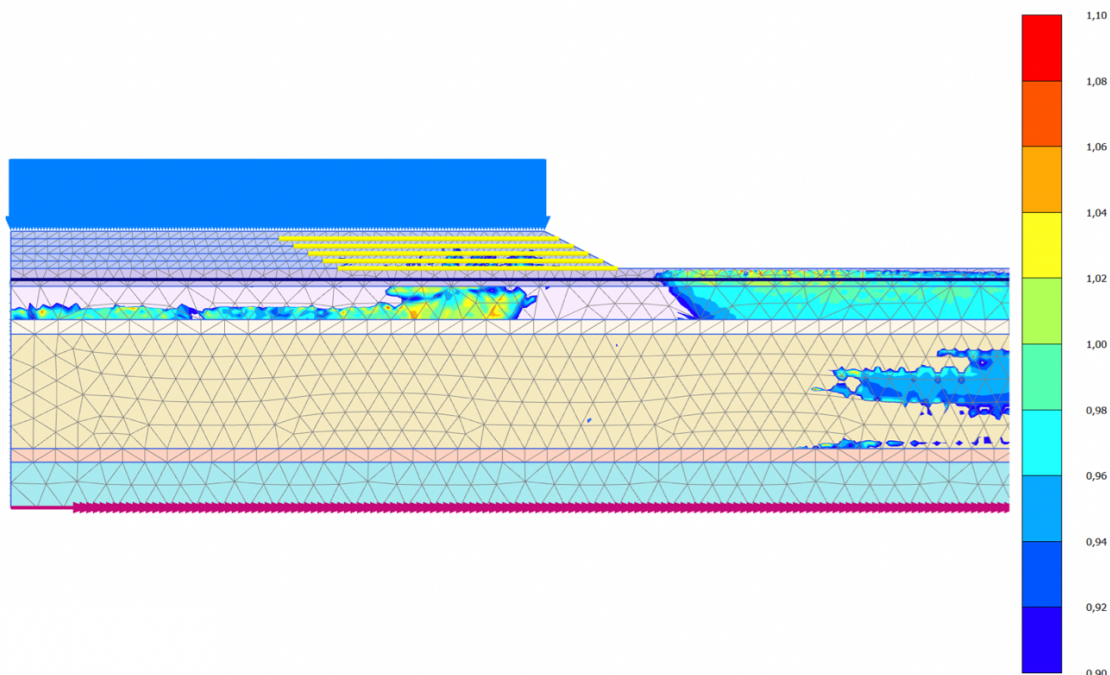


Figure 54. Liquefied areas corresponding to $r_v > 0.9$ at the end of dynamic times for analysis with geotextile

5.3 Optimization of Geotextile

The application of geotextile for slope reinforcement has been discussed in previous chapter. The geotextile-reinforced slope decreases the total displacement at the crest of slope. However, optimization of geotextile based on the tensile strength (and axial stiffness), length, and, number of layers can offer effectiveness on using this material. Therefore, this section discusses these points based on the case of newly-elevated area in Yuriage.

Furthermore, sixty combinations of analyses have been completed to check the influences of each parameter to the total displacement at the crest of the slope. These combinations are based on five different values of tensile strength and axial stiffness, three number of layers, and four lengths of geotextile, which are all summarized in table 19 including the result of analysis on total displacement at the crest of slope.

Table 19. Combination of parameters

Number of layer	Length	Tensile strength	Axial stiffness	Total displacement	Number of layer	Length	Tensile strength	Axial stiffness	Total displacement	Number of layer	Length	Tensile strength	Axial stiffness	Total displacement
[-]	[m]	[kN/m]	[kN/m]	[m]	[-]	[m]	[kN/m]	[kN/m]	[m]	[-]	[m]	[kN/m]	[kN/m]	[m]
5	10	28.8	288	0.532	7	10	28.8	288	0.513	9	10	28.8	288	0.514
		119	1194	0.522			119	1194	0.513			119	1194	0.504
		250	2502	0.518			250	2502	0.510			250	2502	0.504
		500	5004	0.516			500	5004	0.512			500	5004	0.502
		751	6255	0.520			751	6255	0.511			751	6255	0.507
	20	28.8	288	0.512		20	28.8	288	0.496		20	28.8	288	0.487
		119	1194	0.475			119	1194	0.460			119	1194	0.448
		250	2502	0.460			250	2502	0.443			250	2502	0.440
		500	5004	0.452			500	5004	0.443			500	5004	0.436
		751	6255	0.451			751	6255	0.444			751	6255	0.439
	30	28.8	288	0.513		30	28.8	288	0.493		30	28.8	288	0.483
		119	1194	0.469			119	1194	0.446			119	1194	0.435
		250	2502	0.447			250	2502	0.428			250	2502	0.417
		500	5004	0.434			500	5004	0.412			500	5004	0.408
		751	6255	0.431			751	6255	0.410			751	6255	0.398
	40	28.8	288	0.513		40	28.8	288	0.491		40	28.8	288	0.484
		119	1194	0.467			119	1194	0.448			119	1194	0.431
		250	2502	0.439			250	2502	0.414			250	2502	0.406
		500	5004	0.418			500	5004	0.389			500	5004	0.374
		751	6255	0.410			751	6255	0.379			751	6255	0.364

5.3.1 Tensile Strength and Axial Stiffness

The influence of tensile strength and axial stiffness can be taken in to consideration based on the fact that both parameters are correlated with each other. The influence of strength on increasing length of geotextile is given in figure 55 (a), (b), (c), and (d), while for different number of layers is presented in figure 56 (a), (b), and (c).

The influence of strength based on increasing the geotextile’s length is significant as shown in figure 55(a) to 55(d). The influence can be seen with wider ranges of total displacement for each strength, where the largest difference between each value is found in figure 55(d). The variation of strength has no impact in the length of 10m that clearly show that the reinforcement area is inside or slightly outside the failure mechanism. However, the difference between the 500 kN/m and 751 kN/m is too small for each length and number of layers. Thus, the optimum use of strength based on the length of geotextile should be using 500 kN/m.

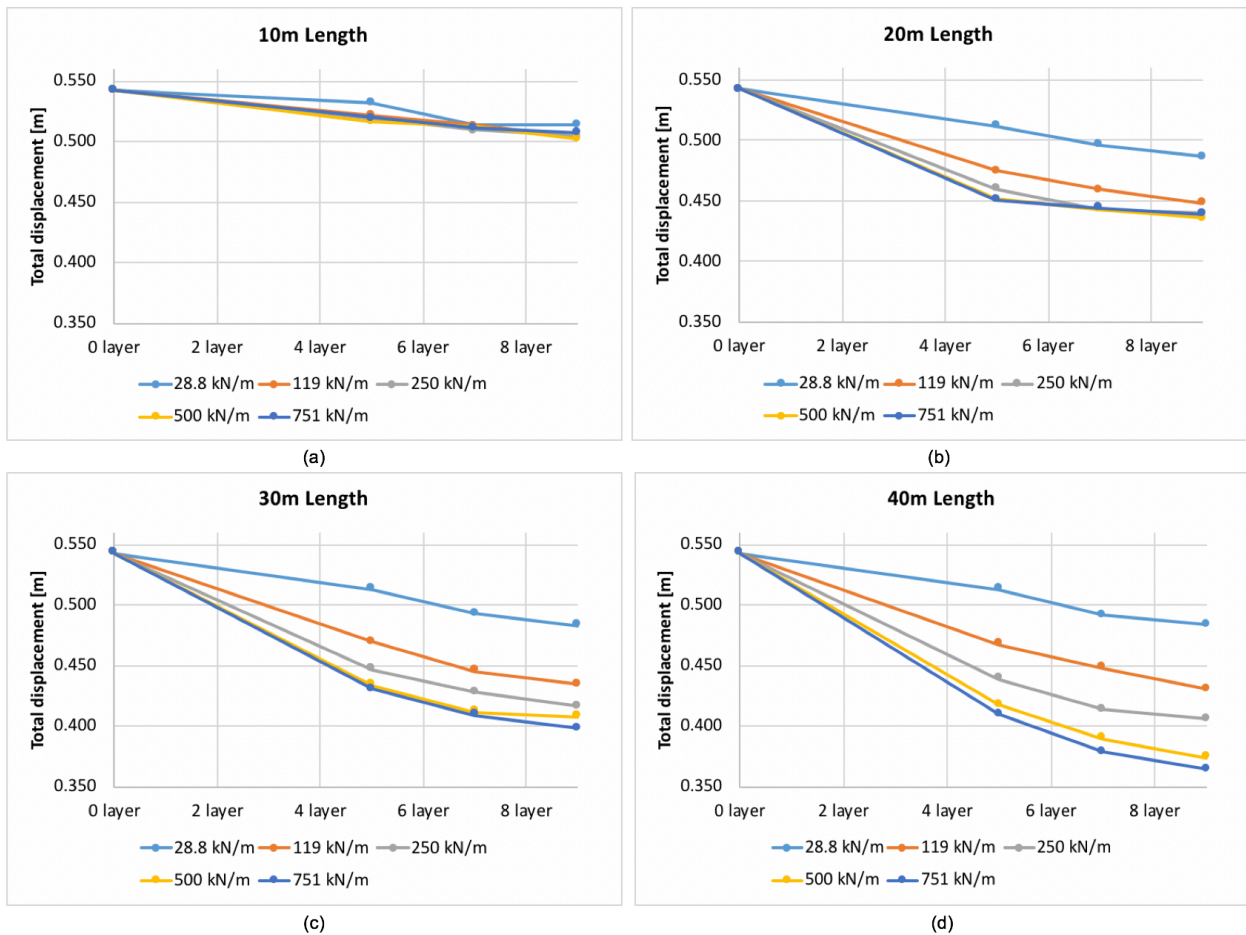


Figure 55. Influence of strength on total displacement for increasing length of geotextile

The influence of strength based on the number of layers is almost similar to the influence based on the length as explained above. However, the difference between each strength is already clear from the 5 layers in figure 56(a). The total displacement decreases significantly in the stronger/stiffer geotextile. The same condition with the length basis, the strength has reached the optimum point of 500 kN/m tensile strength, which means no significant difference can be achieved by increasing strength to 751 kN/m.

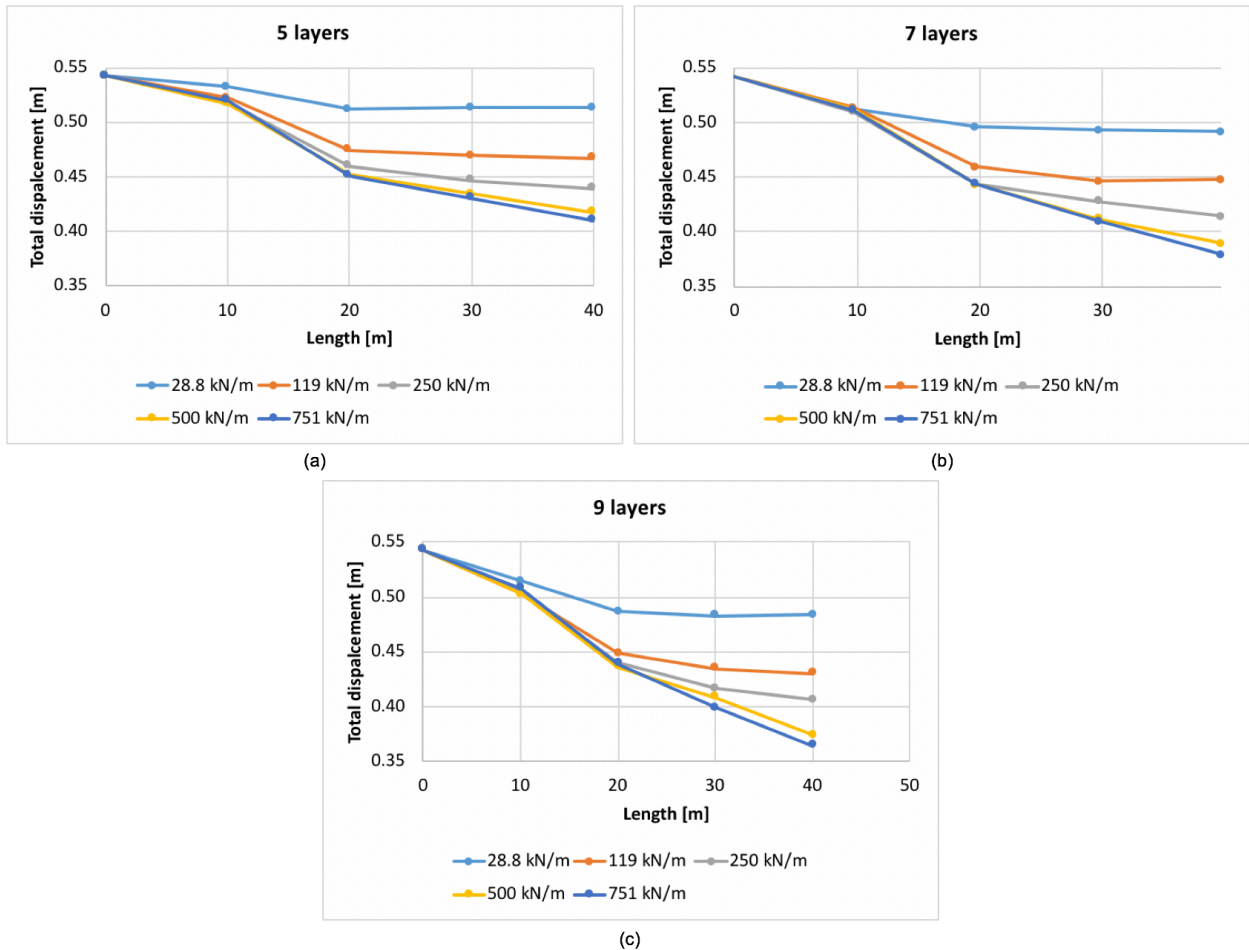


Figure 56. Influence of strength on total displacement for increasing number of layers

Further step is taken to check the influence of strength based on the combination of number of layer and the length for each layer. These two factors lead to total length of geotextile for a project by multiplying both factors, which means comparison can be made based on the total displacement from the (almost) same total length of geotextile. Therefore, the output of the analysis based on the strength in the basis of both factors are shown in figure 57.

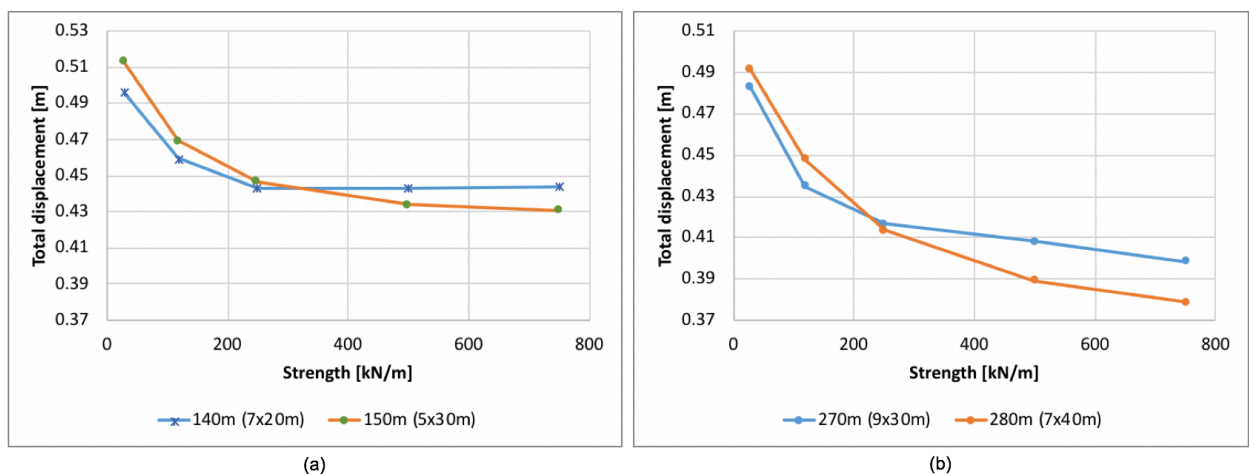


Figure 57. Comparison of total displacement based on the total length

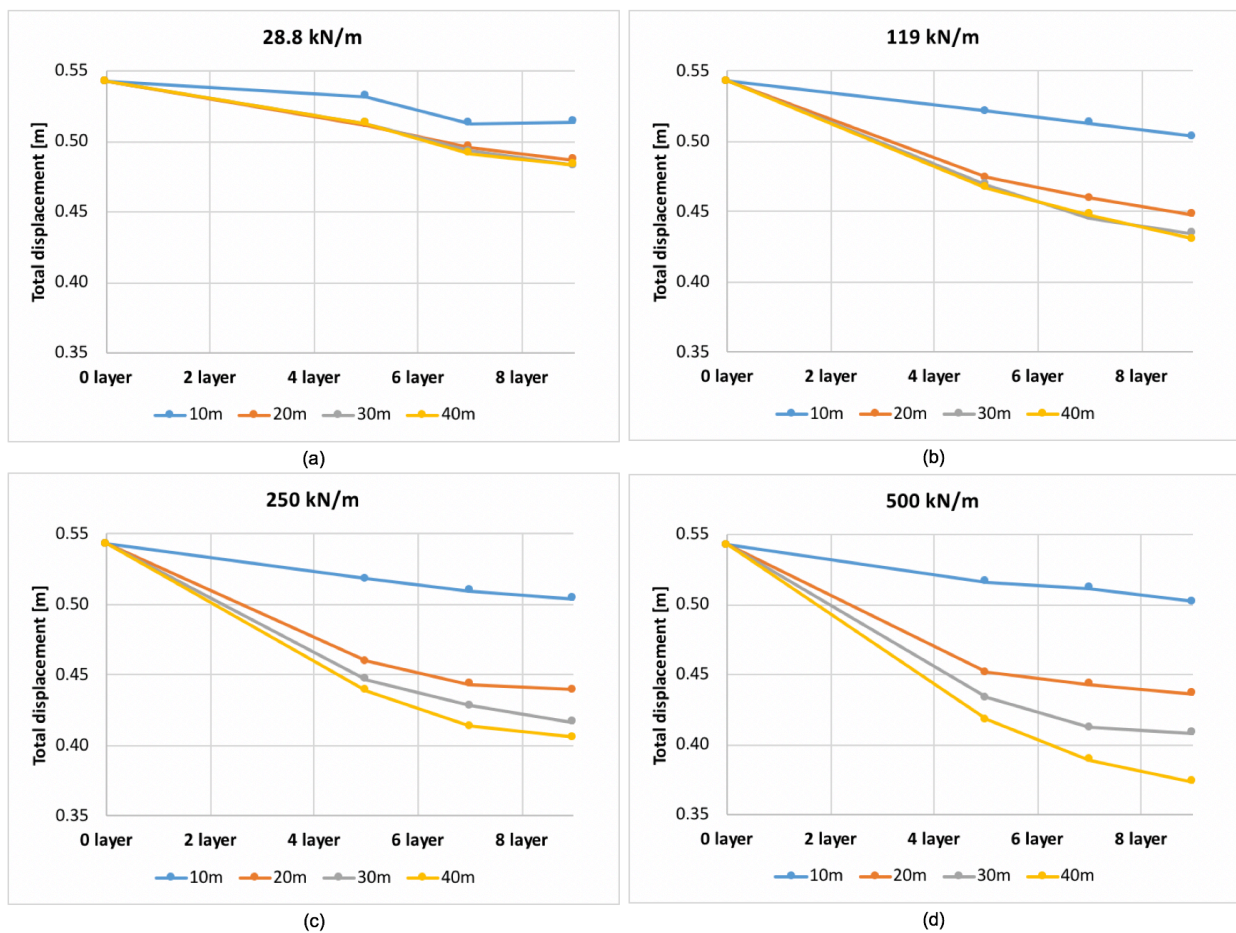
Figure 57 clearly shows that the low strength of geotextile (28.8 kN/m and 119kN/m) gives more influences on the basis of number of layers rather than the length of geotextile. On the other hand, the influence of higher strength (500 kN/m and 751 kN/m) is more significant with the length

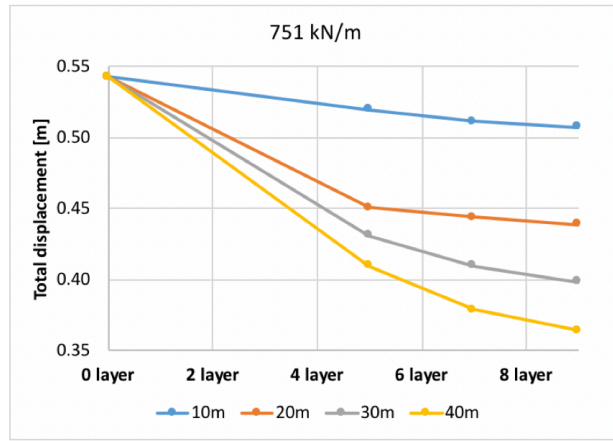
of geotextile rather than number of layers. However, the differences are very small with maximum value 0.02m (2cm) in 751 kN/m strength as shown in figure 52(b).

5.3.2 Length of Geotextile

Length of geotextile variations affect the total displacement with the combination of strength and number of layers. The influences of the length based on the strength of geotextile is given in figure 58, while figure 59 gives the influences of length by varied number of layers.

Another consideration from the influence of length is based on the strength of geotextile, the differences can be seen obviously starting from the strength 250 kN/m but the essential decreases of total displacement is from the strength more than 250 kN/m, especially the highest value of 751 kN/m.

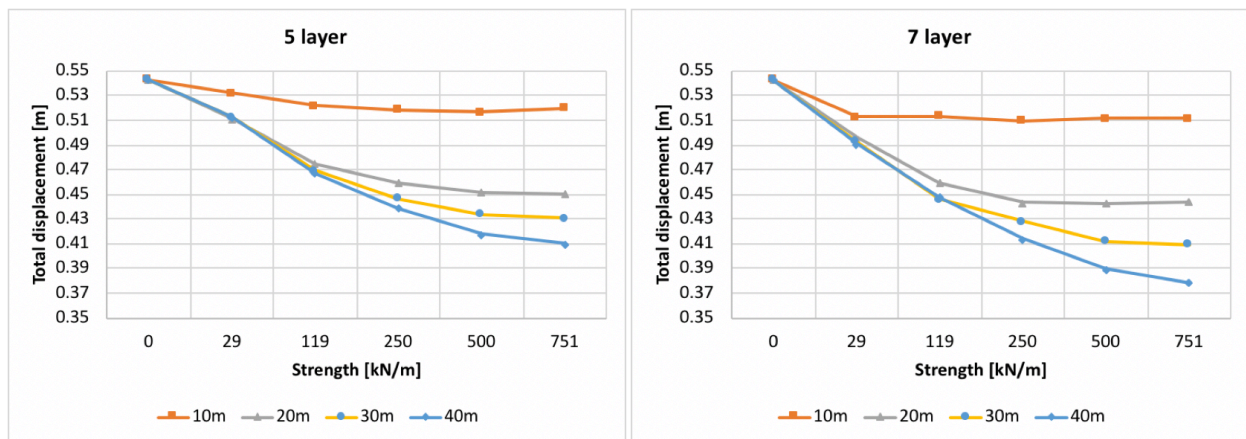




(e)

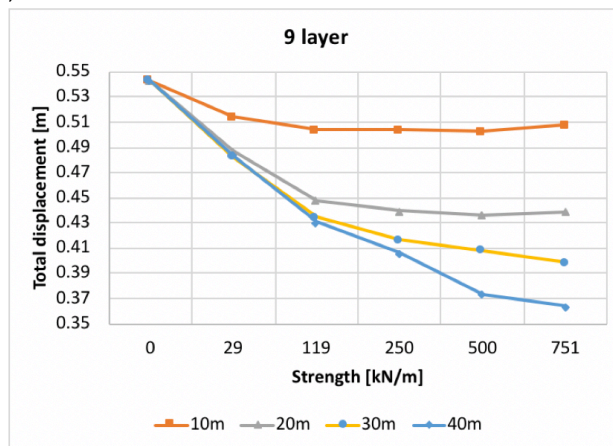
Figure 58. Influence of length on total displacement for increasing strength

The 10m geotextile has negligible influence when increasing the number of layers as shown in figure 59(a), 59(b) and 59(c). The influence of 20m geotextile has most likely the same small influence in decreasing the total displacement. However, the 30m and 40m length of geotextile have better influences in which the increase of number of layers give smaller total displacement.



(a)

(b)



(c)

Figure 59. Influence of length on total displacement for increasing number of layers

5.3.3 Number of Layers

The last part of influence comes from the number of layers, which is in combination of the length and the strength of geotextile as shown in figure 60 and figure 61 respectively. These two figures compare the increase in number of layers to the total displacement at the crest of the slope.

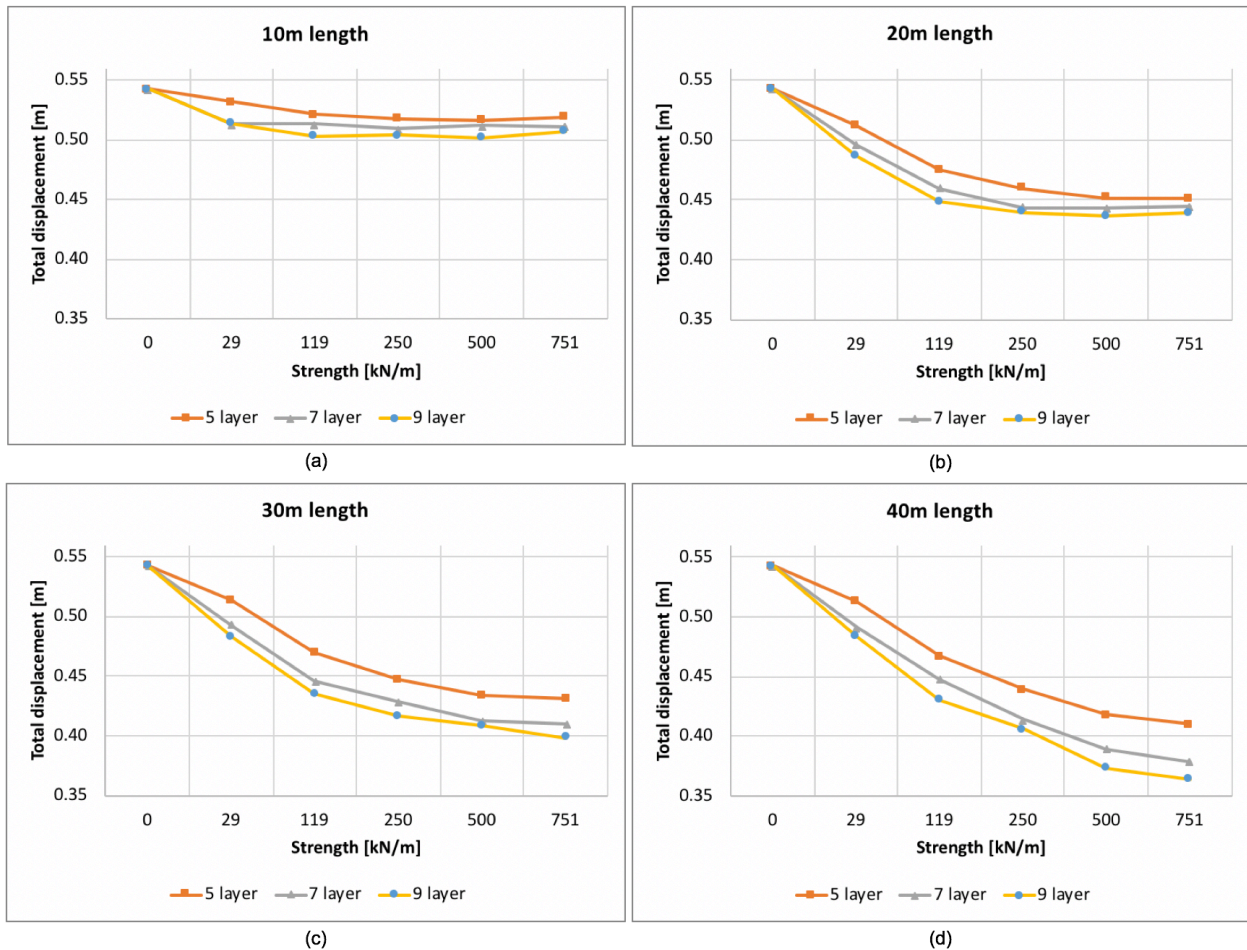


Figure 60. Influence of number of layers on total displacement for increasing length of geotextile

From figure 60 above, the total displacement is decreasing sharply for each number of layers for every length of geotextile. However, the total displacement among the number of layers has insignificant changes, so the minimum layer seems like a better choice and optimum for this Yuriage project.

Furthermore, the influence of number of layers based on the strength has similar trend with the basis of geotextile's length as shown in figure 61. Increasing number of layers show minor influence on total displacement in each strength value. Thus, the optimum number of layers seems to be the lowest one with 5 layers, while if requirement of the project does not reach; the larger value should be taken as rank based on the strength increasing.

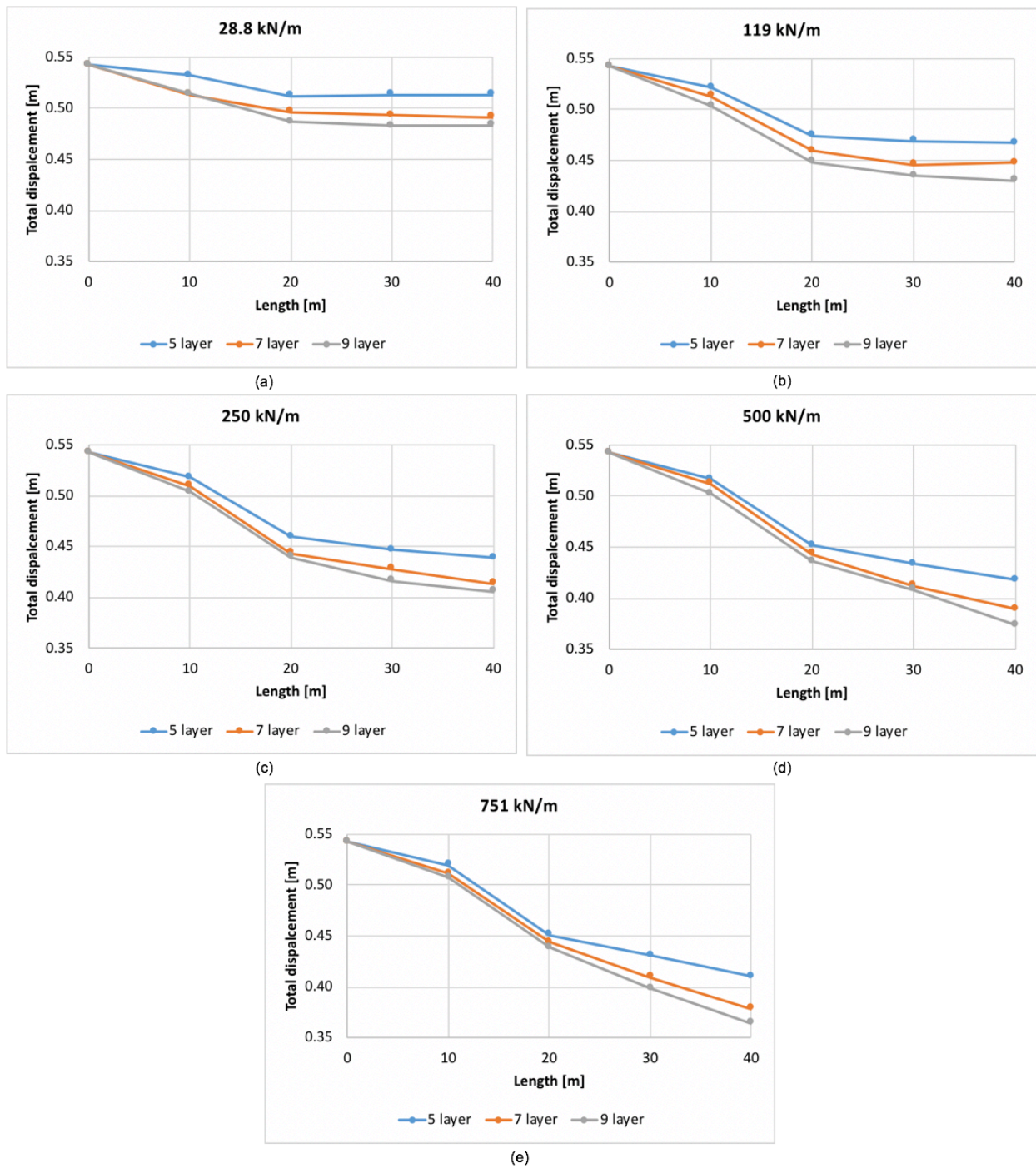


Figure 61. Influence of number of layers on total displacement for increasing strength of geotextile

6 Conclusions and Recommendations

6.1 Conclusions

Main Research Questions

- **How does geotextile reinforcement affect the strength of slope in the newly-elevated area of Yuriage as compared to the compaction method?**

There are three advantages of geotextile that compaction method does not have. First, geotextile produces the reinforcement from the friction of geotextile material and soil that in this case the materials could be in wider ranges of soil type. Second, acts as drainage path, which becomes an important role in preventing liquefaction on sandy soil. Geotextile accelerates the dissipation of seismic induced excess pore pressure. Third, increase the ductility of the soil mass to resist dynamic load.

However, the using of geotextile application has small impact compared to compaction method on decreasing total displacement in this project. There are some possible reasons that were obtained from analysis. First, the weak layer (AC1) induced the instability to the slope and also layers below the embankment (AC1 and AS21) were liquefied during the earthquake. Therefore, the failure of slope will always occur as long as the weak layer remains the same and no improvement on the liquefiable layers. The better parameters of geotextile will decrease the total settlement at crest but in small scale because no improvement is made on the source that make the slope failed. Some possible methods are proposed to improve the soil layer below the slope, such as by replacing the soil material below the slope with stronger materials (AC1) and construct the sand piles to avoid the liquefaction potential under the slope part until the depth of layer AS21, about 6 meters. Finally, the reinforcement using geotextile is not recommended for this project since this method has small impact on decreasing total displacement.

- **What is the optimum utilization of geotextile to meet the requirement of total displacement and economically constructed for the case with geotextile application?**

The optimum application of geotextile for this project is using 500 kN/m tensile strength with axial stiffness 5004 kN/m. Moreover, the shortest total length is preferred with 30m length for each of 5 layers of geotextile to keep the project economically constructed.

Sub Research Questions

- **What type of Constitutive Model is suited for the case of dynamic analysis in PLAXIS 2D software?**

UBCSAND model was used for analysis of slope with earthquake load. This model has some characteristics that suitable for dynamic analysis, especially for this project that concern about

the potential of liquefaction due to the soil profiles are dominated by sandy soil. Apart from capability of this model is able to capture generation of pore pressure during the dynamic time (earthquake) that leads to liquefaction behaviour, UBCSAND is also able to determine strains accumulation in cyclic loading.

However, some layers were not modelled using UBCSAND model for the analysis; bedrock (AG3) that consist of gravel was modelled with Linear Elastic because the material is much stronger and stiffer than the rest of layer and also this bedrock layers is not expected to experience plastic straining. Moreover, the HS Small strain was selected to model AC2 layer because this layer is the cohesive layer that has small possibility to liquified and also it has been deposited for a long time that make the stiffness is even greater.

- **How is the stability of current slope design under a specific seismic condition? Does any failure mechanism appear? What is the maximum total deformation at the crest of the slope?**

The slope was failed under dynamic calculation using Loma Prieta motion with peak acceleration 0.53g. The failure mechanism that goes through the second layer under the slope was found at the end of dynamic time. The weak foundation layer and also liquefied layers under the slope induced the instability of slope under the dynamic loading that is believed the main reason of this failure. Total displacement at the slope crest was found at 0.543m, which is out of the maximum requirement of the project, 0.435m. Furthermore, given the fact that the minimum requirement was not reached, the improvement of slope stability has to be considered, which in this case is using the geotextile application.

The large total displacement is due to plastic strain that was occurred mostly after the peak acceleration motion input at the time around 11. At this stage, the soil particles are restructured due to the shake then could not come back to the initial position (irreversible strain). Pore pressure was developed significantly compared to the result before the earthquake that leads to decreases in effective vertical stress. Therefore, some layers (AC1, AS21, and AS3) were liquefied during the dynamic time based on the pore pressure ratio above 0.9.

- **How different is the total displacement between geotextile method and the compaction method on the dynamic analysis?**

The analysis of slope without earthquake (only compaction method) resulted the total displacement at 0.543m at the end of dynamic time. The appearance of weak foundation layer and liquefied layers were the main reason of this large total displacement. Therefore, the slope strengthening using geotextile (500 kN/m tensile strength, 5004 kN/m axial stiffness, 30m length in 5 layers) decreased the total displacement to 0.434m. In other word, the geotextile application could reduce the total displacement about 0.109m or about 20% smaller.

- **What kind of optimization will be considered to make the total displacement at the crest meet the minimum requirement and economically constructed?**

Optimization of geotextile was considered based on five values of strengths, four difference lengths, and three number of layers. From the combination of these three factors, sixty cases of analysis were done with the result of maximum total displacement must be less than 10% of total height, about 0.435m. Apart from the minimum length that has to be selected, the first factor that has to be considered is the strength of geotextile because this factor gives more influence in the final total displacement. Secondly, with the high strength of geotextile, the length should be considered first rather than the number of layers based on the impact of both factor on the influence of strength to the total of displacement. However, total required length for a project (length of geotextile times the number of layers) could be used for further consideration on selecting the length and number of layers.

6.2 Recommendations and Fields that require further research

To get a more conclusive output and broader understanding, some recommendations are listed as points below:

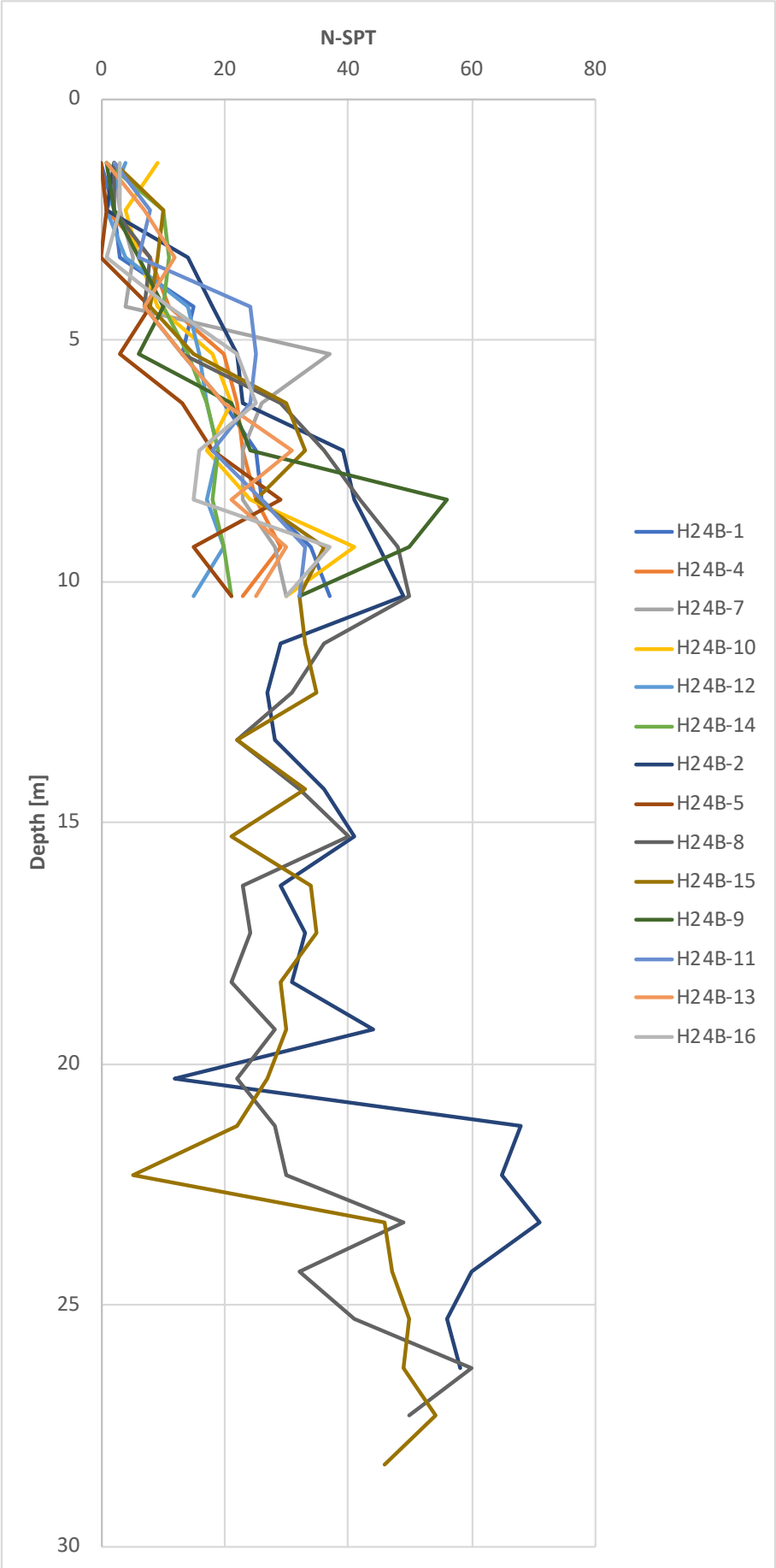
- Laboratory tests should be done for all layers to obtain better input data that perhaps can provide a better result of the analysis. On the other hand, this can be seen as the verification method for the model.
- The motion input based on the original seismic motion data that recorded from the seismometer should be used with further processing (deconvolution) to get the seismic input at the base of engineering rock.
- The optimization of geotextile is only based on one case of slope. However, further optimizations by considering various heights and angles of slope might produce better understanding in the selection of geotextile's parameters.
- The consideration based on the economic (cost of geotextile and construction) can be performed in regards to the priority of choice among those three parameters (strength, length, and number of layers).

Bibliography

- Anbazhagan, P., Uday, A., Moustafa, S. S. R., & Al-Arifi, N. S. N. (2017). Soil void ratio correlation with shear wave velocities and SPT N values for Indo-Gangetic basin. *Journal of the Geological Society of India*, 89(4), 398–406. <https://doi.org/10.1007/s12594-017-0621-z>
- Beatty, M.H., & Byrne, P. (1998). An effective stress model for predicting liquefaction behaviour of sand. *Geotechnical Earthquake Engineering and Soil Dynamics III ASCE Geotechnical Special Publication No.75*, 1:766–777.
- Beatty, M.H., Byrne, P. (2011). UBCSAND constitutive model. Itasca UDM website 904aR.
- Beatty, M. H., & Perlea, V. G. (2011). Several observations on advanced analyses with liquefiable materials. *21st Century Dam Design - Advances and Adaptations, 31st Annual USSD Conference*, 1369–1397.
- Bishop, A. W. (1955). The use of the Slip Circle in the Stability Analysis of Slopes. *Géotechnique*, 5(1), 7–17. <https://doi.org/10.1680/geot.1955.5.1.7>
- Bolton, M. D. (1986). The strength and dilatancy of sands. *Géotechnique*, 36(1), 65–78. <https://doi.org/10.1680/geot.1986.36.1.65>
- Bolton Seed, H., Tokimatsu, K., Harder, L. F., & Chung, R. M. (1985). Influence of SPT Procedures in Soil Liquefaction Resistance Evaluations. *Journal of Geotechnical Engineering*, 111(12), 1425–1445. [https://doi.org/10.1061/\(ASCE\)0733-9410\(1985\)111:12\(1425\)](https://doi.org/10.1061/(ASCE)0733-9410(1985)111:12(1425))
- Bonaparte, R., Holtz, R. D., & Giroud, J. P. (1987). *Soil Reinforcement Design Using Geotextiles and Geogrids*. American Society for Testing and Materials, Philadelphia. Retrieved from www.astm.org
- Brinkgreve, R. B. J., Kumarswamy, S., & Foria, F. (2018). PLAXIS 2D Material Models Manual. Delft: PLAXIS.
- Brinkgreve, R. B. J., Kumarswamy, S., & Foria, F. (2018). PLAXIS 2D Reference Manual. Delft: PLAXIS.
- Brinkgreve, R., & Engin, H. (2010). Validation of empirical formulas to derive model parameters for sands. *Numerical Methods in Geotechnical Engineering*, (June 2010), 137–142. <https://doi.org/10.1201/b10551-25>
- Chian, S. C., Pomonis, A., Saito, K., Fraser, S., Goda, K., Macabuag, J., ... Sammonds, P. (2012). Post Earthquake Field Investigation of the Mw 9.0 Tohoku Earthquake of 11 th March 2011. *15 Wcee*, (March 2011).
- Deltares. (2016). D-Geo Stability. User Manual. Retrieved from www.deltares.com
- Gibbs, H., & Holtz, W. (1957). Research on Determining the Density of Sands by Spoon

- Penetration Testing, 4th ICOSOMEF, 1, 35-39, (3), 35–39. Retrieved from <https://www.issmge.org>
- Hashash, Y. M. A., & Park, D. (2002). Viscous damping formulation and high frequency motion propagation in non-linear site response analysis. *Soil Dynamics and Earthquake Engineering*, 22(7), 611–624. [https://doi.org/10.1016/S0267-7261\(02\)00042-8](https://doi.org/10.1016/S0267-7261(02)00042-8)
- Hudson, M., Idriss, I., Beirkae, M. (1994). QUAD4M User's manual.
- Idriss I.M., Boulanger R.W., 2008, Soil liquefaction during earthquakes, Earthquake Engineering Research Institute, USA.
- Kuhlemeyer R. L. and Lysmer J. (1973). Finite element method for accuracy for wave propagation problems, Journal of Soil Mechanics & Foundation Division, ASCE Vol. 99, No. SM5, pp. 421-427
- Kuwano, J., Miyata, Y., & Koseki, J. (2014). Performance of reinforced soil walls during the 2011 Tohoku earthquake. *Geosynthetics International*, 21(3), 179–196. <https://doi.org/10.1680/gein.14.00008>
- Makra, A. (2013). *Evaluation of the UBC3D-PLM Model Constitutive Model for Prediction of Earthquake induced Liquefaction on Embankment Dams*. Delft University of technology. Retrieved from <https://repository.tudelft.nl>
- Marcuson III, W. F., Hynes, M. E., & Franklin, A. G. (2007). Seismic Design and Analysis of Embankment Dams: The State of Practice. *Proceedings of the 4th Civil Engineering Conference in the Asian Region*, 19. Retrieved from <http://www.columbia.edu/cu/civileng/ling/burmister/2007/Marcuson.pdf>
- Peck, R.B., Hanson, W.E., and Thornburn, T.H., (1974). Foundation Engineering, 2nd ed., John Wiley and Sons, New York, NY.
- Puebla, H., Byrne, P. M., & Phillips, R. (1997). Analysis of CANLEX liquefaction embankments: prototype and centrifuge models. *Canadian Geotechnical Journal*, 34(5), 641–657. <https://doi.org/10.1139/t97-034>
- Robertson, P. K. (1992). Standard penetration test energy measurements using a system based on the personal computer. *Canadian Geotechnical Journal*, (29), 551–557.
- Skempton, A. W. (1986). Standard penetration test procedures and the effects in sands of overburden pressure, relative density, particle size, ageing and overconsolidation. *Géotechnique*, 36(3), 425–447.
- Waltham, T. (2009). *Foundations of Engineering Geology* (3rd ed.). Taylor & Francis, New York. <https://doi.org/10.1017/CBO9781107415324.004>
- Zienkiewicz, O.C., Bicanic, N., Shen, F.Q. (1988). Earthquake input definition and the transmitting boundary conditions. *Advances in Computational Nonlinear Mechanics I*, 109–138.

A Standard Penetration Test Data



B Geotextile Properties from Global Synthetics

PROPERTIES OF ACETex® PET WOVEN GEOTEXTILES

PROPERTY	UNITS	GT 100/50	GT 200/50	GT 300/50	GT 400/50	GT 500/50	GT 600/50	GT 800/50	GT 1000/50	GT 1200/100*	
MECHANICAL PROPERTIES											
Characteristic short term tensile strength	MD	kN/m	100	200	300	400	500	600	800	1000	1200
Characteristic short term tensile strength	CD	kN/m	50	50	50	50	50	50	50	50	100
ISO 10319											
Strain at short term strength ISO 10319	MD	%	10	10	10	10	10	10	10	10	12
Partial factor - creep rupture - f_c											
at 5 years design life			1.33	1.33	1.33	1.33	1.33	1.33	1.33	1.33	1.33
at 10 years design life			1.37	1.37	1.37	1.37	1.37	1.37	1.37	1.37	1.37
at 60 years design life			1.45	1.45	1.45	1.45	1.45	1.45	1.45	1.45	1.45
at 120 years design life			1.5	1.5	1.5	1.5	1.5	1.5	1.5	1.5	1.5
Creep limited strength											
at 5 years design life	MD	kN/m	75	150	226	301	376	451	602	752	902
at 10 years design life	MD	kN/m	73	146	219	292	365	438	584	730	876
at 60 years design life	MD	kN/m	69	138	207	276	345	414	552	690	828
at 120 years design life	MD	kN/m	67	133	200	267	333	400	533	667	800
Partial factor - construction damage - f_d											
in clay, silt or sand			1.1	1.1	1.1	1.05	1.05	1.05	1.05	1.05	1.05
Partial factor - environmental effects in soil environment $2 < \text{soil pH} < 10$ - f_e											
not exceeding 10 years design life			1.0	1.0	1.0	1.0	1.0	1.0	1.0	1.0	1.0
at 60 years design life			1.05	1.05	1.05	1.05	1.05	1.05	1.05	1.05	1.05
at 120 years design life			1.1	1.1	1.1	1.1	1.1	1.1	1.1	1.1	1.1
Long term design strengths - t_d											
in clay, silt or sand											
at 5 years design life	MD	kN/m	68	137	205	286	358	430	573	716	859
at 10 years design life	MD	kN/m	66	133	199	278	348	417	556	695	834
at 60 years design life	MD	kN/m	60	119	179	250	313	375	500	626	751
at 120 years design life	MD	kN/m	55	110	165	231	289	346	462	577	693
Nominal roll width	m		3.8 - 5.2	3.8 - 5.2	3.8 - 5.2	3.8 - 5.2	3.8 - 5.2	3.8 - 5.2	3.8 - 5.2	3.8 - 5.2	3.8 - 5.2
Nominal roll length	m		100	100	100	100	100	100	100	50	50

C Geotextile Properties from TenCate Geosynthetics

TenCate Polyfelt® PEC reinforcing geotextiles are made of high modulus polyester yarns with nonwoven geotextile composites.

Properties of Polyfelt® PEC Reinforcing Geotextiles												
Property	Unit	PEC 35	PEC 50	PEC 75	PEC 100	PEC 150	PEC 200	PEC 35/35	PEC 50/50	PEC 75/75	PEC 100/100	
Characteristic initial strength (ISO 10319)	MD kN/m	35	50	75	100	150	200	35	50	75	100	
Characteristic initial strength (ISO 10319)	CD kN/m	14	14	14	14	14	14	35	50	75	100	
Strain at initial strength	MD %	10	10	10	10	10	10	10	10	10	10	
Partial factor -creep rupture at 120 years design life		1.55	1.55	1.55	1.55	1.55	1.55	1.55	1.55	1.55	1.55	
Creep limited strength at 120 years design life	kN/m	22.6	32.3	48.4	64.5	96.8	129.0	22.6	32.3	48.4	64.5	
Partial factor -construction damage in clay, silt or sand		1.05	1.02	1.00	1.00	1.00	1.00	1.05	1.02	1.00	1.00	
Partial factor -environmental effects soil environment, pH <11 at 120 years design life		1.10	1.10	1.10	1.10	1.10	1.10	1.10	1.10	1.10	1.10	
Long term design strengths at 120 years design life in clay, silt or sand	kN/m	19.6	28.8	44.0	58.7	88.0	117.3	19.6	28.8	44.0	58.7	
Water flow rate normal to the plane (ISO 11058)	mm/s (l/m ² /s)	65	65	65	65	65	65	50	50	50	50	
Water flow rate in the plane: 20kPa (ISO 12958)	10 ³ m ³ /s l/mh	30 11	30 11	30 11	30 11	30 11	30 11	30 11	30 11	30 11	30 11	
Nominal mass (ISO 9864)	g/m ²	265	280	300	330	400	480	330	360	400	500	
Nominal roll width	m	5.2	5.2	5.2	5.2	5.2	5.2	5.2	5.2	5.2	5.2	
Nominal roll length	m	100	100	100	100	100	100	100	100	100	100	
Estimated roll weight (+/- 10%)	kg	147	155	165	181	217	259	181	196	217	269	

D Safety Factor Requirements (Yuriage basic design plan, 2014) (Translated)

○盛土材料定数

盛土材料が決定していないことから、以下に示す盛土-砂相当の値(道路土工盛土工指針 p101)と用いた。
単位体積重量 $\gamma=19\text{kN/m}^3$ 、粘着力 $C=0\text{kN/m}^2$ 、せん断抵抗角 $\phi=30^\circ$

○安定検討

1) 目標安全率

〈道路〉・・・道路土工 軟弱地盤対策工指針

常時：盛土立上り時-1.10、供用時-1.25 [p146]

※沈下速度が速く、盛土立上り時で圧密(強度増加)が完了するため、目標安全率は供用時とする。

地震時：1.0 [p171,p172]

・粘性土：震度法($kh=0.12$: L1 地震動、 $kh=0.24$: L2 地震動・・・Ⅲ種地盤) [p170~171]

・砂質土： ΔU 法 過剰間隙水圧考慮 [p165~175]

(液状化検討時 L1=0.18、L2 タイプ I=0.40、タイプ II=0.60・・・Ⅲ種地盤) [p168]

・ 載荷重 常時：10.8kN/m² を考慮、地震時：考慮しない。[p106~107 を参考]

※載荷重 10.8 kN/m² 【10 kN/m² 建物荷重&交通荷重+積雪荷重 0.8】

〈造成地〉・・・宅地防災マニュアル、UR 都市機構のマニュアル・指針

①常時： $F_s \geq 1.5$ 以上(盛土施工直後)・・・宅防 [I] p8

②地震時： $F_s \geq 1.0$ 以上(大地震時)・・・宅防 [I] p8

・ 震度法 ($kh=0.25$: 大規模地震)

・ 載荷重 安定定検討

(Area construction) Guidelines for the prevention of housing or urban structure.

1) Always: $F_s \geq 1.5$ (immediately after the embankment constructed)

2) Earthquake: $F_s \geq 1.0$ (during a major earthquake)

○沈下検討

・ 沈下量の計算方法： ΔU 法・・・宅防 [II] p50

・ 残留沈下量：宅地部 2.5cm(木造-布基礎の標準値)・・・UR 軟技 pⅢ-11

道路部 10cm・・・道路土工軟弱地盤対策工指針 p119

※砂地盤で全沈下量が少なく即時沈下であるため、10~30cm の小さい方の値を採用。

○道路の重要度及び要求性能・・・次頁以降参照

道路の重要度：県道の重要度について、県道管理者と協議が必要となるが、迂回路があることから“重要度 2”の位置付けとした。

また、重要度 2 の要求性能としては、常時(性能 1)、レベル 1 地震動(性能 2)、レベル 2 地震動(性能 3)となる。レベル 1 地震動(性能 2)は実施するが、性能 3 は「崩壊等により隣接施設等に致命的な影響を与えないこと、安全性を満たすもの(人命を損なうことのないようにするための性能)」と定義しているため、当該地区が該当しないと想定される。

E Disaster category (Yuriage basic design plan, 2014) (Translated)

(3) 応急復旧のための判定

応急復旧のための判定は、上記の応急調査の結果にもとづき道路盛土区間の被災度を判定し、応急復旧、本復旧を含めて何らかの復旧を必要とするか否か、さらに、復旧を必要とする場合には、通行規制の影響および二次災害の防止との関係から、応急復旧を実施する必要があるか否かの判定を行うものである。

1) 被災度判定

道の安 者が に渡 性が 生し って	Level A: Large damage (Whether the embankment is completely collapsed or the vehicle movement is not possible) Level B: Medium Damage (Embankment is partially collapse, and part of the road may interfere with the collapse) Level C: minor damage (small part of embankment is affected, but it interferes the velocity of vehicles) Level D: No damage (especially if no abnormalities are observed in the embankment)
-----------------------------------	---

価され、次のように区分される。

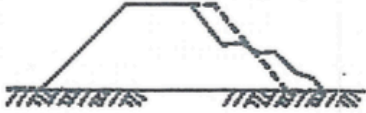




- A : 大被害 (盛土が全面的に崩壊するか、損傷規模が道路車線の大半におよび走行が不可能な場合)
- B : 中被害 (盛土が部分的に崩壊し、道路車線の一部に走行性の支障がある場合)
- C : 小被害 (盛土のごく一部に変状がみとめられるが、走行性に支障のない場合)
- D : 無被害 (盛土にとくに異常が認められない場合)

被災度判定を行う場合は、上述の安定性と走行性を支配する亀裂および段差の位置、深さ、沈下量、形状等の諸量を、被災パターンに分けて判定することが合理的であり、表-3.3.1 および表-3.3.2 のような分類が考えられる。ここでは、盛土を地山の傾斜度により平地盛土と傾斜地盤上の盛土に分類している。また、亀裂の生じた位置および形状により被災パターンを分類し、亀裂の大きさおよび段差量により被災度を区分した。このような分類により、被害の発生機構を推定し、また道路盛土としての機能低下の程度を把

F Damage Level (Yuriage basic design plan, 2014) (Original Document)

表-3.3.1 平地盛土の被災パターンと被災度分類

(1) 被災パターン分類表

被災パターン	被災模式図	被害形態
I型		のり面の流出、崩壊または亀裂の段差の発生が道路車線まで及ばず、のり肩にかぎられるもの。
II型		盛土のすべり崩壊または亀裂、段差の発生が道路車線まで及ぶもの。
III型		破壊が基礎地盤におよび盛土形状が原型をとどめないもの。
IV型		盛土の一律な沈下に伴って、盛土形状をある程度保ちつつ変形したもの。
V型		構造物背面の盛土が沈下および亀裂を起こしたもの。

(2) 被災度分類表

被災パターン	被災度	被災度の説明
I	B	亀裂幅 15cm 以上または段差量 20cm 以上
	C	亀裂幅 15cm 未満、かつ段差量 20cm 未満
II	A	亀裂幅 30cm をこえ、かつ段差量 50cm をこえたもの
	B	亀裂幅 30cm 以下または段差量 50cm 以下
III	A	—
IV	B	沈下量 50cm 以上
	C	沈下量 50cm 未満
V	B	沈下量 20cm 以上
	C	沈下量 20cm 未満

G Unconfined Compression Test for AC1 layer (Yuriage basic design plan, 2014)

JIS A 1216	土の一軸圧縮試験 (強度・変形特性)
------------	--------------------

調査件名 名取市閑上地区土地区画整理事業基本設計委託 試験年月日 平成 25年 3月 2日

試料番号 (深さ) T15-1 (1.00~1.78m) 試験者 八鍬啓一

土質名称	砂質粘土 (低塑性限界) (C19)	供試体 No.	1	2	3
液性限界 w_L (%)	40.6	試料の状態	乱さない	乱さない	乱さない
塑性限界 w_p (%)	23.2	高さ H_s (cm)	7.01	7.03	6.95
ひずみ速度 %/min	1.0	直径 D_s (cm)	3.43	3.41	3.42
特記事項 1) 必要に応じて記載する。		質量 m (g)	113.14	111.49	110.93
		湿潤密度 ρ_w (g/cm ³)	1.747	1.737	1.738
		含水比 w (%)	44.20	45.11	45.75
		一軸圧縮強さ q_u (kN/m ²)	28.9	28.2	30.8
		破壊ひずみ ϵ_f (%)	5.67	5.07	4.16
		変形係数 E_{30} (kN/m ²)	816	1057	1733
		鋭敏比 S_r			

